INFLUENCE OF CHLORINATED SOLVENTS ON THE CORROSION OF IRON IN BORATE BUFFER AND IN SIMULATED GROUNDWATER

By

Pascale M. L. Bonin

A thesis
presented to the University of Waterloo
in fulfilment of the
thesis requirement for the degree of
Doctor of Philosophy
in
Earth Sciences

Waterloo, Ontario, Canada, 1999

© Pascale M. L. Bonin 1999

National Library of Canada
Acquisitions and Bibliographic Services
395 Wellington Street
Ottawa ON K1A 0N4
Canada

Bibliothèque nationale du Canada
Acquisitions et services bibliographiques
395, rue Wellington
Ottawa ON K1A 0N4
Canada

Your file Votre reference

Our file Notre reference

The author has granted a non-exclusive licence allowing the National Library of Canada to reproduce, loan, distribute or sell copies of this thesis in microform, paper or electronic formats.

L'auteur a accordé une licence non exclusive permettant à la Bibliothèque nationale du Canada de reproduire, prêter, distribuer ou vendre des copies de cette thèse sous la forme de microfiche/film, de reproduction sur papier ou sur format électronique.

The author retains ownership of the copyright in this thesis. Neither the thesis nor substantial extracts from it may be printed or otherwise reproduced without the author's permission.

L'auteur conserve la propriété du droit d'auteur qui protège cette thèse. Ni la thèse ni des extraits substantiels de celle-ci ne doivent être imprimés ou autrement reproduits sans son autorisation.

0-612-51180-4

Canada

The University of Waterloo requires the signatures of all persons using or photocopying this thesis. Please sign below, and give address and date.

ABSTRACT

Contact with granular iron has emerged as a significant remediation technology for groundwater contaminated with chlorinated aliphatic hydrocarbons. The degradation of halogenated compounds by iron is a charge transfer process involving oxidation of iron and reduction of the organic compounds. To refine our understanding of the mechanism and kinetics of the charge transfer process, electrochemical and spectroscopic measurements were performed on iron electrodes in borate buffer and in simulated groundwater solutions of calcium carbonate and potassium bromide. These experiments, performed in the presence of two model compounds, a degradable compound (carbon tetrachloride) and a non-degradable compound (dichloromethane), indicated that carbon tetrachloride acts as an oxidizer of the iron surface while dichloromethane is nonreactive i.e., a non-oxidizer.

Based on electrochemical and spectral evidence, a new conceptual model of the reductive dehalogenation of chlorinated aliphatic hydrocarbons by iron is proposed. According to this model, the introduction of an oxidizer such as carbon tetrachloride will result in surface film formation. The composition and protective properties of these films were shown to be dependent on the corrosion behaviour of the iron prior to and after its exposure to the oxidizer, as well as on the ionic composition of the water.

In borate buffer, magnetite and hydrated magnetite were identified as the final products of the surface reactions, while carbonate-containing green rust complexes were detected in aqueous solutions of calcium carbonate. In these two solutions, the introduction of the oxidizer had no effect on the resistance of the iron/solution interface but resulted in an increase of the corrosion rate.

In aqueous solutions of potassium bromide, magnetite, green rusts, $Fe(OH)_3$ and α-FeOOH were identified as the final products of the surface reactions while the resistance of the iron/solution interface increased and the corrosion rate decreased after exposure to carbon tetrachloride. The changes in resistance and corrosion rate could not have been anticipated based on measurements of the potential, since similar positive shifts of potential were observed in all the solutions after exposure to the oxidizer. These changes are, however, in agreement with the fact that, prior to the introduction of the oxidizer, the presence of a film was detected in the potassium bromide solutions; there was no evidence of such a film in the borate and calcium carbonate solutions.

With regard to the practical use of iron for the remediation of groundwater contaminated with chlorinated aliphatic hydrocarbons, the results suggest that surface films may, or may not, affect reaction rates. For example, magnetite and green rust compounds, being non-protective, will not prevent charge transfer at the iron/solution interface; charge transfer will however proceed at a slower rate than on a bare metal surface. In addition, in the case of green rust compounds, they may also play a role as reductants themselves. For $Fe(OH)_3$ and α-FeOOH films, however, the situation is different. Being more protective, their presence could result in localized passivation of the iron, as seen in this study, and therefore be detrimental from a technological point-of-view.

ACKNOWLEDGEMENTS

I would like first to thank my supersivor, Dr. Robert Gillham, for his intellectual and emotional support throughout this degree. Dear Dr. Gillham, thank you for everything! Thank you for believing in me! Thank you for always being there! For being such a patient and caring listener... you have helped me sort things out so often! Thank you also for guiding me while respecting my goals and aspirations...this made the whole experience even more valuable to me!

I would then like to thank my mentor, Dr. Marek Odziemkowski. Dear Marek, how could I ever thank you enough for everything that you have done for me! Without your guidance and your determination, this thesis would never have been possible! You have taught me so much and you have helped me so much! Many thanks also for pushing my limits and always requiring the best out of me...at times, it was not easy but in hindsight, I agree that there was no other way!

I would also like to thank the members of my committee: Dr. Don Irish, Dr. Eric Reardon and Dr. Rick Devlin for their time and support throughout this degree. Dr. Irish, thanks so much for welcoming me in your laboratory and for constructively reviewing my first manuscript. A special thank you also to you, Eric, for reviewing my second manuscript.

My sincere thanks to Dr. Jacek Lipkowski at the University of Guelph who helped me journey in the world of electrochemistry and also for warmly welcoming me into his laboratory. Jacek, your kindness and generosity, both in class and in the laboratory, made it so much easier for me. Thanks also for letting me work with Dr. Wojtek Jędral while he was visiting in your laboratory.

A sincere thank you also to Dr.Wojtek Jędral. Dear Wojtek, I wish I could have had more time to work with you. You are so generous, so dedicated and you are such an amazing teacher. I really value the time I spent with you and the work we did together! Thank you also for your constructive comments on my third manuscript!

Many thanks also to Stephanie O'Hannesin, Greg Friday and Wayne Noble for their support during the experimental phase of this thesis. Dear Stephanie, Greg and Wayne, you have answered my numerous requests with so much patience and diligence! Thank you!

A special thought to Dr. John Cherry, Dr. James Barker and Robin Jowett who presented me with numerous challenges through my involvement, as a guest speaker, in a series of short courses related to groundwater remediation.

Many warm and sincere thoughts to Paul and Gabriel...for their unconditional support and love. Thanks also to my parents, brother and parents-in-law (specially my mother and mother-in-law) for being there when I needed them the most. I would never have made it without you! I love you all a lot! Je vous aime! Thanks so much! Merci!

Finally, I would like to thank the Natural Sciences and Engineering Research Council (NSERC) and CRESTech for their financial support.

DEDICATION

THIS THESIS IS DEDICATED TO MAREK ODZIEMKOWSKI
TO HIS INTEGRITY
AND HIS LOVE OF SCIENCE.

TABLE OF CONTENTS

ABSTRACT iv

ACKNOWLEDGEMENTS v

DEDICATION vi

TABLE OF CONTENTS vii

LIST OF FIGURES ix

LIST OF TABLES xii

1.0 INTRODUCTION 1

1.1 Background and goal 1

1.2 Literature review 2

1.3 Objectives 5

1.4 Thesis organization and format 8

1.5 References 10

2.0 INTRODUCTION TO CONCEPTS 14

2.1 Concepts related to corrosion of iron 14

2.2 Concepts related to surface films on iron 26

2.3 References 31

3.0 INFLUENCE OF CHLORINATED SOLVENTS ON POLARIZATION AND CORROSION BEHAVIOUR OF IRON IN BORATE BUFFER 35

3.1 Cover page 35

3.2 Introduction 36

3.3 Experimental methods 38

3.4 Results 40

3.4.1 Potentiodynamic polarization measurements in borate buffer 40

3.4.2 Open circuit potential-time measurements in borate buffer 46

3.4.3 Raman spectroscopy in borate buffer 49

3.5 Discussion 55

3.6 Conclusion 61

3.7 Appendix 62

3.8 References 62

4.0 *IN SITU* IDENTIFICATION OF CARBONATE-CONTAINING GREEN RUST ON IRON ELECTRODES IN SOLUTIONS SIMULATING GROUNDWATER 67

4.1 Cover page 67

4.2 Introduction 68

4.3 Experimental methods 70

4.4 Results and Discussion 72

4.5 Conclusion 83

4.6 References 84

5.0 ELECTROCHEMICAL AND RAMAN SPECTROSCOPIC STUDIES OF THE INFLUENCE OF CHLORINATED SOLVENTS ON THE CORROSION BEHAVIOUR OF IRON IN BORATE BUFFER AND IN SIMULATED GROUNDWATER 88

5.1 Cover page 88

5.2 Introduction 89

5.3 Experimental methods 93

5.4 Results and Discussion 97
5.4.1 Open circuit potential-time measurements on stationary iron electrodes 97
5.4.2 *In situ* Raman measurements on stationary iron electrodes 100
5.4.3 Tafel plot measurements on iron rotating disk electrodes 107
5.4.4 Corrosion rate measurements on iron rotating disk electrodes 109

5.5 Conclusion 113

5.6 References 114

6.0 CONCLUSION AND FUTURE WORK 118

6.1 Conclusion 118

6.2 Future Work 123

6.3 References 125

LIST OF FIGURES

Figure 2. 1 Schematic of behaviour of iron in pH 8.4 borate buffer (adapted from Figure 9.18 in Fontana and Greene, 1978). 15

Figure 2. 2 Schematic of behaviour of iron in pH 8.4 borate buffer containing some ferric ions (adapted from Figure 9.19 in Fontana and Greene, 1978). 17

Figure 2. 3 Polarization curve for an active-passive metal such as iron (adapted from Figure 9.24 in Fontana and Greene, 1978). 19

Figure 2. 4 Tafel plot where β_c and β_a represent the cathodic and anodic Tafel slopes, respectively (adapted from Figure 2 in Siebert, 1985) 21

Figure 2. 5 The four types of control of a reaction: diffusion-controlled, kinetic-controlled, mixed-kinetics and diffusion-controlled with partial blocking of active-dissolution sites (adapted from Figure 5.10 in Zembura, 1991). 25

Figure 2. 6 Various proposed structures of passive films (adapted from Figure 6 in Cohen, 1978). 27

Figure 3. 1 Potentiodynamic polarization curves in solvent-free borate buffer, in the presence of 8.52×10^{-4}M of CCl_4 and in the presence of 5.11×10^{-3}M of CH_2Cl_2. Sweep rate (dE/dt) was 1 mV/s. 41

Figure 3. 2 Influence of CCl_4 concentration. Potentiodynamic polarization curves in borate buffer in the presence of 2.02×10^{-4}M and 8.52×10^{-4}M of CCl_4. Sweep rate (dE/dt) was 1 mV/s. 43

Figure 3. 3 Influence of CH_2Cl_2 concentration. Potentiodynamic polarization curves in borate buffer in the presence of 5.89×10^{-4}M and 5.11×10^{-3}M of CH_2Cl_2. Sweep rate (dE/dt) was 1 mV/s. 44

Figure 3. 4 Cyclic voltammogram of Fe in solvent-free borate buffer, in the presence of 8.52×10^{-4} M of CCl_4 and in the presence of 5.11×10^{-3}M of CH_2Cl_2. Sweep rate (dE/dt) was 1 mV/s. 45

Figure 3. 5 Open circuit potential-time measurements in borate buffer. (a) injection of CH_2Cl_2 - electrode freshly cleaned; (b) injection of CH_2Cl_2 - electrode immersed for 24 h; (c) injection of CCl_4 - electrode freshly cleaned; (d) injection of CCl_4 - electrode immersed for 24 h; (e) injection of CCl_4 - electrode immersed for 68 h. 46

Figure 3. 6 Plot of the maximum (solid symbols) and final (open symbols) potentials reached in the open circuit potential-time measurements with CCl_4 (freshly cleaned electrode, 24 and 68 h of immersion) on the polarization curve obtained in solvent-free borate buffer. 47

Figure 3. 7 *In situ* Raman spectra of the Fe surface, preoxidized for 24 h, before (a) and after the injection of CCl_4 (b,c,d). 50

Figure 3. 8 *In situ* Raman spectra of the Fe surface, preoxidized for 68 h, before (a) and after the injection of CCl_4 (b,c). 52

Figure 3. 9 Bandfitting of the *in situ* Raman spectra of the Fe surface, preoxidized for 24 h, after the injection of CCl_4. Lower portion of the figure: spectrum 3.7(b); upper portion: spectrum 3.7(d). 54

Figure 3. 10 Bandfitting of the *in situ* Raman spectra of the Fe surface, preoxidized for 68 h, after the injection of CCl_4. Lower portion of the figure: spectrum 3.8(b); upper portion: spectrum 3.8(c) 55

Figure 3. 11 Stability regions for Fe solid species in borate buffer (pH 8.4). This figure was made using the thermodynamic data of Refait and Génin [54] following a format used by Sagoe-Crentsil and Glasser [55]. 58

Figure 3. 12 Conceptual model for the reductive dehalogenation of chlorinated solvents by iron in borate buffer. Cases of a fresh cathodically-cleaned Fe surface and of a pre-oxidized Fe surface. A^{n-} represents anions in solution: OH^-, $(B_4O_7)^{2-}$and $(BO_3)^{3-}$. The "?" indicates uncertainties; see text for details. 60

Figure 4. 1 Open circuit potential (OCP) - time measurements. (1) Freshly cathodically-cleaned iron electrode; (2) Iron electrode pre-oxidized for 17 h. 72

Figure 4. 2 *In situ* Raman spectra of the Fe surface pre-oxidized for 17 h in aqueous solution of calcium carbonate. (A, B) two different locations on the electrode before the injection of CCl_4; (C, D) two different locations on the electrode 1 hour after the injection of CCl_4. 74

Figure 4. 3 *In situ* Raman spectrum of the Fe surface pre-oxidized for 17 h in aqueous solution of calcium carbonate 1 hour after the injection of CCl_4. 77

Figure 4. 4 *In situ* Raman spectra of the Fe surface pre-oxidized for 17 h. (A) Before the injection of CCl_4 in D_2O solution of calcium carbonate; (B) 1 hour after the injection of CCl_4 in D_2O solution of calcium carbonate; (C) 1 hour after the injection of CCl_4 in aqueous solution of calcium carbonate 79

Figure 4. 5 *In situ* Raman spectra of the Fe surface pre-oxidized for 17 h in D_2O solution of calcium carbonate 1 hour after the injection of CCl_4. A) and B) were obtained at two different locations on the electrode. 81

Figure 4. 6 Pourbaix diagram of iron in carbonate-containing aqueous solutions. Pre-oxidized electrode: (■) maximum potential of -0.40 V, (❑) final potential of -0.44 V, pH of 6.7, and $CaCO_3$ concentration of $1.2x10^{-3}$M. Freshly cathodically-cleaned electrode: (Δ) final potential of -0.46 V, pH of 6.4, and $CaCO_3$ concentration of $1.2x10^{-3}$M. *By permission of the publisher. Copyright ©1995 by Elsevier Science Ltd.* 82

Figure 5. 1 Open circuit potential-time measurements in low pH KBr solution. 1) injection of CCl_4 - electrode freshly cleaned; 2) injection of CH_2Cl_2 - electrode freshly cleaned; 3a) injection of CCl_4 - electrode immersed for 17 h; 3b) injection of CCl_4 - electrode immersed for 70 h; 4) injection of CH_2Cl_2 - electrode immersed for 17 h.....98

Figure 5. 2 Open circuit potential-time measurements in high pH KBr solution. 1) injection of CCl_4 - electrode freshly cleaned; 2) injection of CH_2Cl_2 - electrode freshly cleaned; 3) injection of CCl_4 - electrode immersed for 17 h; 4) injection of CH_2Cl_2 - electrode immersed for 17 h. 99

Figure 5. 3 *In situ* Raman spectra of the Fe surface pre-oxidized for 70 h in low pH KBr solution, before (a) and after (b) the injection of CCl_4.....101

Figure 5. 4 *In situ* Raman spectra of the Fe surface pre-oxidized for 17 h in high pH KBr solution, before (a) and at two different locations after (b,c) the injection of CCl_4.....104

Figure 5. 5 Bandfitting of the *in situ* Raman spectra of the Fe surface pre-oxidized for 17 h in high pH KBr solution after the injection of CCl_4. Lower portion of the figure: spectrum 5.4(b); upper portion: spectrum 5.4(c). 106

Figure 5. 6 Tafel plot in borate buffer, before (❑, ——) and after (○, -----) the injection of CCl_4. 108

Figure 5. 7 Tafel plot in calcium carbonate solution, before (❑, ——) and after (○, -----) the injection of CCl_4. 109

LIST OF TABLES

Table 4. 1 Raman bands (in cm^{-1}) and band assignments. 76

Table 5. 1 OCP-time measurements, on freshly cathodically cleaned and pre-oxidized iron electrodes, in the 4 solutions (all potentials in mV NHE). 100

Table 5. 2 Raman bands (in cm^{-1}) observed on pre-oxidized iron electrodes, after the injection of CCl_4, in the 4 solutions 102

Table 5. 3 Corrosion rate measurements in the 4 solutions. 110

Table 6. 1 Summary of the results of the electrochemical and spectroscopic experiments performed on iron stationary and rotating disk electrodes in borate buffer and in simulated groundwater. 118

1.0 INTRODUCTION

1.1 Background and goal

The *in situ* use of granular iron for degradation of chlorinated aliphatic hydrocarbons (Gillham and O'Hannesin, 1994) has emerged as a significant new technology for remediation of contaminated groundwater. The degradation of halogenated compounds by iron is a charge transfer process involving oxidation of iron and reduction of the organic compounds. Though considerable research effort has focused on the degradation pathways and rates of reduction for different organic compounds (Gillham and O'Hannesin, 1992, 1994; Matheson and Tratnyek, 1994; Roberts *et al.*, 1996; Gillham, 1996; Focht *et al.*, 1996; Johnson *et al.*, 1996), many aspects of the charge transfer reactions remain highly speculative. In particular, questions related to the corrosion behaviour of iron, rather than to the fate of the contaminants, are still to be answered. For example, little is known of the influence of the organic molecules on the corrosion potential and corrosion rate of iron, and on the structure and properties of the iron/solution interface.

Approaches centered on the corrosion behaviour of iron, rather than on the contaminant behaviour, were taken in studies of iron particles in contact with water of different ionic compositions by Odziemkowski *et al.* (1998) and Reardon (1995). In the first, Raman spectroscopy was used to identify the surface films formed on electrolytic iron particles during contact with simulated groundwater; in the second, corrosion rates were measured by monitoring the hydrogen pressure increase in sealed cells containing low alloyed scrap steel granules and water. These studies, which were limited to contaminant-free solutions, showed that the nature of surface films and the corrosion rate are affected by the ionic composition of the aqueous solutions. Finally, Scherer *et al.* (1997), who used an iron rotating disk electrode to study the

kinetics of carbon tetrachloride reduction, identified the conditions under which mass transfer effects are negligible and the degradation reactions are controlled by charge transfer.

Following these lines of work, the present study was initiated to investigate the combined influence of chlorinated aliphatic compounds and water with different ionic compositions on the corrosion behaviour of iron and the structure of the iron/solution interface. By focusing on corrosion related issues, the goal was to gain insight concerning mechanistic and kinetic aspects of the degradation of halogenated compounds by iron. In addition, passivation of iron surfaces and longevity of field applications of the iron technology remain important practical questions. It was anticipated that the results of this study would contribute to a better understanding of these issues as well.

1.2 Literature review

The subjects of iron corrosion and passivity have been studied extensively for the last 200 years (Sato, 1990). Most of that research was driven by the need to prevent the deterioration of metallic structures by corrosion processes. Defining the conditions under which a passive film would form or breakdown was therefore often the main objective. In that light, the possible use of organic compounds as inhibitors was considered. It was found that the corrosion rates of many metals and alloys in media ranging from acidic to alkaline could be regulated over wide ranges with the aid of organic inhibitors (Damaskin *et al.*, 1971). The protective properties of these materials, which usually contain nitrogen, sulfur, or hydroxyl groups, were generally attributed to their adsorption onto the metal surfaces (Cohen, 1978).

Another avenue of research is the domain of organic electrochemistry where the synthesis or reduction/oxidation of organic compounds by reaction on different electrode materials, including iron, is studied. The electroreduction of halogenated organic compounds, with substitution of halogen by hydrogen, has been shown to take place under a variety of conditions: in aqueous or non-aqueous media, and on non transition or transition metals (Criddle and McCarty, 1991; Bukhtiarov *et al.*, 1988; Feoktistov, 1983; Baciocchi, 1983). For example, Merica *et al.*, (1998) reported the electroreduction of hexachlorobenzene at mercury and iron cathodes in methanol solutions. The current efficiency and extent of dechlorination were, however, larger on mercury than on iron electrodes.

The first experimental investigations concerning the use of metals to remediate water contaminated with halogenated organic compounds were reported in the patent literature about 30 years ago. Koch (1968) developed a cylindrical cell with Mg plates; Sweeny and Fisher (1972, 1973) designed a column reactor with activated metals (including iron) to degrade various halogenated organic contaminants. Others (Senzaki and Kumagai, 1988, 1989; Seeno, 1991; Takemura, 1992; Gillham and O'Hannesin, 1992, 1994; Schlimm and Heitz, 1996) have since considered the use of iron powder or porous metallic bodies of iron and other metals for the removal of halogenated hydrocarbons from contaminated water. The original contribution of the research by Gillham and O'Hannesin (1992, 1994) is that the use of granular iron, for the remediation of water contaminated with chlorinated aliphatic hydrocarbons, was not restricted to reactor-type applications, but was also proposed for use in *in situ* permeable reaction barriers. The concept of such barriers is remarkably simple, involving the construction of a permeable curtain containing granular iron particles across the path of a contaminant plume. As the

contaminated groundwater passes through the curtain, the contaminants are removed through reaction with the iron particles (Gillham, 1996).

The work by Gillham and O'Hannesin (1992, 1994) originated from the results of a study on sampling bias caused by materials used to monitor halocarbons in groundwater, in which it was found that galvanized metallic surfaces have the potential to transform polyhalogenated hydrocarbons (Reynolds *et al.*, 1990). Gillham and O'Hannesin (1992) confirmed the results of that study and extended the work to include other metals such as iron, zinc, aluminum, brass, copper and stainless steel. Higher degradation rates were obtained with iron and zinc. Because of its lower cost and toxicity, the use of granular iron in groundwater remediation systems, consisting of above-ground reactors or *in situ* permeable reaction walls, was proposed (Gillham and O'Hannesin, 1994). Several field demonstrations of the technology have now been completed, and it has also been used commercially at numerous locations in North America and in Europe (USEPA, 1999; Gillham, 1996; Focht *et al.*, 1996).

Present avenues of research where corrosion or electrochemical processes are used to decompose halogenated organic compounds can be divided into two fields. In the first, energy is supplied to the system to promote the degradation reactions, as in an electrolytic cell, while in the second, the reaction occurs spontaneously i.e., under open-circuit conditions, as in granular iron remediation systems. Advantages of the electrolytic approach over open-circuit methods are that it offers more control over the reaction pathway and that higher overpotentials can be reached. This may allow the degradation of otherwise recalcitrant species and/or result in faster degradation rates. Electrolytic methods have however certain disadvantages. As pointed out by

Merica *et al.* (1998), a non-aqueous solvent, an expensive supporting electrolyte and/or electrode materials that are not environmentally friendly might be required depending on the contaminant to be degraded. Finally, the energy required to promote the reactions might render these methods economically unviable, particularly for the remediation of contaminated groundwaters which are typically not conductive and have low contaminant concentrations.

On the other hand, above-ground reactors or *in situ* permeable reaction walls containing granular iron particles offer limited levels of control and may not be practical for remediation of heavily contaminated water; they have, however, numerous advantages. They do not require an external source of energy since the reactions occur spontaneously, and will occur as long as there is charge transfer from the metal to the contaminants. They also do not require the use of additives in term of solvents or electrolytes and the reactions have been shown to proceed in typical low-conductivity groundwater. Finally, the electrode material (iron) and most by-products are environmentally friendly, and iron granules used in commercial applications are relatively inexpensive.

1.3 Objectives

Accepting the view that the degradation of chlorinated aliphatic hydrocarbons by iron involves charge transfer at the iron/solution interface, the present study was initiated to investigate the combined influence of chlorinated molecules and water with different ionic compositions, on the corrosion behaviour of iron and the structure of the solid-solution interface. More specifically, the objectives were to:

1) Investigate the influence of degradable and non-degradable chlorinated aliphatic hydrocarbons on the corrosion behaviour of iron:

a) Determine if electrochemical measurements can help explain why some compounds are degradable while others are not. (For example, are recalcitrant compounds passivating the iron surface?);

b) Determine if the corrosion potential and corrosion rate of iron are affected by the presence of a degradable compound, and if so, in what way;

c) Determine if the corrosion potential and corrosion rate of iron are affected by the presence of a non-degradable compound, and if so, determine if the changes are of the same nature as those observed in the presence of a degradable compound;

d) Determine if the behaviour of the degrading and non-degrading compounds is similar from one solution to another i.e., determine the influence of the ionic composition of the water;

e) Determine if the presence of a film on the iron surface, prior to the introduction of a degradable or non-degradable contaminant, has an influence on the subsequent corrosion behaviour of iron.

2) Investigate the effects of degradable organic molecules on the structure and properties of the iron/solution interface:

a) In the case of a cathodically cleaned iron surface, characterize the changes at the iron/solution interface following exposure to a degradable compound;

b) In the case of an iron surface covered by a surface film prior to the introduction of a degradable compound, characterize the changes at the iron/solution interface following exposure to the compound;

c) Determine the nature and electronic properties of films present before or formed after exposure to a degradable compound;

d) Determine the influence of the ionic composition of the water on all of the above.

3) Generate a conceptual model of the iron/solution interface, in terms of corrosion behaviour and structure of the interface, following exposure to a degradable compound:

a) For the case of a cathodically cleaned iron surface;

b) For the case of an iron surface covered by a surface film prior to the introduction of a degradable compound;

c) For water with different ionic compositions.

To achieve these objectives, the following strategy was adopted. First, the granular iron/ contaminated groundwater system was simplified to an iron electrode/ borate buffer system in the presence of two model compounds, a degradable compound (carbon tetrachloride-CCl_4) and a non-degradable compound (dichloromethane-CH_2Cl_2). The need to simplify the system arose from the fact that granular iron particles used in commercial applications of the technology are in fact granules of various unknown mixtures of low alloyed scrap steel covered by a thick heterogeneous oxide layer. An iron electrode, on the other hand, is made of pure iron, the surface of which can be made oxide-free by electrochemical cleaning procedures. In addition, typical groundwaters are non-conductive compared to electrochemical solutions, they have limited buffering capacity and they usually contain anions, such as carbonates or halides, which can either act as passivating or aggressive agents. A concentrated borate solution, on the other hand, has buffering capacity and is slightly inhibiting only in the presence of oxygen.

Electrochemical and *in situ* Raman spectroscopic measurements were performed on the iron electrode in contaminant-free borate buffer, then in the presence of CCl_4 or CH_2Cl_2. Electrochemical experiments were performed where the potential of the electrode was controlled i.e., the electrode was polarized. These experiments, which included potentiodynamic polarization, Tafel plot and corrosion rate measurements, using various experimental methods, allowed us to gain insight into the kinetic aspects of the reactions in the presence and absence of contaminants. For other experiments, the potential of the freely corroding electrode at open circuit was monitored over time. During these open circuit potential (OCP)-time experiments, *in situ* Raman spectroscopic measurements were performed to investigate the nature of the changes at the interface.

Finally, the investigation was extended to simulated groundwater and the electrochemical and *in situ* Raman spectroscopic measurements were repeated in aqueous solutions of potassium bromide and calcium carbonate.

1.4 Thesis organization and format

This thesis is divided into six chapters. The first and last chapters are the introduction and conclusion, respectively, while chapters 2 to 5 constitute the main body of the thesis.

This study used electrochemical and spectroscopic techniques to gain insight concerning the granular iron remediation technology. Since these techniques are not frequently used in the fields of Earth Sciences and Environmental Chemistry, some important electrochemical and other related concepts will be introduced in Chapter 2.

In the first stage of this study, potentiodynamic polarization, OCP-time and *in situ* Raman spectroscopy measurements were performed in borate buffer. The results of these experiments were published in the journal Corrosion Science (Vol. 40, No. 8, pp. 1391-1409, 1998). The paper, as published, constitutes Chapter 3.

In the second stage of this study, the investigation was extended to simulated groundwater and experiments were repeated in aqueous solutions of calcium carbonate and potassium bromide. Chapter 4 covers the results of OCP-time and *in situ* Raman spectroscopy measurements performed in calcium carbonate solution. The content of Chapter 4 was submitted to the Journal of Solution Chemistry in May 1999; its format is therefore the format of the manuscript as submitted. The focus of the manuscript is on the *in situ* identification of carbonate-containing green rust, and is of particular importance because it is the first time that this compound, as a corrosion product of iron, has been identified *in situ* by any technique.

Chapter 5 covers the results of Tafel plot and corrosion rate measurements performed in borate buffer and in aqueous solutions of potassium bromide and calcium carbonate. It also covers the results of OCP-time and *in situ* Raman spectroscopy measurements in potassium bromide solution. The content of Chapter 5 was submitted to the journal Corrosion Science in September and accepted in November 1999; its format is therefore the format of the manuscript to be published.

1.5 References

Baciocchi, E. (1983). *1,2-Dehalogenations and related reactions.* Chapter 5: The chemistry of halides, pseudo-halides and azides. The chemistry of functional groups, Supplement D. S. Patai and Z. Rappoport (Eds.), John Wiley & Sons Inc., New York, pp. 161-201.

Bukhtiarov, A.V., V.N. Golyshin, A.P. Tomilov and O.V. Kuz'min. (1988). *Cathodic cleavage of the C-H bond. Electrochemical reduction of halogen-containing organic compounds on transition metals.* Translated from Zhurnal Obshchei Khimii, Vol. 58, No. 6, pp.1398-1406.

Cohen, M. (1978). *The passivity and breakdown of passivity on iron.* Passivity of metals, R.P. Frankenthal and J. Kruger (Eds.), The Electrochemical Society, Pennington, New Jersey, pp. 521-545.

Criddle, C.S. and P.L. McCarty. (1991). *Electrolytic model system for reductive dehalogenation in aqueous environments.* Environ. Sci. Technol., Vol. 25, No. 5, pp.973-978.

Damaskin, B.B, O.A. Petrii and V.V. Batrakov. (1971). *Adsorption of organic compounds on electrodes*, Plenum Press Publishers Ltd, New York, pp. 255-319.

Feoktistov, L.G. (1983). *Reduction of halogenated organic compounds.* Organic electrochemistry: an introduction and a guide, M.M. Baizer and H. Lung (Eds.), M. Dekker, New York, pp. 259-284.

Focht, R., J. Vogan and S.F. O'Hannesin. (1996). *Field application of reactive iron walls for in situ degradation of volatile organic compounds in groundwater.* Remediation, Vol. 3, No. 6, pp. 81-94.

Gillham, R.W. and S.F. O'Hannesin. (1994). *Enhanced degradation of halogenated aliphatics by zero-valent iron.* Groundwater, Vol. 32, No. 6, pp. 958-967.

Gillham, R.W. and S.F. O'Hannesin. (1992). *Metal-catalysed abiotic degradation of halogenated organic compounds*. IAH Conference "Modern trends in hydrogeology", Hamilton, Ontario, May 10-13, pp.94-103.

Gillham, R.W. (1996). *In situ treatment of groundwater: metal-enhanced degradation of chlorinated organic contaminants*. Advances in Groundwater Pollution Control and Remediation, M.M. Aral (Ed.), Kluwer Academic Publishers, Printed in the Netherlands, pp. 249-274.

Johnson, T.L., M.M. Scherer and P.G. Tratnyek. (1996). *Kinetics of halogenated organic compound degradation by iron metal*. Environ. Sci. Technol., Vol. 30, No. 8, pp. 2634-2640.

Koch, R. (1968). *Galvanic action water purifier*. U.S. Patent No. 3 392 102-A.

Matheson, L.J. and P.G. Tratnyek. (1994). *Reductive dehalogenation of chlorinated methanes by iron metal*. Environ. Sci. Technol., Vol. 28, No. 12, pp. 2045-2053.

Merica, S.G., N.J. Bunce, W. Jedral and J. Lipkowski. (1998). *Electroreduction of hexachlorobenzene in protic solvent at Hg cathodes*. J. Applied Electrochem., Vol. 28, pp. 645-651.

Odziemkowski, M.S., T.T. Schuhmacher, R.W. Gillham and E.J. Reardon. (1998). *Mechanism of oxide film formation on iron in simulating groundwater solutions: Raman spectroscopic studies*. Corrosion Science, Vol. 40, No. 2/3, pp. 371-389.

Reardon, E.J. (1995). *Anaerobic corrosion of granular iron: measurement and interpretation of hydrogen evolution rates*. Environ. Sci. Technol., Vol. 29, No. 12, pp. 2936-2945.

Reynolds, G.W., T.F. Hoff and R.W. Gillham. (1990). *Sampling bias caused by materials used to monitor halocarbons in groundwater*. Environ. Sci. Technol., Vol. 24, No. 1, pp. 135-142.

Roberts, A.L., L.A. Totten, W.A. Arnold, D.R. Burris, and T.J.Campbell. (1996*)*. *Reductive elimination of chlorinated ethylenes by zero-valent metals*. Environ. Sci. Technol., Vol. 30, No. 8, pp. 2654-2659.

Sato, N. (1990). *An overview on the passivity of metals*. Corrosion Science, Vol. 31, pp. 1-19.

Scherer, M.M., J.C. Westall, M. Ziomek-Moroz and P.G. Tratnyek. (1997). *Kinetics of carbon tetrachloride reduction at an oxide-free iron electrode*. Environ. Sci. Technol., Vol. 31, No. 8, pp. 2385-2391.

Schlimm, C. and E. Heitz. (1996). *Development of a wastewater treatment process: Reductive dehalogenation of chlorinated hydrocarbons by metals*. Environmental Progress, Vol. 15, No. 1, pp. 38-47.

Seeno, K. (1991). *Sewage treatment*, JP 3-106 496(A), Patents Abstracts of Japan, C-853, Vol. 15, p.293.

Senzaki, T. and Y. Kumagai. (1988). *Removal of chlorinated organic compounds from wasterwater by reduction process: Treatment of 1,1,2,2-tetrachloroethane with iron powder*. Kogyo Yoshi, Vol. 357, pp. 2-7 (in Japanese).

Senzaki, T. and Y. Kumagai. (1989). *Removal of chlorinated organic compounds from wasterwater by reduction process: II. Treatment of trichloroethylene with iron powder*. Kogyo Yoshi, Vol. 369, pp. 19-25 (in Japanese).

Sweeny, K.H. and J.R. Fisher. (1972). *Reductive degradation of halogenated pesticides*. U.S. Patent No. 3 640 821.

Sweeny, K.H. and J.R. Fisher. (1973). *Decomposition of halogenated organic compounds using metallic couples*. U.S. Patent No. 3 737 384.

Takemura, Y. (1992). *Method and apparatus for treating water containing organochlorine compounds*, JP 4-100 593(A), Patents Abstracts of Japan, C-965, Vol. 16, p.338.

United States Environmental Protection Agency (1999). *Field applications of in situ remediation technologies: permeable reactive barriers*, April. EPA-542-R-99-002.

2.0 INTRODUCTION TO CONCEPTS

2.1 Concepts related to corrosion of iron

Metallic iron was manufactured by reaction between the ore and carbonaceous material over four thousand years ago and has been corroding for about the same length of time (Cohen, 1978). Corrosion may be defined as a chemical reaction between a metal and its environment (Jones, 1992, p.4). It actually reflects the tendency of the metal to revert to thermodynamically more stable forms such as those in which it occurs naturally on earth. Thus one of the products of atmospheric corrosion of metallic iron is iron oxide (α-Fe_2O_3) which is a form of iron ore (Snoeyink & Jenkins, 1980).

Corrosion potential and corrosion current density [adapted from Fontana and Greene (1978, pp.313-324)]

Corrosion processes usually involve transfer of electronic charges; they are therefore electrochemical in nature (Jones, 1992, p.5). According to the mixed-potential theory (Wagner and Traud, 1938), any electrochemical reaction can be divided into two or more partial oxidation and reduction reactions. There can be no net accumulation of electrical charge during an electrochemical reaction and thus the total rate of oxidation must equal the total rate of reduction. For example, when an iron electrode is immersed in an aqueous solution such as borate buffer, the two reactions occurring are iron dissolution ($Fe \rightarrow Fe^{2+}+2e^-$) and hydrogen evolution ($2H^++2e^- \rightarrow H_2$) (Figure 2.1). The iron dissolution, defined as the anodic reaction, is an oxidation reaction in which the oxidation state of iron increases, liberating electrons, while hydrogen evolution, the cathodic reaction, is a reduction reaction in which the oxidation state of hydrogen decreases, consuming electrons. The steady state of this system occurs at the intersection between the two

redox systems i.e., at a mixed or corrosion potential E_{corr}. This potential is also known as the open-circuit potential (OCP). At this point, the total rate of oxidation is equal to the total rate of reduction. Because the reaction rate is expressed in terms of current density, the current density corresponding to this point is called the corrosion current density i_{corr}.

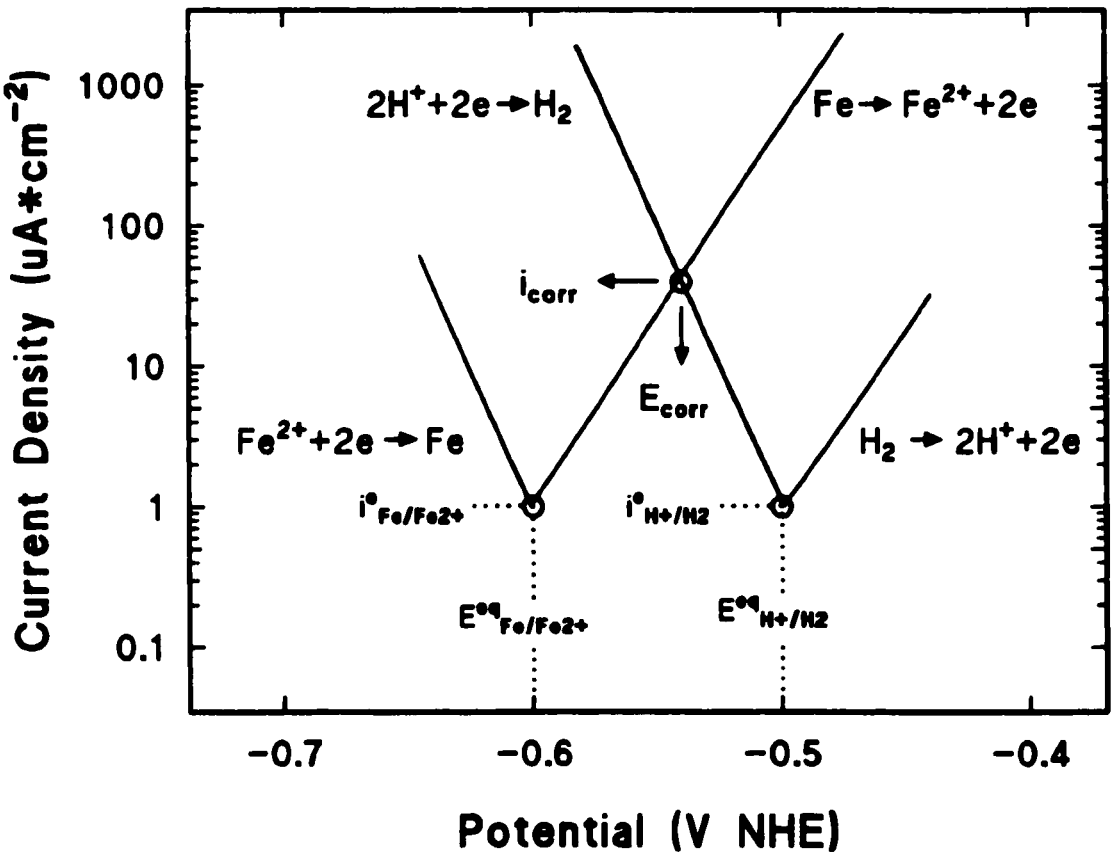


Figure 2. 1 Schematic of behaviour of iron in pH 8.4 borate buffer (adapted from Figure 9.18 in Fontana and Greene, 1978).

The value of the open-circuit or corrosion potential E_{corr} of an iron electrode in an aqueous solution cannot be deduced from the values of the standard electrode potential E° or the equilibrium potential E^{eq} for the Fe/Fe^{2+} or H^{+}/H_2 redox systems. It must however rest between the values for $E^{eq}_{Fe/Fe2+}$ and $E^{eq}_{H+/H2}$.

For example, in the case of an iron electrode immersed in pH 8.4 borate buffer in the presence of 3.4×10^{-6} M of Fe^{2+} ions, a corrosion potential of –0.540 V NHE was measured. In the same solution, the values of $E^{eq}_{Fe/Fe2+}$ and $E^{eq}_{H+/H2}$, calculated using the Nernst equation (Bard and Faulkner, 1980, p.51) where RT/F = 0.02569 V and n = 2:

$$E^{eq}_{Fe/Fe2+} = E^{o}_{Fe/Fe2+} + RT/nF \ln([Fe^{2+}])$$

$$E^{eq}_{H+/H2} = E^{o}_{H+/H2} - 2.3\ RT/F\ pH$$

are -0.602 and -0.496 V NHE, respectively, while the values of $E^{o}_{Fe/Fe2+}$ and $E^{o}_{H+/H2}$, which are constant, are -0.440 and 0 V NHE, respectively. In a similar fashion, the value of the corrosion current density i_{corr} is also different than the exchange current density i_o for the Fe/Fe^{2+} or H^+/H_2 redox systems and again the latter cannot be used to deduce the former.

Oxidizer [adapted from Fontana and Greene (1978, pp.313-324)]

In the example given above, if some ferric salts were added to the borate buffer, three redox systems (Fe/Fe^{2+}, H^+/H_2 and Fe^{3+}/Fe^{2+}) would then be at play (Figure 2.2). The basic principles of the mixed-potential theory also apply to this more complex system. At steady state, the total rate of oxidation must equal the total rate of reduction. The total rate of oxidation follows the iron dissolution rate until $E^{eq}_{H+/H2}$ is reached where it increases because of the addition of hydrogen-oxidation currents and when $E^{eq}_{Fe3+/Fe2+}$ is reached, it increases again due to the addition of ferrous-ion oxidation. Similarly, the total rate of reduction follows the ferric-ion reduction until $E^{eq}_{H+/H2}$ is reached where it increases because of the addition of hydrogen-evolution currents. The point at which the total rates of oxidation and reduction are equal is the mixed or corrosion potential E_{corr} of this system. At this point, the rate of iron dissolution or the

corrosion current density i_{corr} is equal to the summation of the rates of ferric-ion reduction and hydrogen evolution i.e., $i_{corr} = i_{Fe3+/Fe2+} + i_{H+/H2}$.

The presence of the ferric ions resulted in a positive shift of the corrosion potential (from E'_{corr} to E_{corr}), in an increase of the corrosion current density (from i'_{corr} to i_{corr}) and in a decrease of the hydrogen evolution rate (from i'_{corr} to i"). The ferric ions are acting as oxidizers. The effect of an oxidizing agent is dependent on the redox potential of the oxidizer, on its concentration and on its exchange current density on the particular metal.

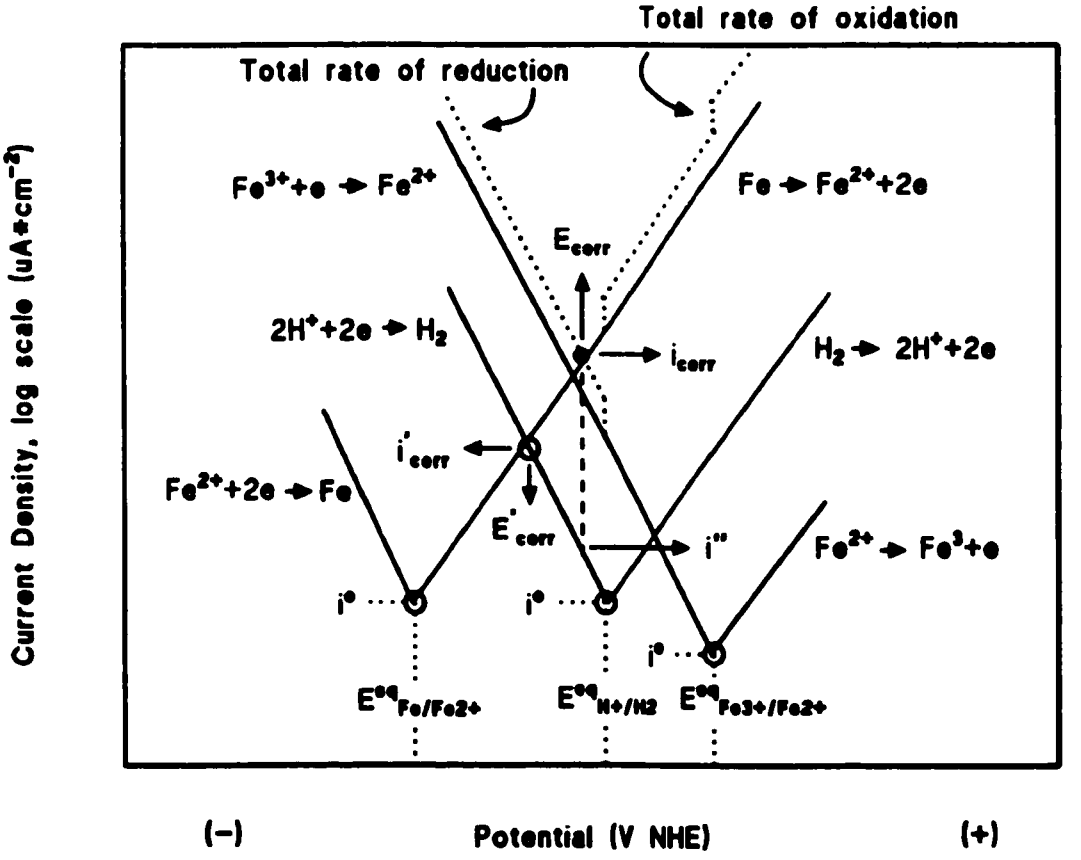


Figure 2. 2 Schematic of behaviour of iron in pH 8.4 borate buffer containing some ferric ions (adapted from Figure 9.19 in Fontana and Greene, 1978).

Passivity [adapted from Fontana and Greene (1978, pp.313-324)]

Iron is considered an active-passive metal. Passivity is a phenomenon observed during the corrosion of certain metals and alloys; it can be defined as a loss of chemical reactivity under certain environmental conditions. This phenomenon was discovered by Keir in 1790, who observed that metallic iron in concentrated nitric acid became suddenly altered (passive) after violent metal dissolution had occurred (active). However, if the iron was scratched with a glass rod, violent metal dissolution recurred (Sato, 1990). From these experiments, one can conclude first that there is a decrease in corrosion rate accompanying the transition from an active to a passive state. Secondly, the passive state is relatively unstable and subject to damage which may result in a transition from the passive to the active state. These characteristics of passivity, with the possibility of using it as a corrosion reduction tool, explain why the subjects of corrosion and passivity have been studied extensively for the last 200 years.

Polarization curve [adapted from Fontana and Greene (1978, pp.313-324)]

The typical behaviour of an active-passive metal such as iron can be illustrated most clearly by a polarization curve, i.e., a current density vs. potential plot (Figure 2.3). As the electrode potential is made more positive than the corrosion potential, the dissolution rate increases exponentially up to a maximum anodic current density corresponding to the primary passive potential E_{pp}. This potential region, between E_{corr} and E_{pp}, is called the active dissolution region. At potentials more positive than E_{pp}, the dissolution rate decreases to a very small value and then remains essentially independent of potential over a considerable potential region. The potential region in which the rate decreases is termed the active-passive transition region, while the region in which the rate is constant is the passive region. At very positive potentials, the dissolution rate again increases

with increasing potential; this region, the transpassive region, corresponds to the destruction of the passive film and the re-activation of the underlying metal. It also corresponds to the onset of oxygen evolution. Finally, at potentials more negative than E_{corr} i.e., in the cathodic region, hydrogen evolution is taking place.

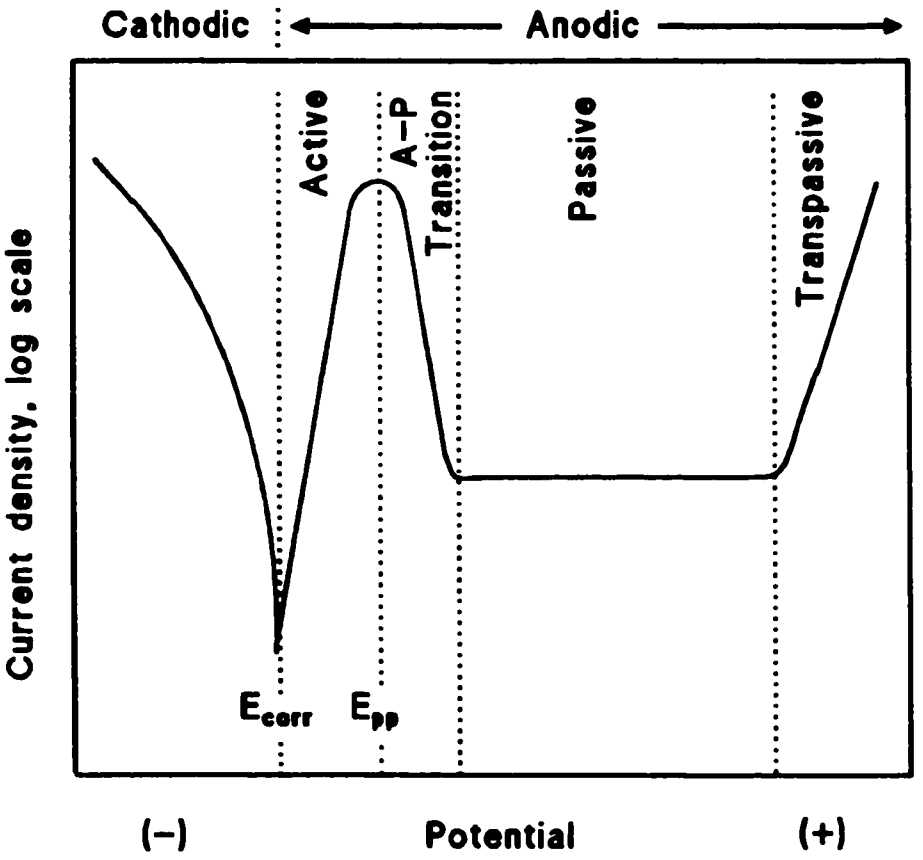


Figure 2. 3 Polarization curve for an active-passive metal such as iron (adapted from Figure 9.24 in Fontana and Greene, 1978).

Potentiostatic vs potentiodynamic procedures [adapted from Jones (1992, pp.122-125)]

Polarization of an active-passive metal such as iron can be performed potentiostatically or potentiodynamically. In potentiostatic procedures, the electrode potential is changed in a step-wise manner and the resulting current response is recorded. (Galvanostatic polarization is also

often performed. In that case, current steps are applied and the potential response is recorded.) During potentiodynamic polarization, the procedure is similar except that the electrode potential is changed continuously instead of step-wise. This allows the automatic recording of a polarization curve. In both procedures, potential is increased in a positive direction (from cathodic to anodic currents). When the reverse sweep is also recorded i.e., from anodic to cathodic currents, a cyclic voltammogram is obtained (Bard & Faulkner, 1980, p.215).

Corrosion rate measurements [adapted from Fontana and Greene (1978, pp.342-345) and Siebert (1985, pp.69-71)]

The mixed-potential theory forms the basis for two electrochemical methods used to determine kinetic paramaters of the charge transfer reactions such as the corrosion current density and the corrosion rate. These are the Tafel extrapolation and the linear polarization techniques.

The Tafel extrapolation method for determining corrosion rate was used by Wagner and Traud (1938) to verify the mixed-potential theory. This technique uses data obtained from cathodic and/or anodic polarization measurements. During cathodic polarization, sufficient current is applied to change the freely corroding potential of an iron electrode in a negative direction from E_{corr}; in anodic polarization, the potential of the electrode is shifted to more positive values. To construct a Tafel plot, the potential of the electrode is plotted against the logarithm of applied current (solid lines on Figure 2.4).

At moderate overpotentials, the cathodic and anodic curves are linear. These regions of linearity are referred to as the Tafel regions. The corrosion potential and the corrosion current density can

be calculated from the intersection between the extrapolations of the two Tafel regions. The corrosion rate is then calculated from the corrosion current density.

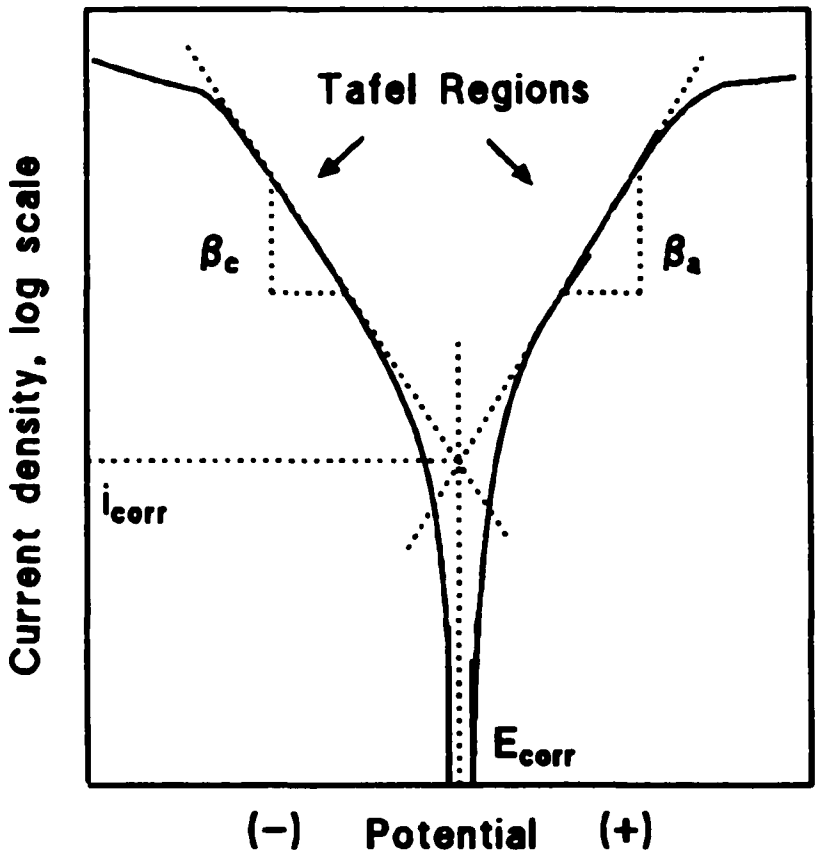


Figure 2. 4 Tafel plot where β_c and β_a represent the cathodic and anodic Tafel slopes, respectively (adapted from Figure 2 in Siebert, 1985).

The main advantages of the Tafel extrapolation technique are that it can be used to measure very low corrosion rates and that it is quick; curves can be generated in an hour or less. There are, however, numerous restrictions. For example, this technique is of limited value where more than one cathodic reaction occurs. It is also often difficult to extrapolate accurately when the Tafel region is not linear over a sufficient potential segment; such is the case when film formation occurs during the anodic polarization of a metal. Finally, since currents in the Tafel region are

one or two orders of magnitude larger on a log scale than the corrosion current, relatively large currents are required to shift the potential from the corrosion potential. The solution must, therefore, be conductive enough such that the IR drop does not significantly obscure the Tafel behaviour. Since the corrosion rate determined by Tafel extrapolation is seldom accurate, the primary use of this technique is to provide a quick check of a given corroding system.

The disadvantages of the Tafel extrapolation method can be overcome by using a linear polarization technique. Within 10 mV more cathodic or more anodic than the corrosion potential, the electrode potential is a linear function of the applied current and the corrosion current density can be calculated from the slope of this line ($\Delta E/\Delta i_{app}$). The corrosion rate is then calculated from the corrosion current density. The linear polarization technique is more versatile and quicker than the Tafel extrapolation method; curves can be generated in minutes. As for the Tafel extrapolation method, the solution must be conductive.

Uncompensated solution resistance [adapted from Mancey (1990, pp. 136-140)]

In any electrochemical technique, the issue of the conductivity of the solution is of importance. The potential of interest is the potential at the electrode/solution interface. However, the potential controlled or measured by a potentiostat is the cell potential. If any part of the current path in the cell, other than the interface, resists the passage of current, then an additional potential drop will occur in the cell, causing the cell potential to differ from the interfacial potential. This additional potential drop is often the result of the solution resistance

The potential drop or IR drop is the product of the current flowing (I) and of the uncompensated solution resistance (R_u), where R_u is the sum of the resistance of the electrode/solution interface and of the solution resistance. Compensation for IR drop can be performed post-factum or on-line (Britz, 1978). In post-factum compensation, the IR effect is measured during the experiment and the IR compensation is achieved by subsequent data manipulation, while in on-line compensation, the cell potential is corrected for the IR effect in real time. In both cases, the value of R_u can be assumed constant for the duration of the experiment or it can be measured at intervals during the course of the experiment. When dealing with a system where film growth can occur on the working electrode, the value of R_u cannot be assumed constant and therefore it has to be measured periodically or continuously. This is why, when performing Tafel plot measurements on iron electrodes, a value for R_u has to be determined at each current pulse increase. Alternatively, when using a linear polarization technique, the potential being within ±10 mV from the corrosion potential, film growth is unlikely to be significant and a value for R_u can be determined prior to the beginning of the experiment and used to program the potentiostat for the subsequent measurements. This last point is only valid however when the measurements are very fast (i.e., 7-10 min.); for longer measurements, the possible formation of a film should be considered.

Diffusion (mass transfer) control vs kinetic (charge transfer) control [adapted from Zembura (1991, pp. 152-179)]

Corrosion processes, like all heterogeneous reactions, proceed through a number of consecutive steps. Reactants reach the reaction surface (mass transfer) to undergo a chemical transformation (charge transfer), then the reaction products leave the reaction surface (mass transfer). The rate

of the overall reaction is limited by the rate of the slowest step: mass transfer and/or charge transfer.

In the case of corrosion of solids in liquids with the formation of soluble products, the transfer of reactants to and from the reaction surface is accomplished in the liquid phase by convection or molecular diffusion. In the bulk of the liquid, the solute is transported by convection. Upon approaching the solid surface, the liquid moves increasingly more slowly in relation to the surface, while the motion, in most cases, ceases at the interface itself. In the liquid layer adjacent to the solid, the transfer of reactants is therefore accomplished by molecular diffusion.

For a rotating disk system, a solution of the convection-diffusion equation for a solute in a liquid at steady state conditions (i.e., $\delta c/\delta t = 0$) has been provided by Levich (1959):

$$j = D\,(dc/dz)_{z=0} = D\,(c^0 - c^l)/\,\delta$$

$$\delta = 1.61 D^{(1/3)} \nu^{(1/6)} \omega^{(-1/2)}$$

where j is the diffusion flux, D is the diffusion coefficient of the reactant, c^0 is its concentration in the bulk of the solution, c^l is concentration at the disk surface, δ is the diffusion layer thickness, ν is the kinematic viscosity, and ω is the angular velocity of the disk. A point to note is that, in a rotating disk system, the thickness of the diffusion layer is a simple function of the angular velocity of the disk.

If the rate of a reaction at the interface is much faster than the rate of reactant transfer, the reaction is said to be controlled by mass transfer, i.e., under diffusion or concentration control.

For such a reaction, $c^1=0$ at the disk surface and the corrosion rate varies linearly with the square root of the angular velocity of the disk (Figure 2.5).

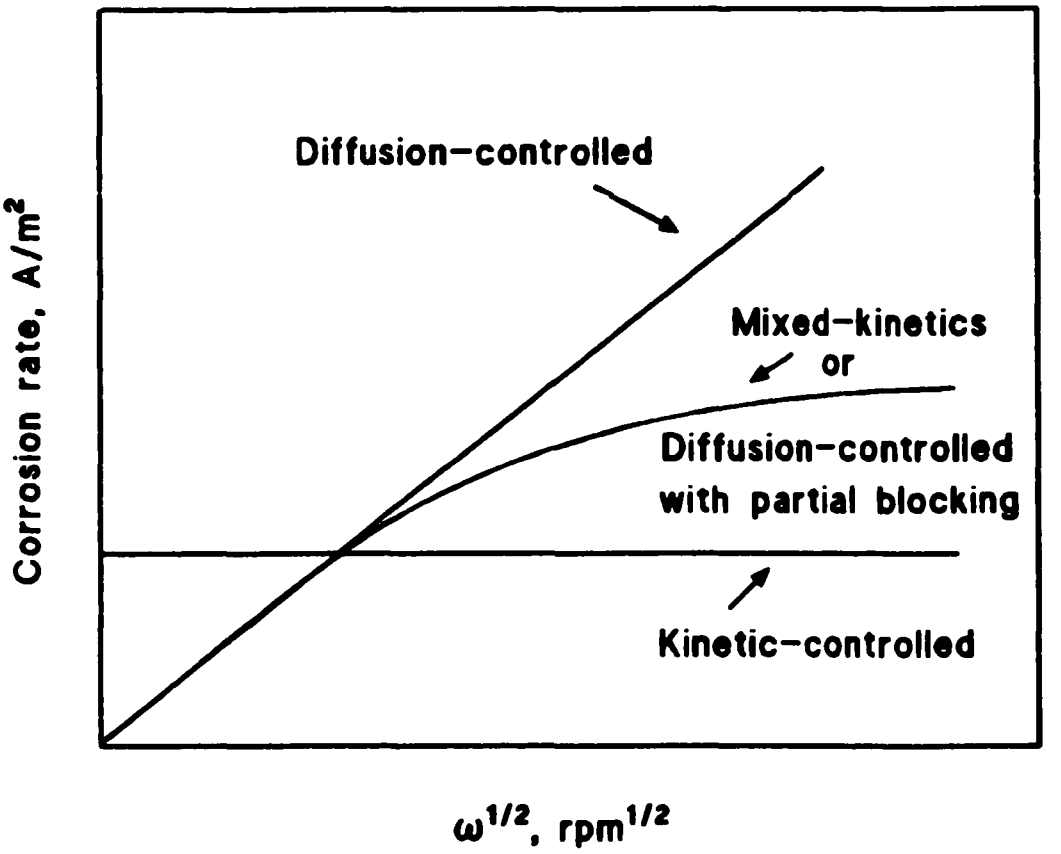


Figure 2. 5 The four types of control of a reaction: diffusion-controlled, kinetic-controlled, mixed-kinetics and diffusion-controlled with partial blocking of active-dissolution sites (adapted from Figure 5.10 in Zembura, 1991).

Alternatively, if the rate of transport greatly exceeds the reaction rate, the reaction is controlled by charge transfer, i.e., under kinetic or activation control. For such a reaction, $c^1 \approx c^0$ on the disk surface and the corrosion rate is independent of the disk speed. In intermediate cases, the reaction occurs in a mixed-kinetics region. Finally, a fourth type of kinetics occurs when a reaction is diffusion-controlled but there is partial blocking of the disk surface by reaction

products; the behaviour is then similar to mixed-kinetics. Such behaviour might also be an artifact due to a large IR drop when dealing with low conductivity solutions.

2.2 Concepts related to surface films on iron

The active-passive behaviour of iron is the result of film formation. The nature of this film is still the subject of extensive research throughout the world. However there is general agreement that the composition and protective properties of this film, in a given aqueous solution, differ from one potential region to another (Gui and Devine, 1991). In alkaline aqueous solutions, the initial stages of iron oxidation result in the formation of Fe/OH_{ads} species with the simultaneous displacement of pre-adsorbed hydrogen (created by cathodic polarization or cleaning procedure) (Burke and Lyons, 1986). In the active dissolution region, the formation of an Fe(II)-rich film is expected, while at potentials more positive than the E_{pp}, the formation of an Fe(III)-rich film is expected. The film formed in the active and active-passive transition region is considered non-protective, while the film formed in the passive region is protective. In the transpassive region, it is the breakdown of this protective film that results in an increase of the iron dissolution rate.

Different models of the passive film on iron have been proposed; these models involve either one or two layers which contain different combinations and arrangements of iron hydroxides, oxides or oxy-hydroxides (Figure 2.6). Early studies by Vetter (1958) and Nagayama and Cohen (1962) pointed to a sandwich of inner Fe_3O_4 / outer γ-Fe_2O_3 as the structure of the passive film (Figure 2.6A).

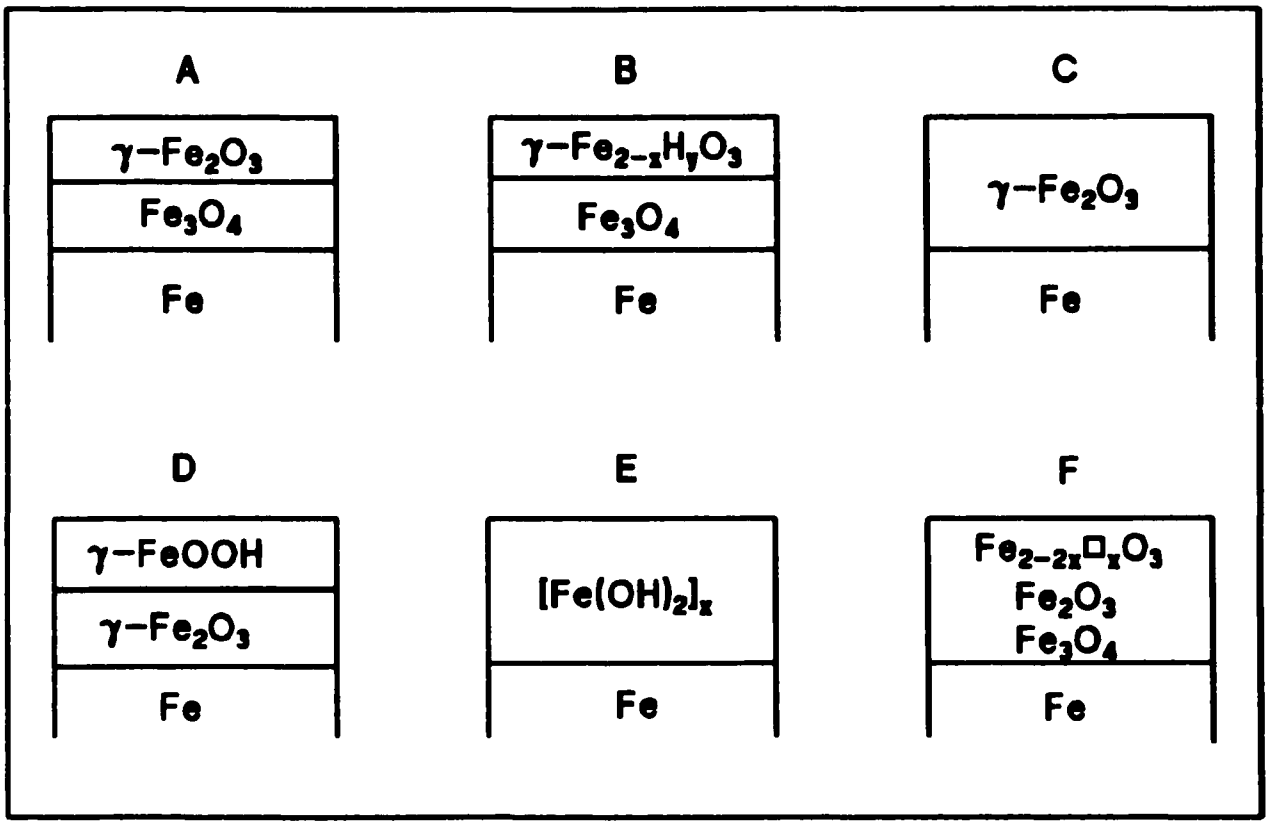


Figure 2. 6 Various proposed structures of passive films (adapted from Figure 6 in Cohen, 1978).

Foley *et al.* (1967) also supported the idea of a bi-layer model. In their case, however, they found that when the potential was in the passive region, γ-Fe_2O_3 was found along with Fe_3O_4 but at lower potentials, Fe_3O_4 and/or oxy-hydroxides were observed. Discrepancies also exist with regards to the electronic properties of the passive film. Depending on the model, the higher valency outer portion of the passive film should be considered an n-type semiconductor (Schultze, 1978), an insulator (Cohen, 1978) or a combination of both, i.e., a chemi-conductor (Chen and Cahan, 1982); the inner Fe_3O_4 is regarded as conductive (Schultze, 1978). Finally, other questions that are still debated relate to the thickness and mechanical properties of the passive film.

Precipitate vs surface film

A precipitate is an insoluble substance produced by a chemical reaction in solution (e.g., the spontaneous formation of magnetite on electrolytic iron particles [Odziemkowski *et al.*, 1998]). "Surface film" is a broader term; it includes precipitates, adsorbed species and films formed by other mechanisms than precipitation (e.g., the native film on commercial iron materials which is formed by a very specific mechanism of high temperature oxidation [Odziemkowski and Gillham, 1997]).

Ex situ vs *in situ* techniques

The current pictures of the film formed on iron result from the use of a variety of electrochemical and non-electrochemical techniques, both *ex situ* and *in situ*. There is however evidence that *ex situ* techniques deal with an altered or decomposed film (Uhlig, 1978). In fact, the problem with ex situ techniques is that potential and/or environmental control is lost in order to study a sample (Chen and Cahan, 1982). For example, in the use of electron microscopy to study the passive film on iron, one must open the circuit (losing potential control), wash and dry the electrode (losing control of pH, etc.,), put the sample in a vacuum environment (losing control of O_2 pressure), and bombard the sample with electrons (which are highly reducing and heat the specimen). Even if exposure to vacuum and heating by electrons did not change the passive film structurally, recent *in situ* studies by Mössbauer spectroscopy and EXAFS have revealed that removal from aqueous solution and the change or elimination of potential control have changed the composition of the passive film by eliminating some hydrogen-containing species (Kruger, 1989). Finally, according to Gui and Devine (1991), the validity of ex situ techniques is even

more in question when dealing with films formed in the active and active-passive transition regions.

Raman Spectroscopy

An important advantage of Raman spectroscopy over other methods of surface analysis is its ability to analyze samples in aqueous solutions *in situ*. Raman spectra are obtained by irradiating a sample with a powerful laser source of monochromatic radiation. During irradiation, most of the radiation will be transmitted without change but, in addition, some inelastic scattering of the radiation will occur (Long, 1977). The scattering of radiation without change of frequency (or wavenumber) is called Rayleigh scattering while the scattering of radiation with change of frequency is called Raman scattering. When the radiation is scattered to lower frequencies (i.e., the irradiated molecules gain energy), Stokes Raman bands arise; when the radiation is scattered to higher frequencies (i.e., the irradiated molecules lose energy), anti-Stokes Raman bands are produced. Anti-Stokes bands are usually less intense than the corresponding Stokes bands. For this reason, the Stokes part of a spectrum is generally used.

The normal Raman effect is defined as weak because the intensity of Rayleigh scattering is generally a thousandth of the intensity of the exciting radiation and the intensity of strong Raman bands is generally about a thousandth of the intensity of Rayleigh scattering (Long, 1977). Typically, a measurable intensity of Raman scattering will occur only if a sufficiently high flux of photons is incident on the sample and if a large number of scattering entities are present. The latter requirement explains why it is nearly impossible to detect Raman scattering from a very thin film (Gui and Devine, 1991). Raman scattering from submonolayer quantities of material

adsorbed on silver electrodes immersed in aqueous solutions has, however, been detected by surface enhanced Raman spectroscopy (SERS). It has to be noted that, for normal as well as for surface enhanced Raman spectroscopy, the development of more sensitive detectors in the last decade has enabled thinner films to be studied with more accuracy. Research projects related to iron have benefited from such developments. For example, in the work by Schuhmacher (1995) performed using a Dilor OMARS-89 spectrometer, normal Raman spectroscopy (NRS) did not reveal the existence of any surface film on an iron electrode held at OCP for 17 hours in deaerated pH 10 KBr solution ($Fe(OH)_2$ and magnetite were however detected by SERS), while in the present study, performed with a Renishaw 1000 system, green rust and α-FeOOH were detected by NRS on an iron electrode under the same conditions.

The difference in frequency between the exciting radiation and Raman bands is independent of the wavelength of the exciting radiation and characteristic of the vibrational (or rotational) energy change of the sample molecules. Vibrational spectra of samples in solutions often consist of broad and overlapped bands as a result of collisional broadening and near concurrent frequencies (Semmler, 1989). In order to interpret and quantify these spectra, one has to manipulate the data by mathematical techniques. Examples of data treatments include baseline correction (where a baseline is fitted to a spectrum before any other data treatment), smoothing (where the noise is removed) and band fitting (where overlapped bands in composite profiles are resolved).

Raman spectroscopy will not differentiate between the inner and outer layer of the film (Melendres *et al.*, 1992). However, because of the high penetration depth of the Raman laser

beam, it is possible to obtain spectra from the inner and outer portion of the film simultaneously. The laser penetration depth can be estimated by a procedure described by Dünnwald and Otto (1989). The penetration depth of light, d, is a function of the imaginary part, k, of the complex refractive index, $n + ik$, of the surface film. It is defined as $d = \lambda/2k$, where λ is the wavelength of light in vacuum. For an energy of 1.96 eV, a k value of $\approx$0.5 was measured for natural Fe_3O_4 (Buchenau and Müller, 1972), while a k value of $\approx$0.3 was found for the passive film on Fe in pH 8.4 borate buffer (Azumi et al., 1986). Using a 632.8 nm wavelength laser (corresponding to 1.96 eV), the laser penetration depth for Fe_3O_4 and the passive film would therefore be 632.8 and 1055 nm, respectively.

2.3 References

Azumi, K., T. Ohtsuka and N. Sato. (1986). *Spectroscopic photoreponse of the passive film formed on iron.* J. Electrochem. Soc., Vol. 33, No. 7, pp. 1326-1328.

Bard, A. J. and L.R. Faulkner. (1980). *Electrochemical methods. Fundamentals and applications.* John Wiley & Sons Inc., New York, pp. 51 and 215.

Britz, D. (1978). *IR elimination in electrochemical cells.* J. Electroanal. Chem., Vol. 88, pp.309-352.

Buchenau, U. and I. Müller. (1972). *Optical properties of magnetite.* Sol. State Commun., Vol. 11, pp. 1291-1293.

Burke, L.D. and M.E.G. Lyons. (1986). *The formation and stability of hydrous oxide films on iron under potential cycling conditions in aqueous solution at high pH.* J. Electroanal. Chem., Vol. 198, pp.347-368.

Chen, C.T. and B.D. Cahan. (1982). *The nature of the passive film on iron. I. Automatic ellipsometric spectroscopy studies. II. A-C impedance studies. III. The chemi-conductor model and further supporting evidence.* J. Electrochem. Soc., Vol. 129, pp. 17-26 (I); 474-480 (II); 921-925 (III).

Cohen, M. (1978). *The passivity and breakdown of passivity on iron.* Passivity of metals, R.P. Frankenthal and J. Kruger (Eds.), The Electrochemical Society, Pennington, New Jersey, pp. 521-545.

Dünnwald, J. and A. Otto. (1989). *An investigation of phase transitions in rust layers using Raman spectroscopy.* Corrosion Science, Vol. 29, No. 9, pp. 1167-1176.

Foley, C.L., J. Kruger and C.J. Bechtoldt. (1967). J. Electrochem. Soc., Vol. 114, p. 944.

Fontana, M.G. and N.D. Greene. (1978). *Corrosion engineering.* 2nd ed., McGraw-Hill Inc., New York, pp. 313-324 and 342-345.

Gui, J. and T.M. Devine. (1991). *In situ vibrational spectra of the passive film on iron in buffered borate solution.* Corrosion Science, Vol. 32, No. 10, pp. 1105-1124.

Jones, D.A. (1992). *Principles and prevention of corrosion.* Macmillan Pub. Co., New York, pp. 4-5 and 122-125.

Keir, J. (1790). Phil. Trans., Vol. 80, p.359.

Kruger, J. (1989). *The nature of the passive film on iron and ferrous alloys.* Corrosion Science, Vol. 29, No. 2/3, pp.149-162.

Levich, V.G. (1959). *Physical hydrodynamics.* Nauka, Moskva (in Russian).

Long, D.A. (1977). *Raman spectroscopy.* Mc-Graw-Hill Inc., New York, pp. 1-13.

Mancey, D.S. (1990). *The dissolution of iron and magnetite.* Ph.D. Thesis, University of Guelph, Guelph, Ontario, pp. 136-140.

Melendres, C.A., M. Pankuch, Y.S. Li and R.L. Knight. (1992). *Surface enhanced Raman spectroelectrochemical studies of the corrosion films on iron and chromium in aqueous solution environments.* Electrochim. Acta, Vol. 37, No. 15, pp.2747-2754.

Nagayama, M. and M. Cohen. (1962). *The anodic oxidation of iron in neutral solution.* J. Electrochem. Soc., Vol. 109, pp. 781-790.

Odziemkowski, M.S., T.T. Schuhmacher, R.W. Gillham and E.J. Reardon. (1998). *Mechanism of oxide film formation on iron in simulating groundwater solutions: Raman spectroscopic studies.* Corrosion Science, Vol. 40, No. 2/3, pp. 371-389.

Odziemkowski, M.S. and R.W. Gillham. (1997). *Surface redox reactions on commercial grade granular iron (steel) and their influence on the reductive dechlorination of solvent. Micro Raman spectroscopic studies.* 213th ACS National Meeting, San Francisco, CA. Extended Abstracts, Division of Environmental Chemistry, Vol. 37, No. 1, pp. 177-180.

Sato, N. (1990). *An overview on the passivity of metals.* Corrosion Science, Vol. 31, pp. 1-19.

Schuhmacher, T.T. (1995). *Identification of precipitates formed on zero-valent iron in anaerobic aqueous solutions.* M.Sc. Thesis, University of Waterloo, Waterloo, Ontario, pp. 34-43.

Schultze, J.W. (1978). *Electron transfer reactions on passive films.* Passivity of metals, R.P. Frankenthal and J. Kruger (Eds.), The Electrochemical Society, Pennington, New Jersey, pp. 82-101.

Semmler, J. (1989). *Raman spectral studies of organic electrolytes at elevated temperatures and pressures.* Ph.D. Thesis, University of Waterloo, Waterloo, Ontario, pp. 14-24 and 45-64.

Siebert, O.W. (1985). *Laboratory electrochemical test methods.* Laboratory corrosion tests and standards, G.S. Haynes and R. Baboian (Eds.), ASTM STP 866, Philadelphia, pp.69-71.

Snoeyink, V.L. and D. Jenkins. (1980). *Water Chemistry*. John Wiley & Sons Inc., New York, p.363.

Uhlig, H.H. (1978). *History of passivity, experiments and theories.* Passivity of metals, R.P. Frankenthal and J. Kruger (Eds.), The Electrochemical Society, Pennington, New Jersey, pp. 1-28.

Vetter, K.S. (1958). Z. Electrochem., Vol. 62, p.642.

Wagner, C. and W. Traud. (1938). Z. Electrochem. Vol. 44, p. 391.

Zembura, Z. (1991). *Rotating disk studies in the transport of reactants during corrosion of copper, iron, and zinc with hydrogen and oxygen depolarization.* Corrosion of metals and hydrogen-related phenomena, J. Flis (Ed.), Elsevier Science Publishing Co. Inc., New York, pp. 152-179.

3.0 INFLUENCE OF CHLORINATED SOLVENTS ON POLARIZATION AND CORROSION BEHAVIOUR OF IRON IN BORATE BUFFER

The following paper, as published in the journal Corrosion Science (*Corrosion Science*, **40**, pp. 1391-1409, 1998), covers the results of the potentiodymanic polarization, OCP-time and *in situ* Raman spectroscopy measurements performed in borate buffer.

Following publication of the paper, the authors were made aware of the convention according to which Tafel slopes are to be expressed as absolute values. Therefore, the "decrease of the cathodic Tafel slope (from –180 to –280 mV/decade)" reported on p.42 should be replaced by "an increase of the cathodic Tafel slope (from 180 to 280 mV/decade)".

3.1 Cover page

INFLUENCE OF CHLORINATED SOLVENTS ON POLARIZATION AND CORROSION BEHAVIOUR OF IRON IN BORATE BUFFER

PASCALE M. L. BONIN, MAREK S. ODZIEMKOWSKI and ROBERT W. GILLHAM

Department of Earth Sciences, University of Waterloo,
Waterloo, Ontario, Canada N2L 3G1

Abstract - A new remediation technology for groundwater contaminated with chlorinated solvents is through contact with granular iron. To refine our understanding of the reaction mechanism, electrochemical and spectroscopic measurements were performed on iron electrodes in deaerated borate buffer containing an amount of a degradable (carbon tetrachloride) or non-degradable (dichloromethane) compound. The results of polarization measurements indicated that carbon tetrachloride acts as an oxidizer towards iron while dichloromethane is nonreactive. Magnetite and hydrated magnetite, identified by Raman spectroscopy, are the final products of the surface redox reactions. Based on electrochemical and spectral evidence, a new conceptual model for the reductive reactions is proposed.

Keywords: A. iron, borate, chlorinated solvents, iron oxides, B. Raman spectroscopy.

3.2 Introduction

Chlorinated solvents such as tetrachloroethene, trichloroethene and carbon tetrachloride are some of the most important groundwater contaminants in North America [1]. These compounds are said to be persistent in the subsurface environment because they do not transform at appreciable rates under most natural biological or abiotic conditions [1].

Several studies have examined ways of enhancing the degradation rates of chlorinated solvents [2-6]. Using granular iron and a wide range of dissolved chlorinated organic compounds, Gillham and O'Hannesin [7] reported half-lives that are 5 to 15 orders of magnitude lower than those reported for natural rates of abiotic degradation. Their work originated from the results of a study on sampling bias caused by materials used to monitor halocarbons in groundwater, in which it was found that galvanized metallic surfaces have the potential to transform polyhalogenated hydrocarbons [8]. Gillham and O'Hannesin [9] confirmed the results of that study and extended the work to include other metals such as iron, zinc, aluminium, brass, copper and stainless steel. Higher degradation rates were obtained with iron and zinc. Because of its lower cost and toxicity, the use of granular iron in groundwater remediation systems, consisting of above- ground reactors or *in situ* permeable reaction walls, was proposed [9]. Several field demonstrations of the technology are now in progress [10-11].

The degradation of chlorinated solvents by iron is a charge transfer process involving oxidation of iron, dissociation of water and reductive dechlorination of the organic compounds according to the following equations [7]:

$$2Fe^0 \rightarrow 2Fe^{2+} + 4e^- \quad (1)$$

$$3H_2O \rightarrow 3H^+ + 3OH^- \quad (2)$$

$$2H^+ + 2e^- \rightarrow H_2 \quad (3)$$

$$X\text{-}Cl + H^+ + 2e^- \rightarrow X\text{-}H + Cl^- \quad (4)$$

Matheson and Tratnyek [12] proposed 3 possible mechanisms for the reductive dehalogenation of chlorinated solvents by iron in aqueous systems: (A) direct electron transfer from iron metal at the metal surface; (B) reduction by Fe^{2+}; (C) catalysed hydrogenolysis by H_2. Acknowledging the fact that the degradation reactions involve charge transfer at the iron/solution interface, the present study was initiated to refine our understanding of the mechanism of the reductive dehalogenation of chlorinated solvents in the presence of iron. The influence of the organic molecules on the polarization and corrosion behaviour of iron, as well as their effect on the structure of the iron/solution interface, was investigated by means of electrochemical and spectral measurements. Potentiodynamic polarization, open circuit potential-time and *in situ* Raman measurements were performed on iron electrodes in deaerated borate buffer to which an amount of a degradable compound (carbon tetrachloride-CCl_4) or non-degradable compound (dichloromethane-CH_2Cl_2) [7] was added.

Borate solution was chosen because of its buffering capacity. The selected ratio of borate to boric acid resulted in a solution pH of 8.4, which is typical of many natural groundwaters [7]. The choice of the borate buffer was also based on the fact that the iron/borate interface has been extensively studied by many electrochemical techniques [13-15] and *in situ* spectroelectrochemical techniques such as Raman spectroscopy [16-19], ellipsometry [20-22] and x-ray adsorption near edge spectroscopy (XANES) [23-25], thus creating an extensive literature background for our study.

3.3 Experimental methods

In all experiments, the working electrode was a disk of polycrystalline iron (99.99% purity) pressed into a Kel-F holder. For the polarization measurements, the iron disk had a diameter of 2 mm. For the open circuit potential-time and Raman measurements, the diameter was 5 mm. The auxiliary electrode was platinum. Potentials were measured against a Ag/AgCl electrode and then converted to NHE. Prior to each experiment, the iron electrode was polished with 1200 grade SiC emery paper, washed in copious amounts of distilled water, and ultrasonically cleaned. The iron electrode was then immersed in deaerated borate buffer and cathodically cleaned for 900 s. The 0.0357M $Na_2B_4O_7$ + 0.15M H_3BO_3 solution, prepared from distilled water, had a pH of 8.4 and a redox potential *Eh*, after deaeration, of 0.3 V NHE.

Potentiodynamic polarization measurements were carried out on a stationary iron electrode using a Model 273 PAR potentiostat /galvanostat, interfaced to a DEC PRO-380 series personal computer via an IEEE-488 interface. Software written in house was used for data acquisition and potentiostat control. Forward and reverse potential sweeps were performed at a rate of 1 mV/s over two ranges of potential: from -0.8 to +1.2 V NHE, and from -0.7 to +1.3 V NHE.

The open circuit potential of the iron electrode was monitored over time using a high impedance (10^{14} ohms) preamplifier. The use of such a preamplifier was required to prevent current flow between the working and the reference electrodes. The high impedance unit was connected to a UPC601-U Universal PC Sensor Interface Card transmitting data to a DTK Corp. 386 computer. The data were recorded at rates of 4 to 60 points/minute. The measurements were repeated at least twice. The data were reproducible within 2%.

In situ Raman spectra were obtained with a Renishaw 1000 Raman microscope system. The instrument consists of an Olympus microscope, a single spectrograph fitted with holographic notch filters for spectroscopy mode, and a Peltier-cooled CCD detector. The optical efficiency of the instrument is high (≥30%), as is its sensitivity. The detection of a very weak signal (1 photon/s) is therefore possible [26]. Excitation was achieved using the 632.8 nm line of a Melles Griot 35mW HeNe laser. All Raman measurements were carried out using backscattering geometry. The long working-length objective lens used in the spectral studies has an objective magnification 50 (OLYMPUS IC50/MSPLAN 50, ∞/0 f = 180, NA = 0.55). It allows the study of a spot size of 2 μm with a confocal depth of field of 3 μm. The laser was operated at its maximum power of 35 mW; this translates to ca. 3 mW at the sample surface. Such low light intensity is unlikely to alter the surface film composition, particularly for *in - situ* measurements. In contrast to our previous work [27], the high sensitivity of the Renishaw 1000 Raman system permits the iron electrode to be located further away from the optical window (ca. 5 mm) allowing the Luggin capillary to be placed 2-3 mm from the electrode. A previously-designed three-electrode spectroelectrochemical cell [28] was modified to accommodate an injection port.

The chlorinated solvent (pure phase CCl_4 or CH_2Cl_2) was injected directly into the aqueous solution through a Teflon septum; 0.2 mL of solvent was injected in the electrochemical cell filled with 300 mL of borate solution while 17 μL was injected into the 25 mL Raman cell (resulting in a ratio of 0.7 μL of solvent per mL of solution in both cells). In the electrochemical cell, deaeration with N_2 was performed in and above the solution prior to the solvent injection, and above the solution after the injection of the solvent. The solution was continuously stirred using a Teflon stir bar. Since there was no headspace in the Raman cell, deaeration stopped once

the cell was filled with deaerated solution. Prior to the introduction of the solution, the cell had been purged with N_2. No stirring was performed.

The pure phase chlorinated solvents that were injected did not dissolve entirely. In addition, the solvents being volatile, the aqueous concentrations decreased over time. Dissolved aqueous concentrations, averaged over the duration of an experiment, are therefore reported. Organic analyses were performed, via a pentane extraction procedure, using a Hewlett Packard 5710A gas chromatograph. The chromatograph was equipped with a ^{63}Ni electron capture detector (ECD) and a glass column packed with 10% squalane on chromasorb P,AW-DMCS (80/100 mesh). The carrier gas was a mixture of 95% argon and 5% methane, with a flow rate of 20 mL/min. Analyses were performed on samples collected during the polarization experiments. No samples were collected during the open circuit potential-time and Raman measurements.

3.4 Results

3.4.1 Potentiodynamic polarization measurements in borate buffer

The anodic polarization of the electrode immersed in solvent-free deaerated borate buffer resulted in a typical anodic polarization curve for an active-passive metal such as iron [29,30] (Figure 3.1 - where only the forward sweep has been plotted). A corrosion potential E_{corr} of -0.53 V NHE was observed while the maximum anodic current density, corresponding to the primary passive potential E_{pp}, occurred at -0.34 V NHE. This is in accord with Rubim and Dunnwald [18] (sweeping rate of 10 mV/s) and Kerkar *et al.* [31] (unspecified rate). Other studies have reported a value of -0.36 V NHE for E_{pp} (sweeping rates of 16-60 mV/s) [20,21,32].

Based on free energy thermodynamic considerations, CCl_4 and CH_2Cl_2 should act as oxidizers of an iron electrode, and by doing so should undergo reductive dechlorination, since their relative half-reaction reduction potentials are +2.2 and +1.0 V NHE, respectively [1]. According to the mixed-potential theory [33], the addition of an oxidizer to a solvent-free solution should result in a positive shift of the corrosion potential, an increase of the corrosion rate as well as a decrease of the overpotential of the cathodic reactions [34] (which is expressed by a decrease of the cathodic Tafel slope [35]). The magnitude of these effects is a function of the redox potential of the oxidizer and its concentration [34].

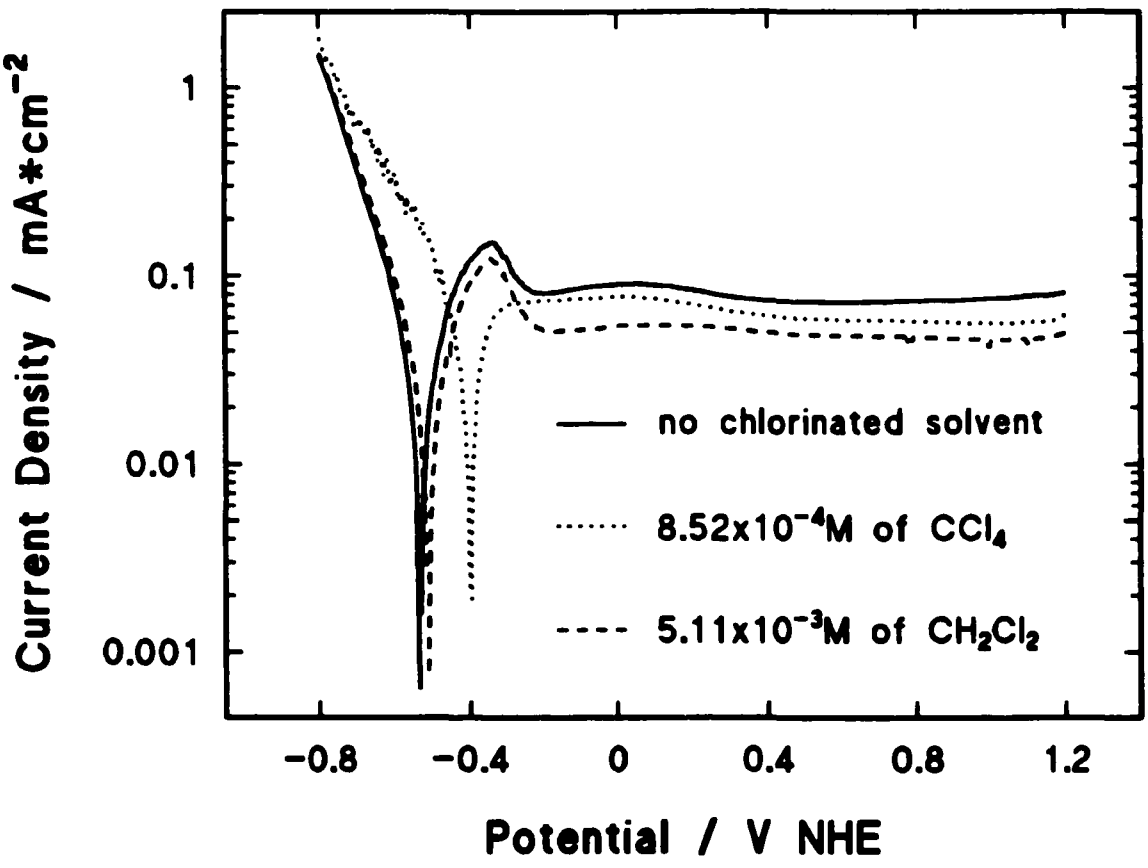


Figure 3. 1 Potentiodynamic polarization curves in solvent-free borate buffer, in the presence of $8.52x10^{-4}$M of CCl_4 and in the presence of $5.11x10^{-3}$M of CH_2Cl_2. Sweep rate (dE/dt) was 1 mV/s.

As shown on Figure 3.1, the polarization of the iron electrode in a borate buffer to which CCl_4 had been added (resulting in an average aqueous concentration of 8.52×10^{-4}M) indicated that CCl_4 indeed acts as an oxidizer (i.e., anodic inhibitor) of the iron electrode. In the presence of CCl_4, there is a positive shift of the corrosion potential (from -0.53 to -0.4 V), an increase in the corrosion current density i_o (from 0.04 to 0.06 mA/cm^2) and a decrease of the cathodic Tafel slope (from –180 to –280 mV/decade). This is accompanied by the disappearance of the active/passive transition region indicating that the iron electrode goes directly from an active dissolution state to a passivated state during its polarization. Finally, in the passive region, the anodic currents are lower than in solvent-free borate buffer.

When the experiment was performed in a solution to which CH_2Cl_2, the non-degradable compound, had been added (resulting in an average aqueous concentration of 5.11×10^{-3}M), the cathodic Tafel slope is unchanged, there is no visible increase in corrosion current density and the shift of the corrosion potential is insignificant. The main effect of CH_2Cl_2 appears in the passive region where the currents were lower than in solvent-free borate buffer, most probably due to adsorption of CH_2Cl_2 on the electrode surface.

Due to volatilization in the headspace above the solution, the concentration of solvent in solution decreased with time. To evaluate the effect of the concentration of CCl_4 or CH_2Cl_2 on the polarization behaviour of iron, some experiments were performed where there was a delay between the injection of the solvent and the beginning of the sweeping. The electrode was not in solution during this delay. As expected, the longer delays resulted in higher volatilization losses i.e., in smaller aqueous concentrations of solvent, which had a lesser influence on the

polarization behaviour of iron. This is shown on Figure 3.2, where for a smaller concentration of CCl_4 ($2.02x10^{-4}$M instead of $8.52x10^{-4}$M after an overnight delay), the changes in corrosion potential and cathodic slope were smaller and there was no visible increase in the corrosion current density. The influence of the aqueous concentration of CH_2Cl_2 ($5.89x10^{-4}$M instead of $5.11x10^{-3}$M after a few hours delay), on the polarization behaviour of iron can be seen in Figure 3.3. Again the main effect lies in the passive region where the anodic currents vary inversely with the CH_2Cl_2 aqueous concentration.

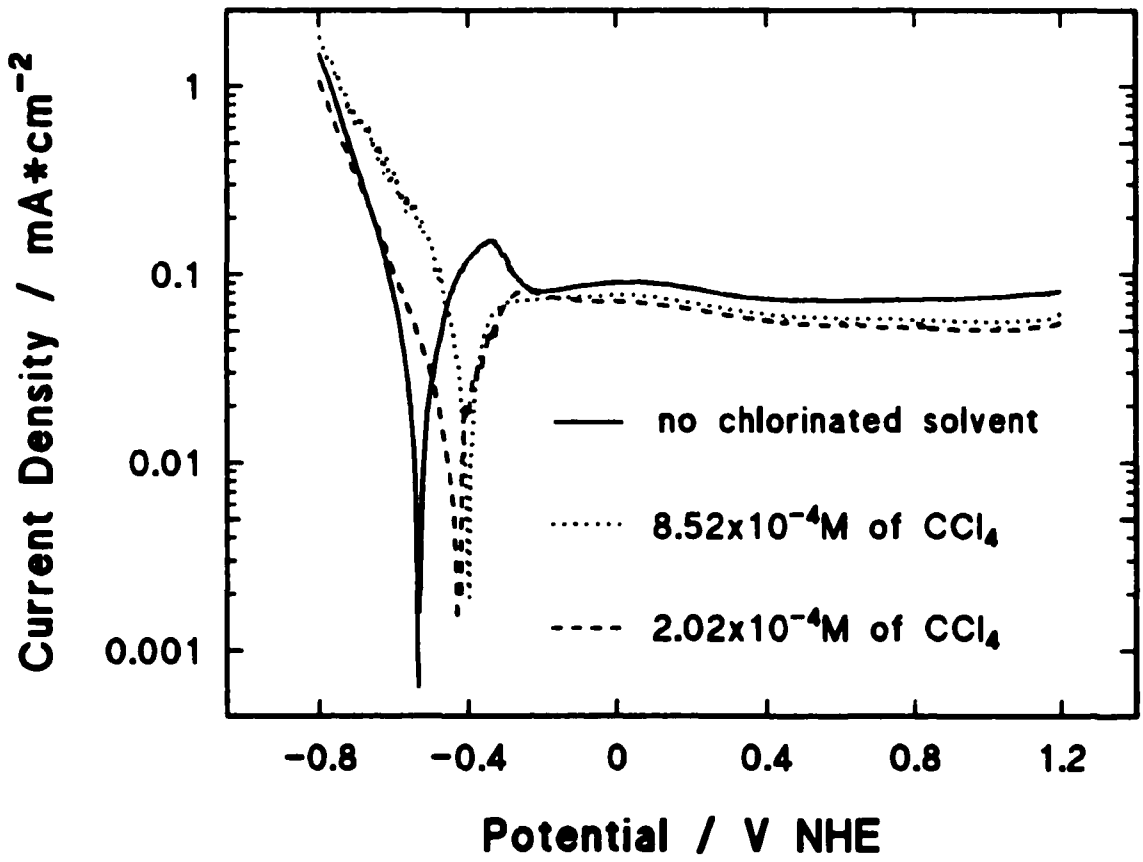


Figure 3. 2 Influence of CCl_4 concentration. Potentiodynamic polarization curves in borate buffer in the presence of $2.02x10^{-4}$M and $8.52x10^{-4}$M of CCl_4. Sweep rate (dE/dt) was 1 mV/s.

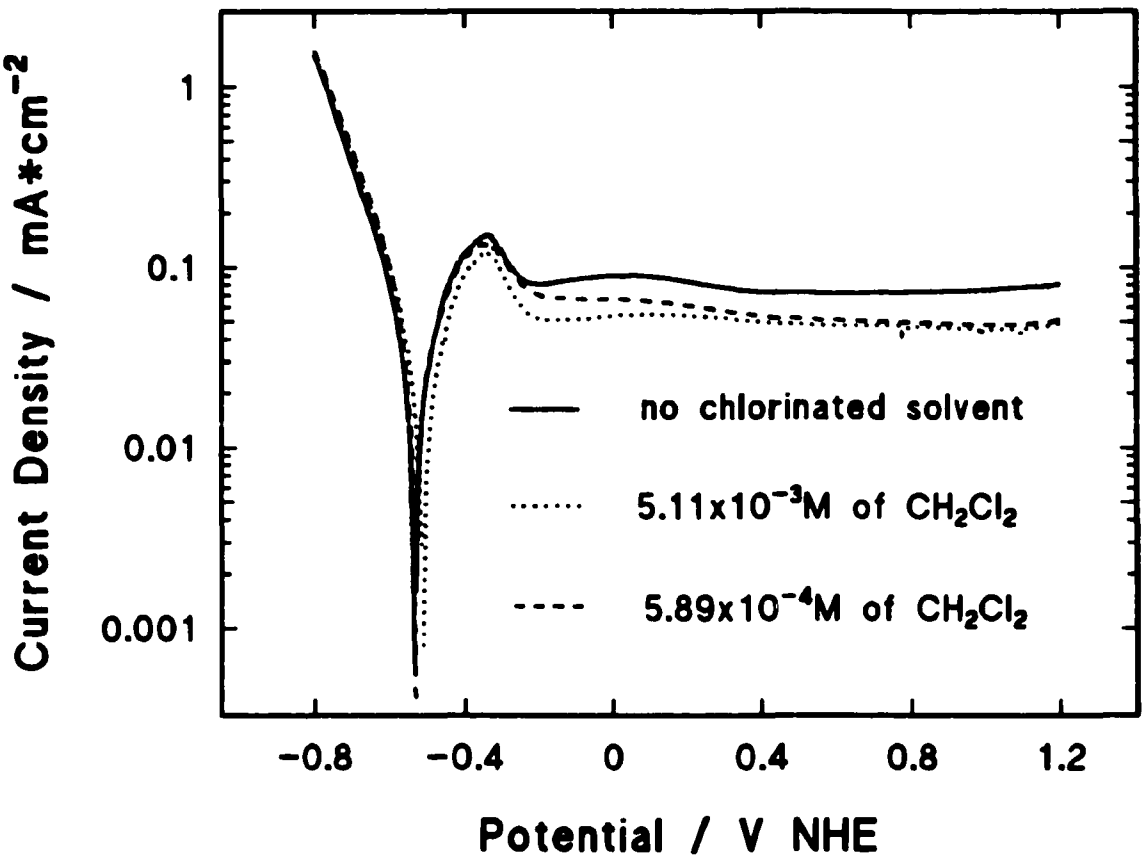


Figure 3. 3 Influence of CH_2Cl_2 concentration. Potentiodynamic polarization curves in borate buffer in the presence of 5.89×10^{-4}M and 5.11×10^{-3}M of CH_2Cl_2. Sweep rate (dE/dt) was 1 mV/s.

By plotting the potentiodynamic polarization curve in the form of a cyclic voltammogram (CV), a peak can be observed at the end of the reverse sweep performed in the solution containing 8.52×10^{-4}M of CCl_4 (Figure 3.4). This cathodic peak could be due to desorption of solvent or dissolution of surface films. The fact that the peak was not observed in the presence of CH_2Cl_2, which did not have a significant influence on the polarization of iron but nevertheless adsorbed on the surface of the electrode in the passive region, suggests that this peak be attributed to the reduction of surface films. To verify this hypothesis, two additional sets of experiments were performed. In the first set, the CV of an Fe electrode immersed in borate buffer spiked with CCl_4 was measured over a potential range of -0.8 to -0.53 V (E_{corr} in solvent-free borate buffer), and

no cathodic peak or hysteresis was observed. For the second set, the upper potential limit was -0.4 V, which corresponds to E_{corr} in borate buffer containing 8.52×10^{-4}M of CCl_4. In this case, at a more positive potential, film formation should be expected and the cathodic reduction of this film resulted in the appearance of the cathodic reduction peak and hysteresis.

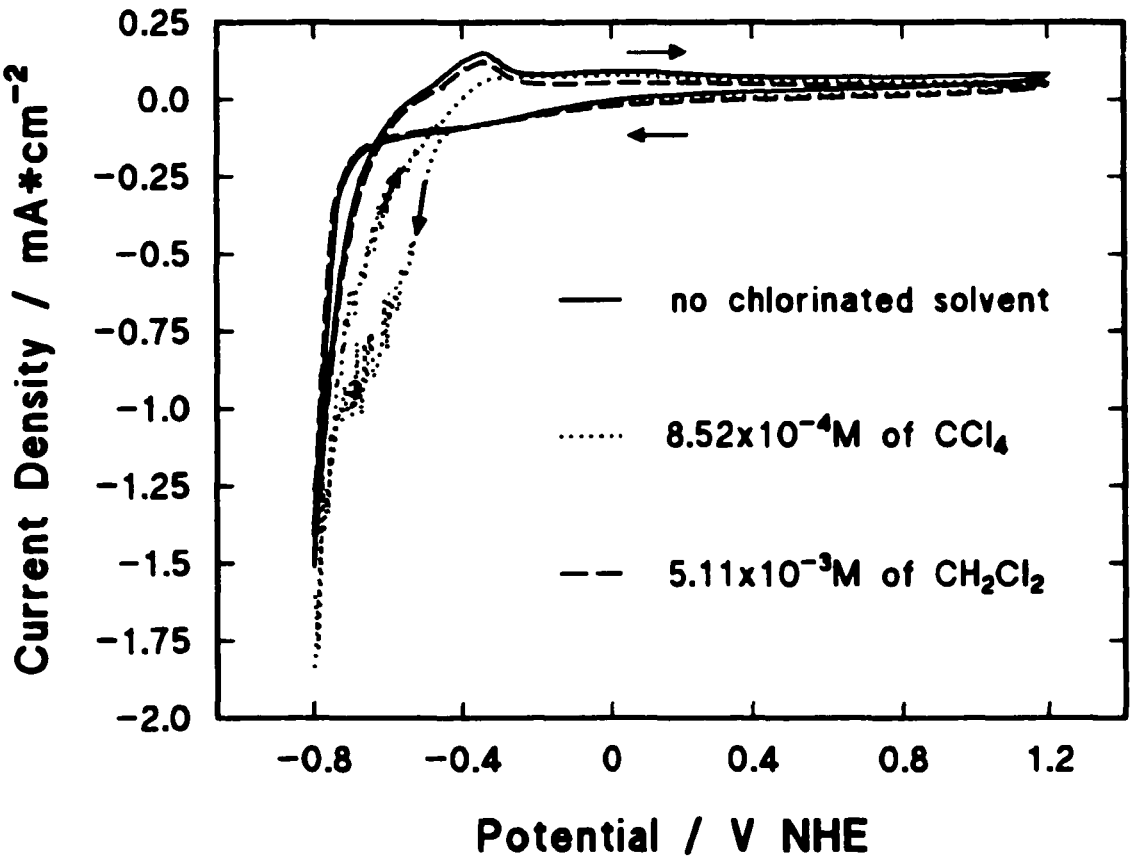


Figure 3. 4 Cyclic voltammogram of Fe in solvent-free borate buffer, in the presence of 8.52×10^{-4} M of CCl_4 and in the presence of 5.11×10^{-3}M of CH_2Cl_2. Sweep rate (dE/dt) was 1 mV/s.

Based on the results of the potentiodynamic polarization experiments performed over a range of -0.7 to + 1.3 V NHE, it appears that both solvents (CCl_4 and CH_2Cl_2) do not have a significant influence on the polarization behaviour of the iron electrode in the transpassive region. These

experiments confirmed that these solvents are more susceptible to degradation by reduction than oxidation, as expected based on their relative half-reaction reduction potentials [1].

3.4.2 Open circuit potential-time measurements in borate buffer

The change of the open circuit potential of an iron electrode, freshly cathodically cleaned or kept immersed in borate buffer for a given time. was monitored over time following the injection of CCl_4 or CH_2Cl_2 (Figure 3.5).

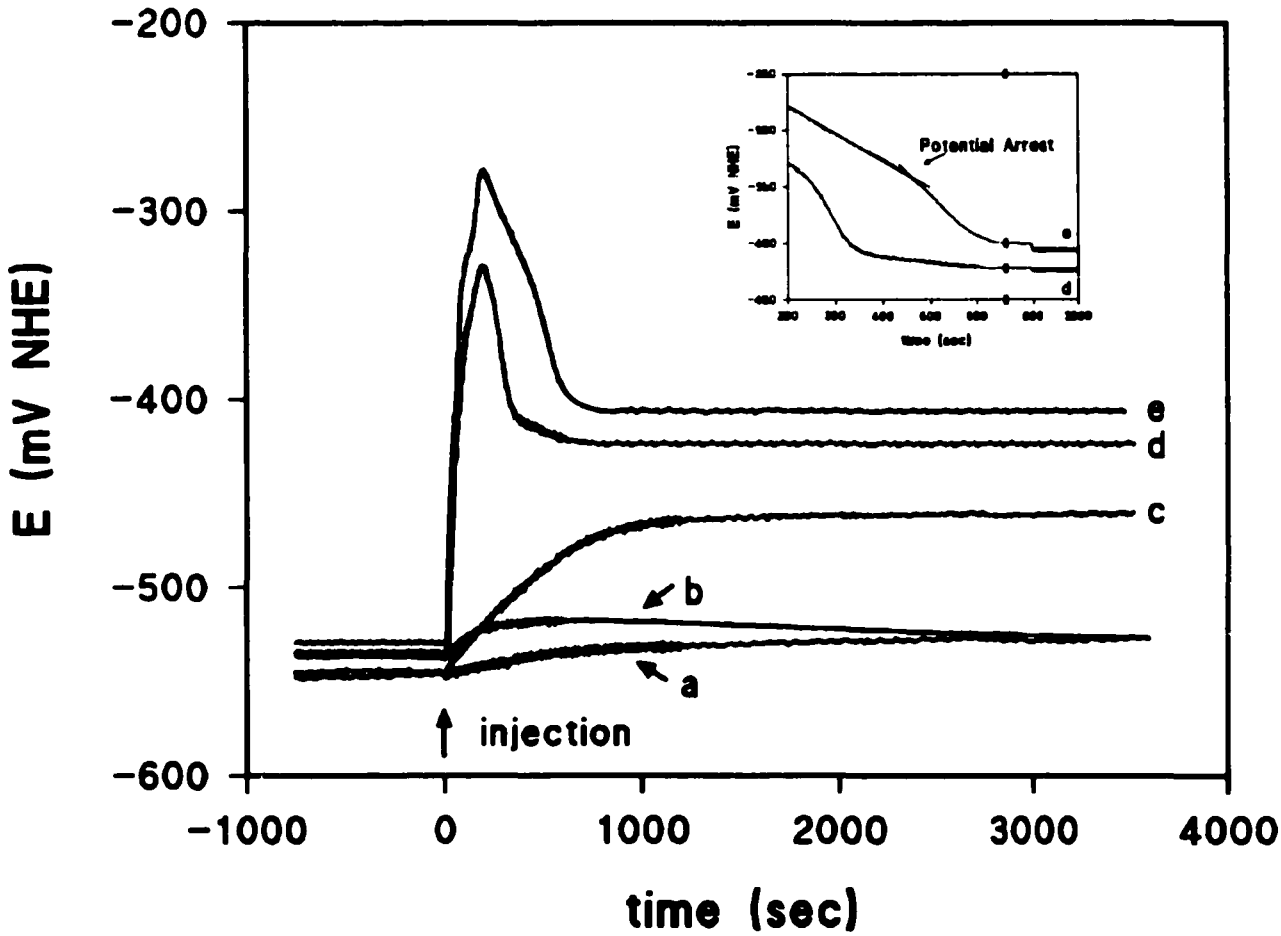


Figure 3. 5 Open circuit potential-time measurements in borate buffer. (a) injection of CH_2Cl_2 - electrode freshly cleaned; (b) injection of CH_2Cl_2 - electrode immersed for 24 h; (c) injection of CCl_4 - electrode freshly cleaned; (d) injection of CCl_4 - electrode immersed for 24 h; (e) injection of CCl_4 - electrode immersed for 68 h.

The injection of CCl_4, at the end of the cathodic cleaning period, resulted in a positive shift in potential to the active dissolution potential region (Figure 3.6). This shift, from -0.54 to -0.46 V, occurred over a period of approximately 1000 s. Once the potential stabilized, it stayed constant until the end of the experiment.

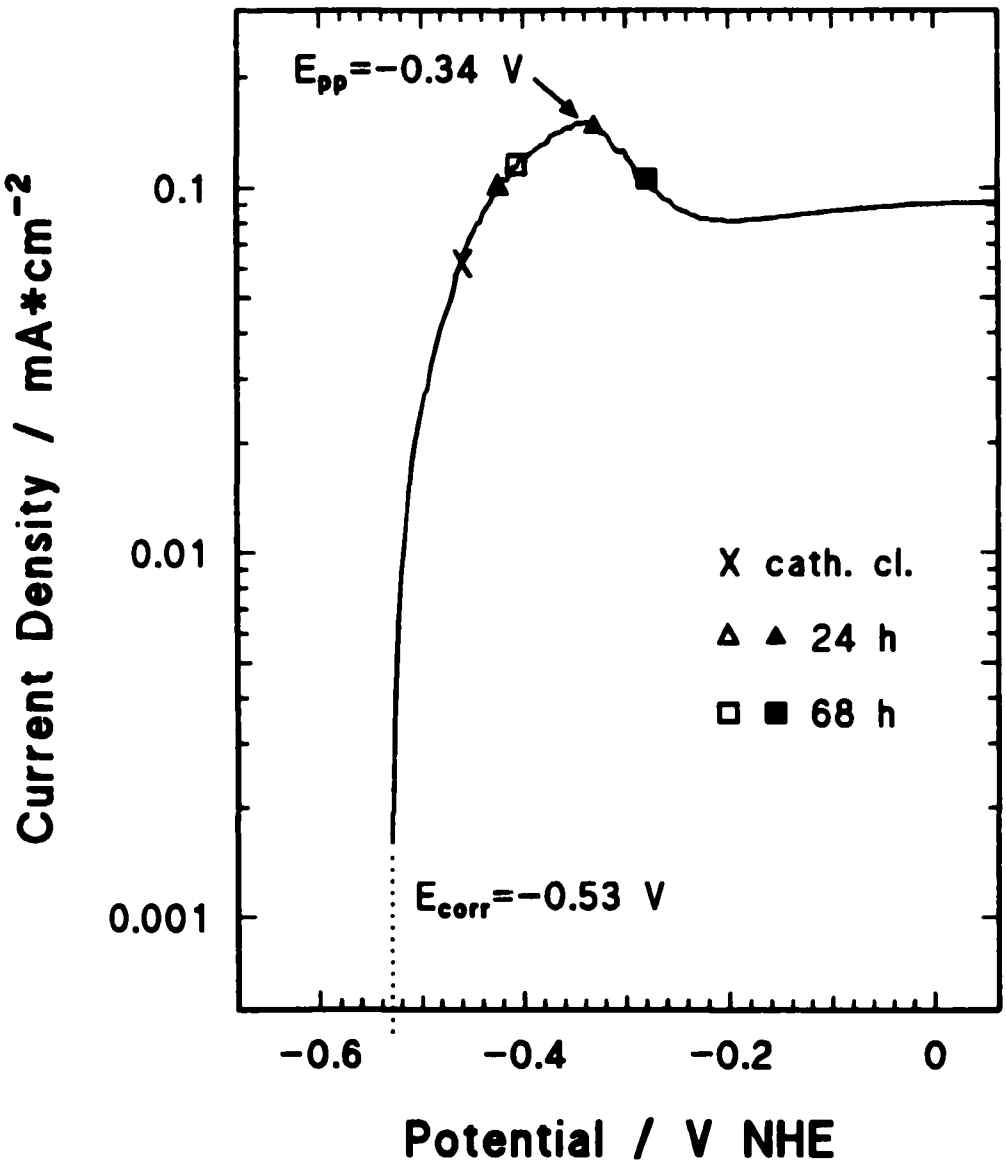


Figure 3. 6 Plot of the maximum (solid symbols) and final (open symbols) potentials reached in the open circuit potential-time measurements with CCl_4 (freshly cleaned electrode, 24 and 68 h of immersion) on the polarization curve obtained in solvent-free borate buffer.

Keeping the iron electrode immersed in solvent-free borate buffer for a given time (24 or 68 h) resulted in pre-oxidation of the Fe electrode. This pre-oxidized Fe surface, upon introduction of an oxidizer in the system, should act as a catalyst in the sense that it should promote faster further oxidation of the iron electrode. This phenomenon, similar to electrocatalysis due to premonolayer oxidation of noble metals [36], was observed when the injection of CCl_4 was performed after 24 and 68 h of immersion. The potential shifts were then larger, reaching the active-passive transition potential region (Figure 3.6), and more rapid. The magnitude of the shifts was related to the time of immersion (+0.20 V after 24h and +0.25 V after 68h).

Subsequent declines of potential, and a potential arrest at -0.34 V, were observed for the pre-oxidation experiments (see insert, Figure 3.5). The potential arrest reflects the passage between the active/passive transition to the active dissolution region and corresponds to the E_{pp}. The potential declines and arrest were attributed to the autoreduction of the higher valency outer portion of the surface film [13]. Chloride ions, released during the reductive dehalogenation of chlorinated solvents[7], might have facilitated the autoreduction of the film [37,38]. Another possible mechanism for film removal, chemical dissolution, is rather unlikely due to the high pH of the borate buffer.

Many studies [13-15,20-22,37,38] have reported a second potential arrest during the galvanostatic cathodic reduction of surface films on iron. This second potential arrest, corresponding to the reduction of the Fe_3O_4 inner layer, appears at potential lower than the equilibrium potential for hydrogen evolution (-0.496 V NHE in a borate buffer of pH 8.4) [13]. For the 24 and 68h

immersion experiments, the final stabilized potentials were -0.42 and -0.41 V respectively, suggesting that the inner Fe_3O_4 layer might not be reduced.

The effect of the injection of CH_2Cl_2, at the end of the cathodic cleaning period or after 24 h of immersion, was similar to the observed background potential drift of the electrode in solvent-free borate buffer (from -0.54 to -0.53 V after 24h of immersion). This shift might be related to an increase of Fe^{2+} ions in solution, as predicted by the Nernst equation [34]. This is assuming, however, that the change of Fe_{total} in solution (from $3.4x10^{-6}$M to $8.1x10^{-6}$M after 24h of immersion), as measured by AA, is representative of an increase of Fe^{2+} ions in solution. In accordance with the polarization experiments, the open circuit potential-time measurements indicated that CCl_4 acts as an oxidizer of the iron electrode while CH_2Cl_2 is nonreactive.

3.4.3 Raman spectroscopy in borate buffer

Consistent with the electrochemical data and independent of the electrode treatment, the injection of CH_2Cl_2 did not result in the formation of a surface film which could be detected by Normal Raman spectroscopy. In the case of a fresh cathodically-cleaned Fe electrode, the injection of CCl_4 caused a shift of potential to the active dissolution potential region. The surface film, being in the initial stage of formation, was most probably too thin to be detected by Normal Raman spectroscopy. In contrast, the pre-oxidation by immersion of the Fe electrode followed by the injection of CCl_4, causing the formation of an Fe(III) surface film followed by its autoreduction, resulted in measurable spectral change. Since all Raman spectral measurements were performed 3600 s after the injection of the solvent, they represent the final products of the surface redox reactions.

In Figure 3.7, the spectrum of the Fe surface after 24 h of immersion in solvent-free borate buffer [Figure 3.7(a)], which shows only the Raman signal of borate ion in solution at 878 cm^{-1}, is compared with the Raman spectra obtained from three randomly selected areas of the electrode surface after the injection of CCl_4 [Figure 3.7 (b,c,d)].

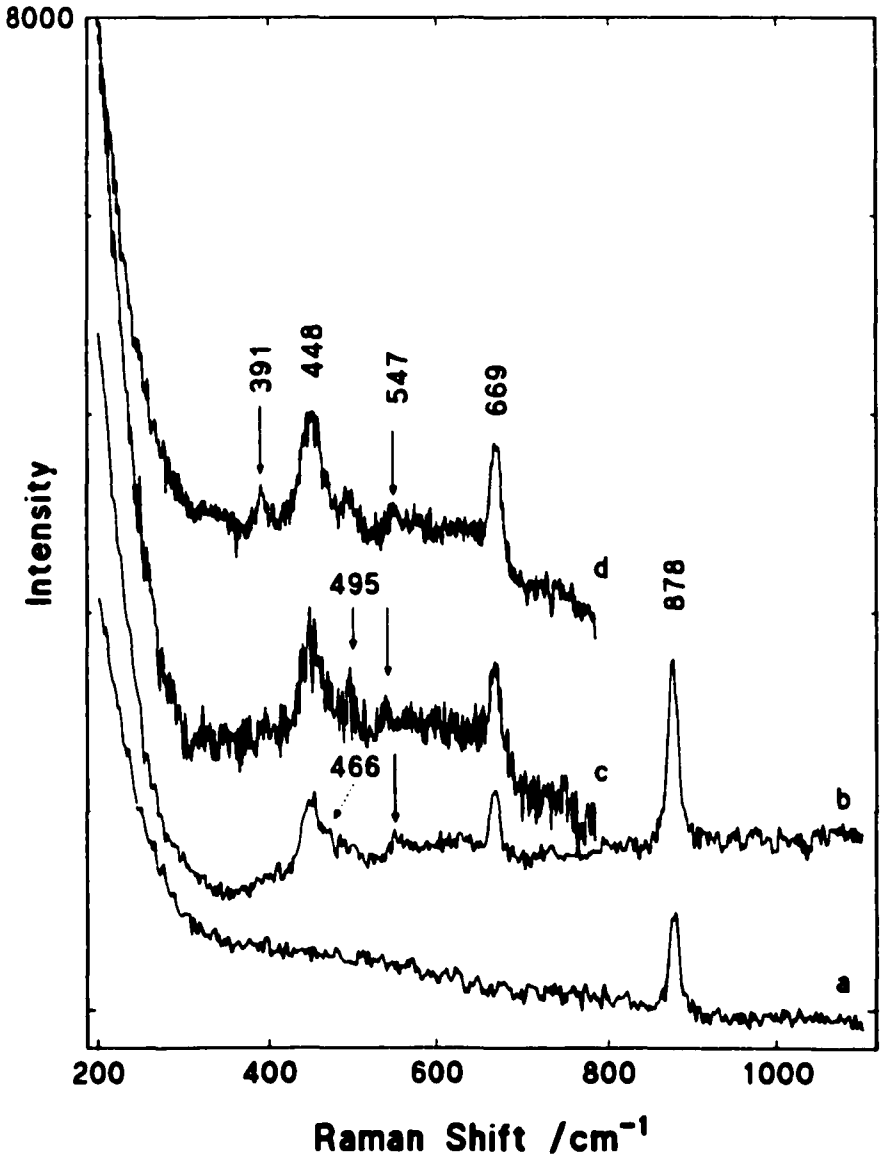


Figure 3. 7 *In situ* Raman spectra of the Fe surface, preoxidized for 24 h, before (a) and after the injection of CCl_4 (b,c,d).

The Raman band at 669 cm^{-1} is attributed to the strongest A_{1g} mode of Fe_3O_4 [27,39]. γ-Fe_2O_3 is also characterized by a main peak around 650-700 cm^{-1} [40]. Discrimination between the different spinel structures is usually based on the broadness and shape of the peak [40]. In the case of Fe_3O_4, a single symmetric band is observed, while for γ-Fe_2O_3, the band observed in that region is very broad and has two shoulders [27,40]. Finally, the fact that the potential reached the active/passive transition region (and not the passive region) followed by the autoreduction of the film reinforces the assignment of this band to the strongest A_{1g} mode of magnetite.

The assignment of the band at 547 cm^{-1} is more difficult. It might be attributed to the T_{2g} mode of magnetite (540 cm^{-1}) [27,39] or to one of the vibrational modes of $Fe(OH)_2$ [41]. The intensity ratio of the A_{1g}/T_{2g} modes in a standard Fe_3O_4 sample is 6.6 [27]. The average intensity ratio of the bands I_{669}/I_{547} measured for the data presented in Figure 3.7 is 5.02 ± 0.24, indicating that the band at 547 cm^{-1} is stronger than expected for a magnetite sample. Therefore it might be attributed to the combination of the T_{2g} mode of magnetite and an $Fe(OH)_2$ band at 550 cm^{-1} [41] (i.e., I_{547} = $I_{540}(Fe_3O_4) + I_{550}(Fe(OH)_2)$). The latter was further suggested by the observation of a shoulder at 466 cm^{-1} in Figure 3.7(b,d) which may be due to the presence of $Fe(OH)_2$ [41]. A band at 460 cm^{-1} has been reported for laboratory-synthesized $Fe(OH)_2$ [41]; according to Gui and Devine [16], it represents the E_g mode of $Fe(OH)_2$. The increase in pre-oxidation time from 24 to 68 h [Figure 3.8 (a,b,c)] caused the increase of the I_{669}/I_{547} ratio to 5.53 ± 0.17. Further calculations performed on the baseline corrected and bandfitted data (Figure 3.9 and Figure 3.10) indicate that, for a longer pre-oxidation time, the increase of the ratio can be attributed to a decrease of the contribution of the $Fe(OH)_2$ band at 550 cm^{-1} to the total intensity of the 547 cm^{-1} band. This change was accompanied by the disappearance of the shoulder at 466 cm^{-1}, as would be expected

if our band assignment is correct. The band at ca. 391 cm^{-1} is assigned to iron oxyhydroxide species since it falls at the same frequency as the strongest bands of α - FeOOH [42,43]. Similarly the band at 479 cm^{-1}, visible only in Figure 3.8(c), might be attributed to α - FeOOH [42,43].

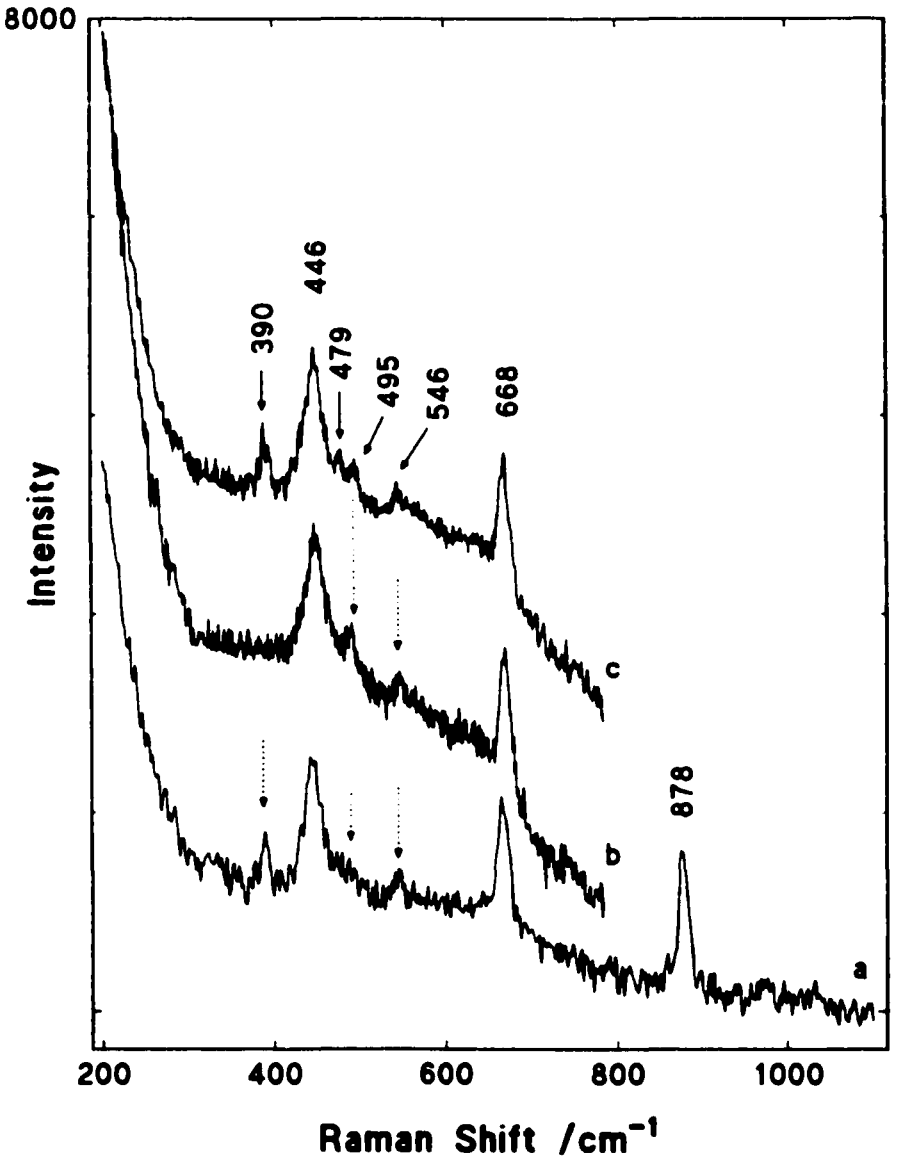


Figure 3. 8 *In situ* Raman spectra of the Fe surface, preoxidized for 68 h, before (a) and after the injection of CCl_4 (b,c).

The broad, complex bands observed at ca. 448 and ca. 495 cm^{-1} do not correlate with any known iron oxide, hydroxide or oxyhydroxide species (see Table 2 in Ref. 19). Kanno and Hiraishi [44] observed similar bands in a glassy $Fe(NO_3)_3$ solution at 450 and 506 cm^{-1}; in a glassy $FeCl_3$ solution these bands were detected at 440 and 485 cm^{-1}. In both cases the bands were assigned to the E_g and A_{1g} stretching modes of $[Fe(OH_2)_6]^{3+}$, respectively. In borate buffer after 10 min of cathodic reduction at -900 mV SCE, Oblonsky and Devine [19] observed two bands at 405 and 490 cm^{-1}. They attributed these bands to symmetric stretching modes of Fe^{2+} - OH_2 and Fe^{3+} - OH_2. Comparable bands at ca. 420 and ca. 505 cm^{-1} were observed in 'green rust' complexes and were assigned to Fe^{2+} - OH and Fe^{3+} - OH stretching modes, respectively [45]. Very similar bands at 434 and 510 cm^{-1} were observed by Simard *et al.*[46] during pitting corrosion of steel in bicarbonate buffer. In the latter experiment, the correctness of the band assignments was confirmed by an experiment with heavy water [46]. In all these cases, the bands at 405 - 434 and 490 - 510 cm^{-1} are the results of the destruction of the surface film by pitting corrosion [45,46] or by electrochemical reduction [19]. Deconvolution of the broad, asymmetric band at ca. 448 cm^{-1} indicated the existence of two bands under a broad envelope, one ranging from 425 (Figure 3.10) to 442 cm^{-1} (Figure 3.9) and a band at ca. 450 cm^{-1}. In the light of previous findings [19,44,45,46], the bands at ca. 448 and ca. 495 cm^{-1} should be attributed to the E_g and A_{1g} stretching vibrations* of the double layer species Fe^{3+} - OH_2, while the lowest frequency band might be assigned to the stretching mode of the double layer species Fe^{2+} - OH or Fe^{2+} - OH_2.

In the presence of Cl^-, which is a product of the dechlorination reaction [7], one or more water molecules in the $[Fe(H_2O)_6]^{3+}$ solution species will be replaced by chloride. This will shift the

* Considering the O_h symmetry of the $[Fe(OH_2)_6]^{3+}$ cation, the deformation vibration H_2O - Fe^{3+} - OH_2 at 325 cm^{-1} should be the weakest of all bands; therefore it is not surprising that it was not observed in this study.

Fe^{3+} - OH_2 vibrations; Kanno and Hiraishi [44] suggest that the $[FeCl(H_2O)_5]^{2+}$ species has a Fe - OH_2 band at 485 cm^{-1} and that the $[FeCl_2(H_2O)_4]^{+}$ species has a Fe - OH_2 band at 440 cm^{-1}. The E_g mode of $[Fe(H_2O)_6]^{3+}$ is expected to be weaker than the A_{1g} mode. No Raman spectral evidence was observed in our measurements for Fe-Cl vibrations; these would occur at 332 cm^{-1} or less [47]. However the formation of $[Fe(OH)(H_2O)_5]^{2+}$ cannot be ruled out; such a species would account for a lower frequency of Fe^{3+} - OH_2 vibration than for $[Fe(H_2O)_6]^{3+}$.

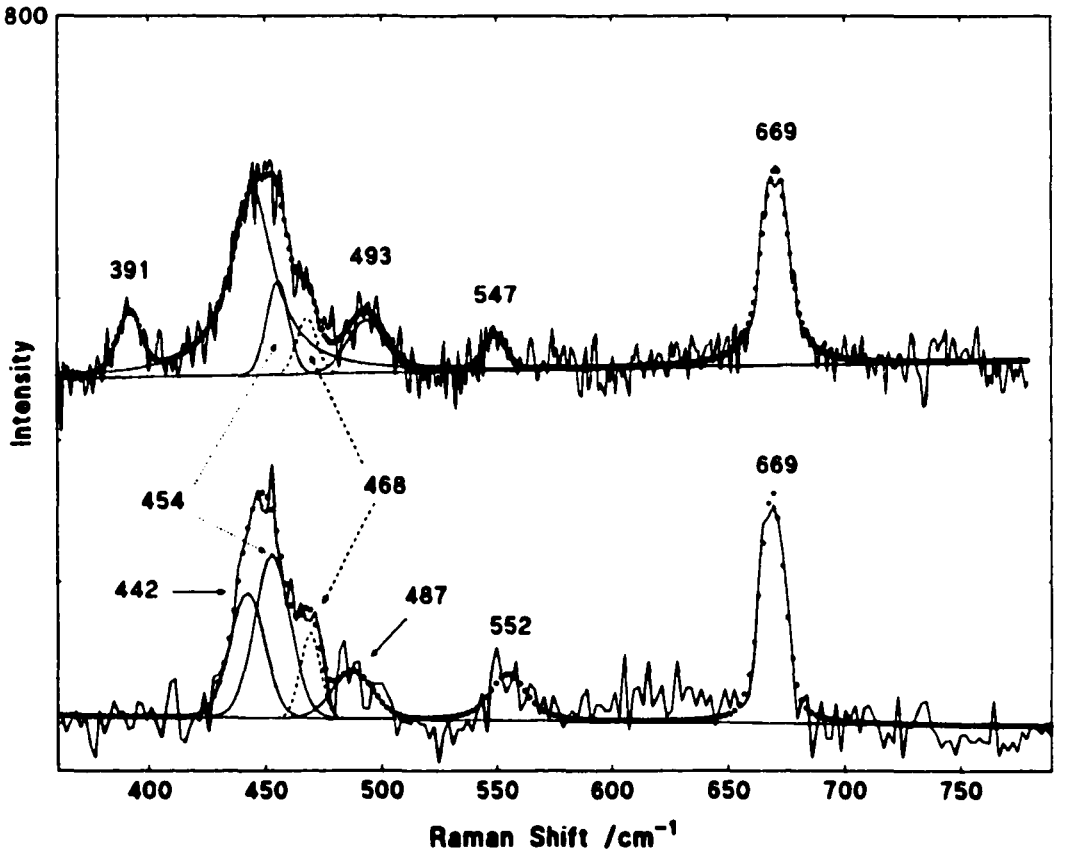


Figure 3. 9 Bandfitting of the *in situ* Raman spectra of the Fe surface, preoxidized for 24 h, after the injection of CCl_4. Lower portion of the figure: spectrum 3.7(b); upper portion: spectrum 3.7(d).

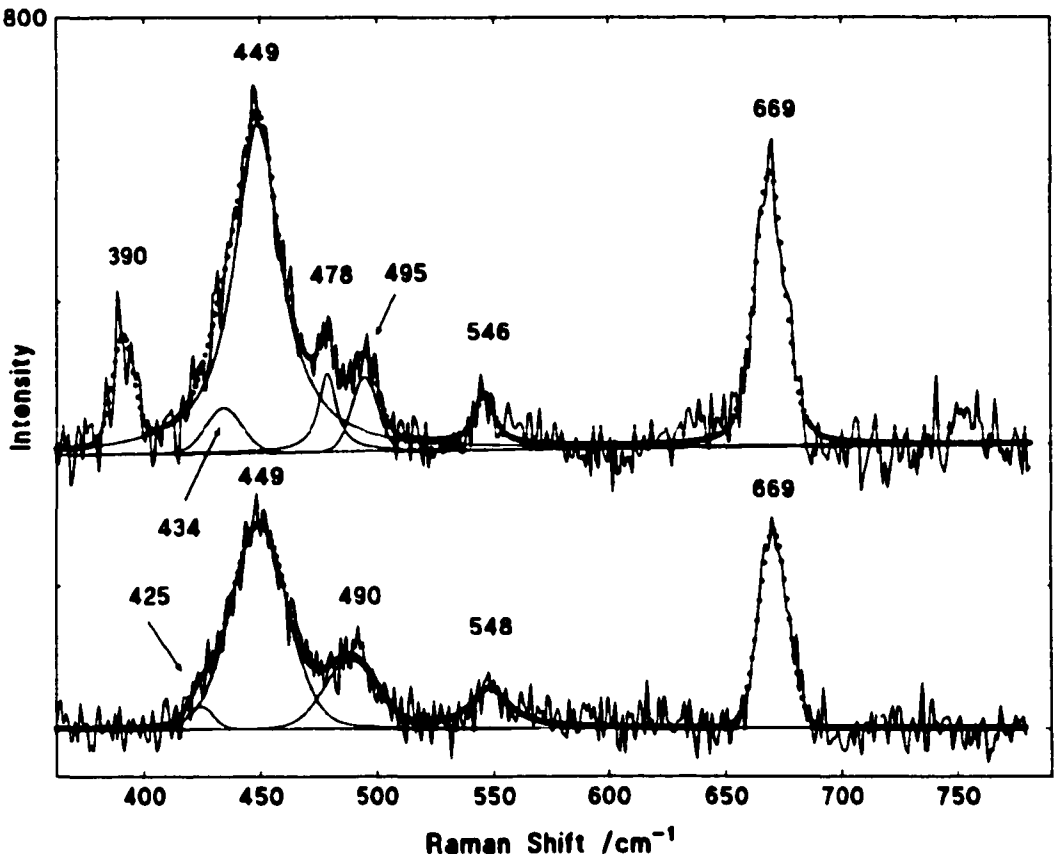


Figure 3. 10 Bandfitting of the *in situ* Raman spectra of the Fe surface, preoxidized for 68 h, after the injection of CCl_4. Lower portion of the figure: spectrum 3.8(b); upper portion: spectrum 3.8(c).

3.5 Discussion

There are discrepancies between the different models of the passive film on iron [30]. Depending on the model, the higher valency outer portion of the passive film should be considered an n-type semiconductor [48], an insulator [30] or a combination of both i.e., a chemi-conductor [21]. According to the semiconductor model [48], when the potential of an electrode is more cathodic than the flat band potential (-10 mV NHE in solvent-free borate buffer pH 8.4 [25]), the oxide/electrolyte interface will be negatively charged and will therefore repel negatively-charged ions or molecules [23]. At potentials more anodic than the flat band potential, the oxide surface will be

positively charged and will therefore attract negatively-charged ions or molecules [23]. Non-polar aliphatic chlorinated solvents such as CCl_4 and CH_2Cl_2, due to charge separation between carbon and chlorine atoms, develop momentary central-electron-poor and peripheral-electron-rich structural regions [49]. This is why, in the polarization experiments, the only significant effect of CH_2Cl_2 is in the passive region where, due to adsorption of CH_2Cl_2 molecules on the surface of the electrode, the currents were lower than in solvent-free borate buffer.

The injection of CCl_4 into a borate buffer hosting an iron electrode, freshly cathodically-cleaned or pre-oxidized, resulted in positive shifts of potential which corresponded to surface film formation. The composition and protective properties of the film are dependent on the potential history of the iron electrode after its exposure to the oxidizing solvent. In the case of a fresh cathodically-cleaned iron electrode, the injection of CCl_4 resulted in a potential shift from the corrosion potential to the active dissolution potential region. The surface film, being in an early stage of formation, was most probably too thin to be detected by Normal Raman spectroscopy. According to Burke and Lyons [50], the initial stages of Fe oxidation in aqueous alkaline solutions result in the formation of Fe/OH_{ads} species with simultaneous displacement of pre-adsorbed hydrogen created by the cathodic cleaning procedure:

$$Fe + OH^- \rightarrow Fe/OH_{ads} + e^- \qquad (5)$$

$$Fe/H_{ads} \rightarrow Fe + H^+ + e^- \qquad (6)$$

As noted by Simpraga and Conway [51], the oxidation state of Fe in such a film is an indeterminate quantity, though some degree of electronic charge transfer from Fe to the OH_{ads} species is

expected. In consequence the formation of a quasi-bulk film of $Fe(OH)_2$ / non-stoichiometric magnetite might be expected [13,52]. $Fe(OH)_2$, being unstable, will convert over time to Fe_3O_4 [52].

In the case of an iron electrode that has been pre-oxidized, the injection of CCl_4 resulted in a potential shift from the corrosion potential to the active/passive transition potential region. At more positive potentials than the E_{pp}, an Fe(III) film is expected [17,27]. This film, being formed in the active/passive transition region, is expected to be less protective than a film formed in the passive region. Therefore some degree of charge transfer through the film might be expected causing both the reductive dechlorination of the solvent and the autoreduction of the film. Following the autoreduction of the Fe(III) film and the stabilization of the potential in the active dissolution region, the main components of the film, as seen in the Raman spectra, will be magnetite and hydrated magnetite $Fe(OH)_2 \bullet 2FeOOH$. Upon aging, hydrated magnetite should convert to magnetite. Ionic species in a solution of general formula $[Fe(OH)_n(OH_2)_{6-n}]^{(3-n)+}$ are the products of the hydrolysis of Fe_{aq}^{3+} and Fe_{aq}^{2+} [47]. These latter, in our case, result from corrosion and autoreduction reactions. Raman results indicate that the dominant ionic species at the interphase are $[Fe(OH)(OH_2)_5]^{2+}$ or $[Fe(OH_2)_6]^{3+}$ while Fe_{aq}^{2+} species are depleted. The depletion of Fe_{aq}^{2+} in the interphase might result from the formation of magnetite:

$$3Fe_{aq}^{2+} + 4H_2O \rightarrow Fe_3O_4 + 6H^+ + H_{2(g)} \quad (7)$$

or/and non-stoichiometric magnetite (where $2n+3m=8$):

$$nFe^{2+} + mFe^{3+} + 4H_2O \rightarrow Fe_n^{2+}Fe_m^{3+}O_4 + 8H^+ \quad (8)$$

The supporting evidence for the above are the decrease of the lowest frequency band, attributed to the Fe^{2+} - OH or Fe^{2+} - OH_2 stretching vibration, and the simultaneous increase of the Fe_3O_4 band, for longer pre-oxidation times.

A product of the reductive dehalogenation of CCl_4 are chlorine ions [7]. However, the Raman spectra of the pre-oxidized Fe surface obtained after the injection of CCl_4 did not reveal the presence of a Cl^- peak (Figs 3.7 and 3.8). This might be due to the fact that, even if all the CCl_4 in solution ($\approx 1x10^{-3}$ M) were reduced, the maximum concentration of Cl^- ions in solution ($2x10^{-3}$ M) would not be sufficient to result in a Raman signal. The formation of Cl-green rust is therefore unlikely (Figure 3.11). The formation of borate-green rust is also rather unlikely since no change in the borate peak was observed after the injection of CCl_4 (Figure 3.7).

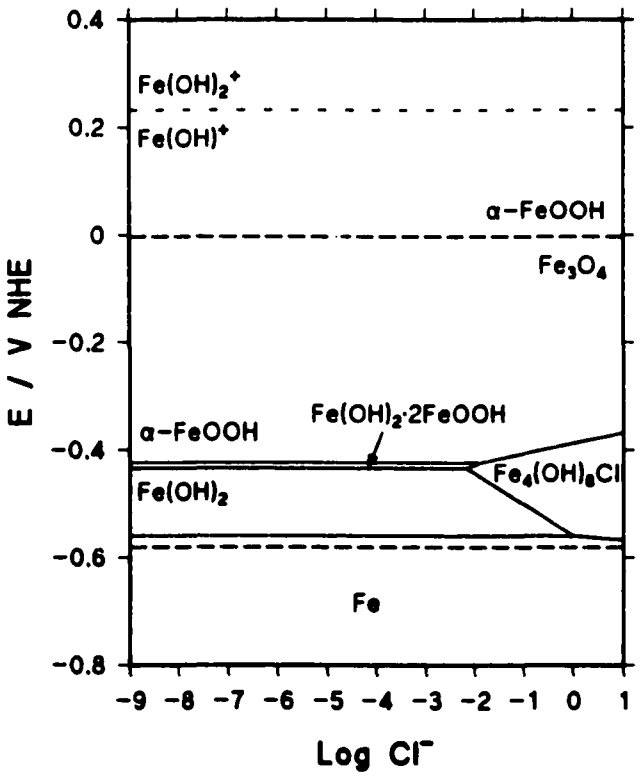


Figure 3. 11 Stability regions for Fe solid species in borate buffer (pH 8.4). This figure was made using the thermodynamic data of Refait and Génin [54] following a format used by Sagoe-Crentsil and Glasser [55].

Raman spectroscopy will not differentiate between inner and outer layers of the film [53]. However, because of the high penetration depth of the Raman laser beam (see Appendix), it is possible to obtain spectra from the inner and outer portion of the film simultaneously. In addition, it is logical to assume that the denser species will be located in the inner portion of the interface. Magnetite, being the denser species [20], should therefore occupy the inner layer of the film. Based on this evidence, it is now possible to conceptualize the solid/electrolyte interface for the cases of a fresh, cathodically-cleaned, Fe surface and of a pre-oxidized Fe surface in borate buffer after exposure to CCl_4 (Figure 3.12). For both cases, upon aging of the film, the main surface product will be magnetite. From a technological point-of-view, this is very important. Magnetite, being electronically conductive [48], will allow for charge transfer through the interphase and, as a consequence, reductive dechlorination will continue to proceed. The degradation will, however, be proceeding at a slower rate since charge transfer rate is slower through an oxide than on bare metal surface [48]. Another possible mechanism for the degradation of the chlorinated solvents, as proposed by Matheson and Tratnyek [12], is catalysed hydrogenolysis by molecular H_2. However, based on Marcus and Protopopoff's theoretical calculations [56], atomic H is adsorbed on a magnetite covered surface. Therefore atomic H_{ads}, rather than molecular H_2, will play a role in that mechanism.

It has been advanced [12] that the corrosion behaviour of iron will differ from a highly conductive medium (such as borate buffer) to low conductivity simulated groundwater solutions. To evaluate this, electrochemical and spectral measurements were performed in solutions of potassium bromide and calcium carbonate prepared to simulate groundwater [43]. The electrochemical experiments gave results very similar to those observed in borate buffer. The

spectroscopic results however indicated that the structure of the interface and the nature of the surface films differ from one solution to another. Therefore, the conceptual model proposed here is only valid in borate buffer; in solutions typical of groundwater, a model of the interface is still to be proposed [43].

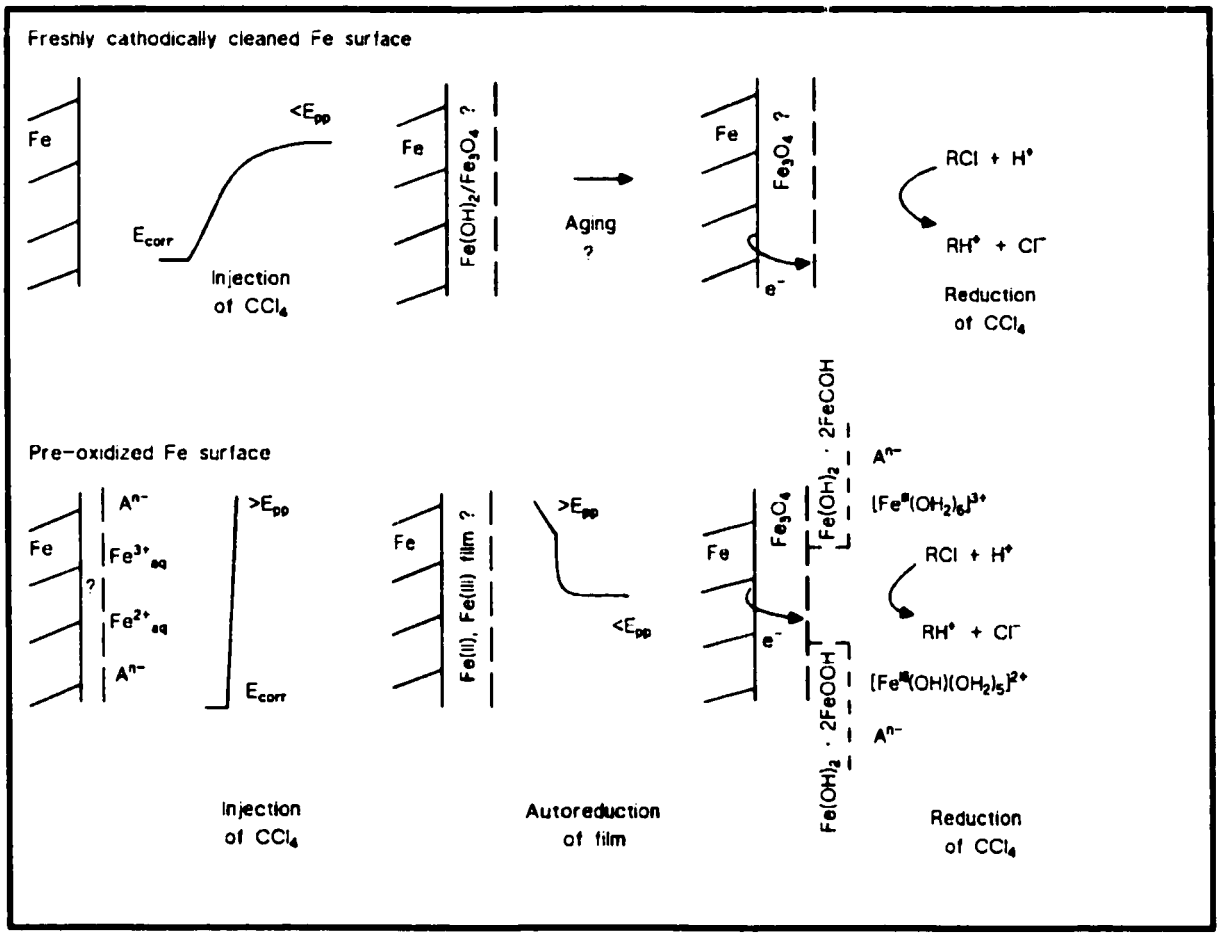


Figure 3. 12 Conceptual model for the reductive dehalogenation of chlorinated solvents by iron in borate buffer. Cases of a fresh cathodically-cleaned Fe surface and of a pre-oxidized Fe surface. A^{n-} represents anions in solution: OH^-, $(B_4O_7)^{2-}$and $(BO_3)^{3-}$. The "?" indicates uncertainties; see text for details.

3.6 Conclusion

Based on the electrochemical and Raman spectral results obtained in the present study, combined with literature data [17], a new conceptual model of the reductive dehalogenation of chlorinated solvents by iron is proposed. According to this model, the introduction of an oxidizer will result in surface film formation. Based on free energy thermodynamic considerations, both CCl_4 and CH_2Cl_2 should act as oxidizers of an iron electrode, but as shown in the present study, only CCl_4 has the ability to oxidize the Fe surface while CH_2Cl_2 is nonreactive. In the case of a fresh cathodically- cleaned Fe surface, a quasi-bulk $Fe(OH)_2/Fe_3O_4$ film should be expected. For a pre-oxidized Fe surface, an Fe(III) film should form, then be reduced resulting in the formation of a $Fe_3O_4/Fe(OH)_2 \bullet 2FeOOH$ film. Excess of $[Fe(OH)(OH_2)_5]^{2+}$ or $[Fe(OH_2)_6]^{3+}$ ions should also be present in the double layer region as a result of hydrolysis reactions. For both cases, upon aging of the film, the main surface product will be magnetite. Magnetite, being electronically conductive [48], will allow for charge transfer and therefore for reductive dechlorination. Another mechanism, catalysed hydrogenolysis by H_{ads} on the magnetite surface, might also play a role in the reduction of the chlorinated solvents.

Acknowledgements - The authors wish to thank Professor Donald Irish, from the Department of Chemistry at the University of Waterloo, and Dr. Piotr Kedzierzawski, from the Département de Chimie Appliquée à l'Université de Genève, for helpful discussions. We would also like to acknowledge the Natural Sciences and Engineering Research Council of Canada for financial support.

3.7 Appendix

The laser penetration depth can be estimated by the procedure described by Dünnwald and Otto[57]. Raman spectra were measured using the 632.8 nm (1.96 eV) line of an HeNe laser with ca. 3 mW power at the electrode surface. It is known that the penetration depth of light, d, is a function of the imaginary part, k, of the complex refractive index, $n + ik$, of the surface film [57]. It is defined as $d = c/2k\upsilon = \lambda/2k$, where υ, λ, and c are, respectively, the frequency, wavelength, and velocity of light in vacuum. The imaginary part of the refractive index for natural Fe_3O_4 for 1.96 eV was measured to be about 0.5 [58]; thus the laser penetration depth for Fe_3O_4 is approximately 632 nm. Iron hydroxides and oxyhydroxides, which were detected in this study, are characterized by smaller k values. Thus a deeper laser penetration depth should be expected for these compounds. The passive film on Fe in borate buffer (pH=8.4) for 1.96 eV exhibits the k value of 0.3 [59]; thus a laser penetration depth of 1055 nm for such a film is expected.

3.8 References

1. T.M. Vogel, C.S. Criddle and P.L. McCarty, *Environ. Sci. Technol.*, **21**, 722 (1987).
2. C.S. Criddle and P.L. McCarty, *Environ. Sci. Technol.*, **25**, 973 (1991).
3. C.A. Schanke and L.P. Wackett, *Environ. Sci. Technol.*, **26**, 830 (1992).
4. C.J. Gantzer and L.P. Wackett, *Environ. Sci. Technol.*, **25**, 715 (1991).
5. M.R. Kriegman-King and M. Reinhard, *Environ. Sci. Technol.*, **28**, 692 (1994).
6. M.R. Kriegman-King and M. Reinhard, *Environ. Sci. Technol.*, **26**, 2198 (1992).
7. R.W. Gillham and S.F. O'Hannesin, *Groundwater*, **32**, 958 (1994).
8. G.W. Reynolds, T.F. Hoff and R.W. Gillham, *Environ. Sci. Technol.*, **24**, 135 (1990).

9. R.W. Gillham and S.F. O'Hannesin, Modern trends in hydrogeology. Paper presented at the IAH Conference, Hamilton, Ontario, May 10-13, p.94 (1992).

10. R.W. Gillham, in *Advances in Groundwater Pollution Control and Remediation*, ed. M.M. Aral. Kluwer Academic Publishers, Printed in the Netherlands, p.249 (1996).

11. R. Focht, J. Vogan and S.F. O'Hannesin, *Remediation* , **6**, 81 (1996).

12. L.J. Matheson and P.G. Tratnyek, *Environ. Sci. Technol.*, **28**, 2045 (1994).

13. M. Nagayama and M. Cohen, *J. Electrochem. Soc.*, **109**, 781 (1962).

14. S. Haruyama and T. Tsuru, *Corrosion Science*, **13**, 275 (1973).

15. M. Cohen and K. Hashimoto, *J. Electrochem. Soc.*, **121**, 42 (1974).

16. J. Gui and T.M. Devine, *Corrosion Science*, **36**, 441 (1994).

17. J. Gui and T.M. Devine, *Corrosion Science*, **32**, 1105 (1991).

18. J.C. Rubim and J. Dunnwald, *J. Electroanal. Chem.*, **258**, 327 (1989).

19. L.J. Oblonsky and T.M. Devine, *Corrosion Science*, **37**, 17 (1995).

20. Z. Szklarska-Smialowska and W. Kozlowski, *J. Electrochem. Soc.*, **131**, 234(I) and 499(II) (1984).

21. C. Chen and B.D. Cahan, *J. Electrochem. Soc.*, **129**, 17(I), 474(II) and 921(III) (1982).

22. N. Sato, K. Kudo and T. Noda, *Electrochim. Acta*, **16**, 1909 (1971).

23. S. Virtanen, P. Schmuki, A.J. Davenport and C.M. Vitus, *J. Electrochem. Soc.*, **144**, 198 (1997).

24. P. Schmuki, S. Virtanen, A.J. Davenport and C.M. Vitus, *J. Electrochem. Soc.*, **143**, 574 (1996).

25. S. Virtanen, P. Schmuki, H. Bohni, P. Vuoristo and T. Mantyla, *J. Electrochem. Soc.*, **142**, 3067 (1995).

26. K.P.J. Williams, I.C. Wilcok, I.P. Hayward, and A. Whitley, *Spectroscopy*, **11**, 45 (1996).

27. M. Odziemkowski, J. Flis and D.E. Irish, *Electrochim. Acta*, **39**, 2225 (1994).

28. M. Odziemkowski, M. Krell and D.E. Irish, *J. Electrochem. Soc.*, **139**, 3052 (1992).

29. N. Sato, in *Passivity of Metals*, eds. R.P. Frankenthal and J. Kruger. Electrochem. Soc., Princeton, NJ, p.29 (1978).

30. M. Cohen, in *Passivity of Metals*, eds. R.P. Frankenthal and J. Kruger. Electrochem. Soc., Princeton, NJ, p.521 (1978).

31. M. Kerkar, J. Robinson and A.J. Forty, *Faraday Discuss.*, **89**, 31 (1990).

32. A. Cakir and J.C. Scully, in *Passivity of Metals*, eds. R.P. Frankenthal and J. Kruger. Electrochem. Soc., Princeton, NJ, p.385 (1978).

33. C. Wagner and W. Traud, *Z. Electrochem.*, **44**, 391 (1938).

34. M.G. Fontana and N.D. Greene, in *Corrosion Engineering*. McGraw-Hill Inc., New York, p.325 (1978).

35. B.B. Damaskin, O.A. Petrii and V.V. Batrakov, in *Adsorption of Organic Compounds on Electrodes*. Plenum Press Publishers Ltd, p.304 (1971).

36. L.D. Burke, *Electrochim. Acta*, **39**, 1841 (1994).

37. K. Ogura, S. Haruyama and K. Nagasaki, *J. Electrochem. Soc. Japan*, **37**, 102 (1968).

38. S. Haruyama, K. Ogura and K. Nagasaki, *J. Electrochem. Soc. Japan*, **37**, 38 (1968).

39. T.R. Hart, H. Temkin and S.B. Adams, in *Light Scattering in Solids*, eds. M. Balkanski, R. Leite and S. Porto. Flammarion Sciences, Paris, p.254 (1976).

40. N. Boucherit, A. Hugot-Le Goff and S. Joiret, *Corrosion Science*, **32**, 497 (1991).

41. I.C.G. Thanos, *Electrochim. Acta*, **31**, 811 (1986).

42. T. Ohtsuka, K.Kubo and N. Sato, *Corrosion*, **42**, 476 (1986).

43. P.M.L. Bonin, W. Jedral, M.S. Odziemkowski and R.W. Gillham, *Corrosion Science* (in press).

44. H. Kanno and J. Hiraishi, *J. Raman Spectrosc.*, **12**, 224 (1982).

45. N. Boucherit and A. Hugot-Le Goff, *Faraday Discuss.*, **94**, 137 (1992).

46. S. Simard, M. Odziemkowski, D.E. Irish, L. Brossard and H. Ménard, in 191st Meeting of the Electrochemical Society, Montreal, Quebec. Meeting Abstract Vol. 97-1, p.279 (1997).

47. K. Murata, D.E. Irish and G.E. Toogood, *Can. J. Chem.*, **67**, 517 (1989).

48. J.W. Schultze, in *Passivity of Metals*, eds. R.P. Frankenthal and J. Kruger. Electrochem. Soc., Princeton, NJ, p.82 (1978).

49. R.P. Schwarzenbach, P.M. Gshwend and D.M. Imboden, in *Environmental Organic Chemistry*, A Wiley-Interscience Publication, John Wiley & Sons Inc., New York, p.63 (1993).

50. L.D Burke and M.E.G. Lyons, *J. Electroanal. Chem.*, **198**, 347 (1986).

51. R. Simpraga and B.E. Conway, in *Proceedings of the Symposium on Oxide Films on Metals and Alloys*, Proc. Vol. 92-22, eds B.R. MacDougall, R.S. Alwitt and T.A. Ramanarayana, The Electrochem. Soc., Princeton, NJ (1992).

52. M.S. Odziemkowski, T.T. Schumacher, R.W. Gillham and E.J. Reardon, *Corrosion Science*, **40**, 371 (1998).

53. C.A. Melendres, M. Pankuch, Y.S. Li and R.L. Knight, *Electrochim. Acta*, **37**, 2747 (1992).

54. PH. Refait and J.M.R. Génin, *Corrosion Science*, **34**, 797 (1993).

55. K.K. Sagoe-Crentsil and F.P. Glasser, *Corrosion*, **49**, 457 (1993).

56. P. Marcus and E. Protopopoff, Private communication in 191st Meeting of the Electrochemical Society, Montreal, Quebec, May 4-9 (1997).

57. J. Dünnwald and A. Otto, *Corrosion Science*, **29**, 1167 (1989).

58. U. Buchenau and I. Müller, *Sol. State Commun.*, **11**, 1291 (1972).

59. K. Azumi, T. Ohtsuka and N. Sato, *J. Electochem. Soc.*, **133**, 1326 (1986).

4.0 *IN SITU* IDENTIFICATION OF CARBONATE-CONTAINING GREEN RUST ON IRON ELECTRODES IN SOLUTIONS SIMULATING GROUNDWATER

The following manuscript, as submitted to the Journal of Solution Chemistry, covers the results of open circuit potential-time and *in situ* Raman measurements performed in aqueous solution of calcium carbonate.

4.1 Cover page

IN SITU IDENTIFICATION OF CARBONATE-CONTAINING GREEN RUST ON IRON ELECTRODES IN SOLUTIONS SIMULATING GROUNDWATER*

P.M.L. BONIN, M.S. ODZIEMKOWSKI, E.J. REARDON and R.W. GILLHAM

Department of Earth Sciences, University of Waterloo,
Waterloo, Ontario, Canada N2L 3G1

* Dedicated to Professor Donald E. Irish on the occasion of his retirement and in recognition of his contribution to solution chemistry and metal/electrolyte interface studies.

Abstract - Open circuit potential-time and spectral measurements were performed on iron electrodes in aqueous solutions containing calcium carbonate to simulate groundwater, to which an amount of carbon tetrachloride was added. In the case of a pre-oxidized iron electrode, the injection of the chlorinated aliphatic hydrocarbon resulted in the formation of carbonate-containing green rust. *In situ* identification, performed by Raman spectroscopy, was based on bands at ca. 433, 509 and 1053 cm^{-1} which were assigned respectively to the Fe^{2+}- OH stretching mode of green rust, the Fe^{3+}- OH stretching mode of green rust and the stretching vibrations of carbonate ions in the interlayer regions of the green rust. The assignment of the Fe^{2+} - OH and Fe^{3+} - OH stretching mode bands was confirmed by parallel experiments using D_2O solution. The results of the open circuit potential-time experiments are in good agreement with literature thermodynamic data for iron in carbonate-containing aqueous solutions.

Keywords: Open circuit potential; Raman spectroscopy; iron; green rust; carbon tetrachloride; calcium carbonate; deuterated water; thermodynamic data.

4.2 Introduction

A new remediation technology for groundwater contaminated with chlorinated aliphatic hydrocarbons involves contact with granular iron [1]. The nature and electronic properties of surface films formed during the degradation reactions could influence the longevity of field installations. In a previous study [2], where column experiments were performed in an attempt to identify precipitates formed on granular iron following exposure to solutions simulating groundwater, the formation of green rust was not observed. In the present study, electrochemical and spectral measurements were performed on iron electrodes in aqueous solutions of calcium carbonate to which an amount of a degradable chlorinated compound (carbon tetrachloride-CCl_4) was added. In the presence of the contaminant, which acts as an oxidizer [3], carbonate-containing green rust was identified *in situ* by Raman spectroscopy.

Green rusts are Fe^{2+}-Fe^{3+} layered double hydroxide (LDH) compounds belonging to the hydrotalcite mineral group [4]. LDH compounds consist of positively-charged brucite-like layers separated by interlayers of anions and water molecules. These interlayer regions have been used as reaction galleries to promote organic synthesis reactions [4] and reductive dechlorination of organic compounds such as carbon tetrachloride [5]. There are two types of green rusts: green rust one (GR1) with planar anions such as Cl^- [6] and CO_3^{2-} [7], and green rust two (GR2) with three-dimensional anions in the interlayers such as SO_4^{2-} [8].

Carbonate-containing green rust was discovered , as a corrosion product of iron, in municipal water pipes by Stampfl [7]. It has been extensively studied by Taylor and Murad [9-13] and Hansen [14], among others. Drissi et al. [15], who synthesized stoichiometric GR1(CO_3^{2-}) by oxidation of $Fe(OH)_2$

in aqueous solution, determined its chemical formula to be $[Fe^{(II)}Fe^{(III)}(OH)_{12}][CO_3 \cdot 2H_2O]$. Based on their estimate of the standard free energy of formation of stoichiometric GR1(CO_3^{2-}), they also drew the Pourbaix diagram of iron in carbonate-containing aqueous solution illustrating its stability region in terms of potential and pH. In a study by Abdelmoula et al. [16], devoted to checking the validity of the Pourbaix diagram devised by Drissi et al. [15], the formation of carbonate-containing green rust by corrosion of metallic iron disks in $NaHCO_3$ solutions was reported. Identification of the green rust compound was, however, performed *ex situ*, by X-ray diffraction (XRD) and Mössbauer spectroscopy. For these methods, the iron disks were removed from solution then quickly dried before analysis. In addition, both techniques involved exposure to air [15]: during scanning for the XRD analyses and in the transfer to the cryostat in the case of Mössbauer spectroscopy. Green rust, an intermediate transient compound between metallic iron and common rust [16], oxidizes quickly in air [15]. Finally, since the validity of *ex situ* surface analysis for the study of passive films on Fe has often been questioned [17 and references there in], it is reasonable to question its validity in the case of transient films such as green rusts. A more valid approach is to study these films *in situ*, i.e., without losing potential or environmental control [18-19], by an *in situ* technique such as Raman spectroscopy, for example.

Raman spectra of green rusts as products of pitting corrosion [20-22] or autoreduction of Fe(III) oxide films [23] as well as of synthetic green rusts [24-25] and natural green rust minerals [24-25] have been previously reported. Of particular interest is the work of Simard et al. [22] who were the first to obtain spectral evidence of chloride and phosphate ions in the interlayers of green rust structures formed in bicarbonate and phosphate solutions. In the present study, Raman spectra of carbonate-containing green rust formed as a corrosion product of iron are reported.

4.3 Experimental methods

In all experiments, the working electrode was a 5 mm diameter disk of polycrystalline iron (99.99% purity) pressed in a Kel-F holder. The auxiliary electrode was platinum. Potentials were measured against a Ag/AgCl electrode and then converted to NHE. Prior to each experiment, the iron electrode was polished with 1200 grade SiC emery paper, washed in copious amounts of distilled water and ultrasonically cleaned. The iron electrode was then immersed in a deaerated aqueous solution of calcium carbonate and cathodically cleaned for 900s. The $1.2x10^{-3}$M $CaCO_3$ solution, prepared from distilled water, was deaerated and equilibrated with a 5% CO_2 / 95% N_2 gas mixture. After this procedure, the pH and redox potential Eh (in V) of the solution were respectively 6.4 and 0.3.

The open circuit potential (OCP) of the iron electrode was monitored over time using a high impedance (10^{14} ohms) preamplifier to prevent current flow between the working and the reference electrodes. The high impedance unit was connected to a UPC601-U Universal PC Sensor Interface Card which transmitted data to a DTK Corp. 386 computer. The data were recorded at rates of 4 to 60 points / minute.

In situ Raman spectra were obtained with a Renishaw 1000 Raman microscope system. The instrument consists of an Olympus microscope, a single spectrograph fitted with holographic notch filters for spectroscopy mode, and a Peltier-cooled CCD detector. The optical efficiency of the instrument is high (≥30%), as is its sensitivity, allowing the detection of a very weak signal (1 photon/s). Excitation was achieved using the 632.8 nm line of a Melles Griot 35 mW HeNe laser. All Raman measurements were carried out using backscattering geometry. The objective lens used

in this study has a magnification of 50. When set-up in confocal mode, it allows the study of a spot size of 2 μm^2 with a focal depth of field of 4 μm. In non-confocal mode, the focal depth is 26 μm. In the present study, the non-confocal mode was used. The laser was operated at its maximum power of 35 mW; this translates to ca. 3 mW at the sample surface. Such low light intensity is unlikely to alter the surface film composition, particularly for *in situ* measurements. A three-electrode spectroelectrochemical cell with an injection port, as illustrated by Brolo et al. [26], was used.

The chlorinated hydrocarbon (pure phase CCl_4) was injected directly into the solution through a Teflon septum; 0.2 mL of contaminant was injected into the electrochemical cell filled with 300 mL of $CaCO_3$ solution while 17 μL was injected into the 25 mL Raman cell (resulting in a ratio of 0.7 μL of chlorinated hydrocarbon per mL of solution in both cells). In the electrochemical cell, deaeration with the 5% CO_2 / 95% N_2 gas mixture was performed in and above the solution prior to contaminant injection, and above the solution after injection. The solution was continuously stirred using a Teflon stir bar. Since there was no headspace in the Raman cell, deaeration stopped once the cell was filled with deaerated solution. Prior to the introduction of the solution, the cell had been purged with N_2. No stirring was performed.

In situ Raman measurements were repeated in a D_2O solution of calcium carbonate to confirm the band assignment of species containing OH^- functional groups.

4.4 Results and Discussion

As previously reported [3], the polarization of an iron electrode in pH 8.4 borate buffer to which an amount of pure phase carbon tetrachloride had been added indicated that CCl_4 acts as an oxidizer of iron. In the presence of the contaminant, there was a positive shift of the corrosion potential, an increase in the corrosion current density and an increase of the cathodic Tafel slope. The change of the OCP of a freshly cathodically-cleaned iron electrode, in deaerated aqueous solution of calcium carbonate, following the injection of carbon tetrachloride (0.2 mL of pure phase CCl_4 in 300 mL of solution) was monitored over time (Figure 4.1). As observed in borate buffer [3], the injection of the contaminant resulted in a positive shift of potential (curve 1: from -0.54 to -0.46 V in about 600 s).

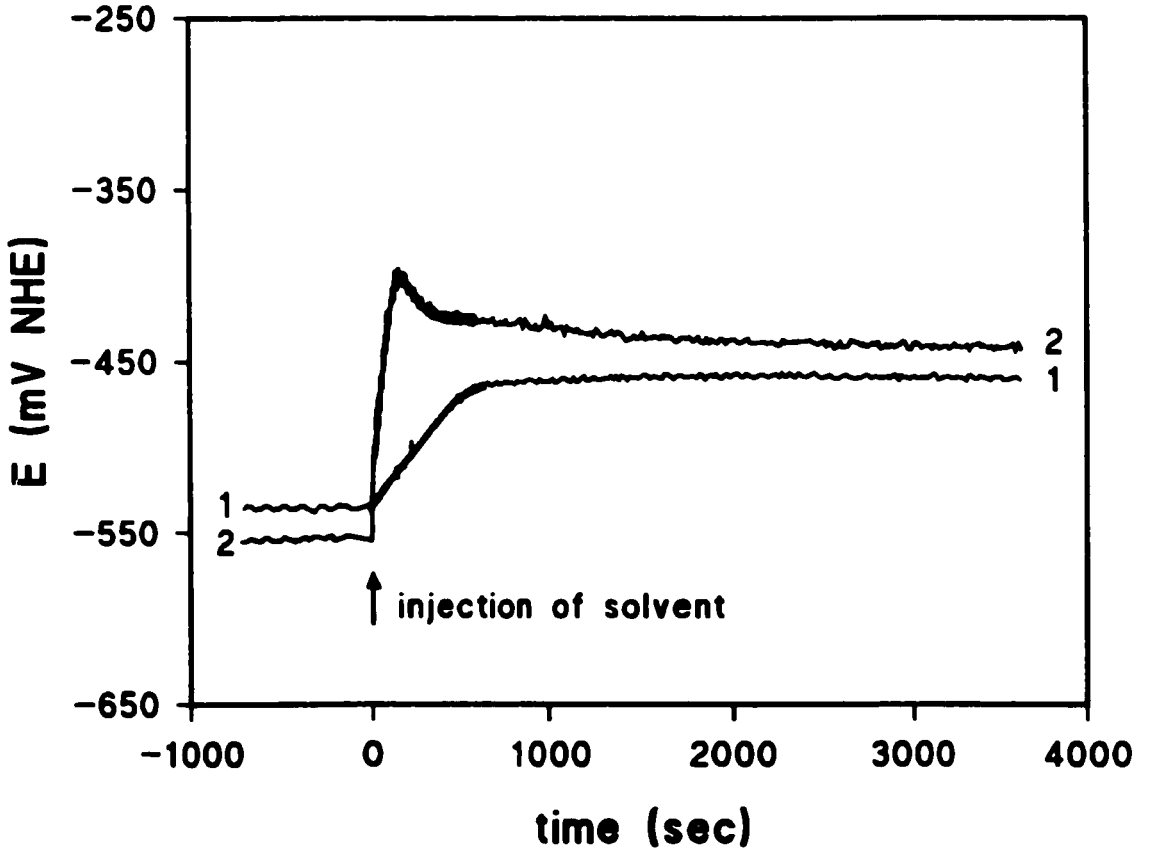


Figure 4. 1 Open circuit potential (OCP) - time measurements. (1) Freshly cathodically-cleaned iron electrode; (2) Iron electrode pre-oxidized for 17 h.

Keeping the iron electrode immersed in a contaminant-free aqueous solution of calcium carbonate for a given time (17h) resulted in the pre-oxidation of the Fe electrode, and probably in the formation of ferrous hydroxide as observed in 3.4×10^{-4}M KBr solution [2]. This pre-oxidized Fe surface, upon introduction of an oxidizer (CCl_4), should act as a catalyst in the sense that it should promote faster and further oxidation of the iron electrode and/or the $Fe(OH)_2$ film covering the electrode surface. This phenomenon, similar to electrocatalysis due to premonolayer oxidation of noble metals[27], was observed when the injection of the chlorinated hydrocarbon was performed after 17 h of immersion. The potential shifts were then larger and more rapid (curve 2: from -0.56 to -0.40 V in about 150 s). A subsequent decline of potential was observed (from -0.40 to -0.44 V). This decline may be a consequence of a change in impedance of the metal/solution interface.

The OCP of the iron electrode drifted during the immersion time in contaminant-free solution (from -0.54 to -0.56 V in 17 h). This drift is related to local changes of pH. From the Nernst equation[28], a shift of -0.02 V corresponds to an increase in pH of 0.3 (from 6.4 to 6.7) in the vicinity of the electrode.

In the case of a freshly cathodically-cleaned iron electrode, the injection of CCl_4 caused a shift of potential but the surface film, being in the initial stage of formation, was probably too thin to be detected by Normal Raman spectroscopy.

Raman measurements were also performed on the iron electrode, kept immersed for 17 h in deaerated aqueous solution of calcium carbonate. Before the injection of CCl_4, the surface was free of precipitates (spectrum A, Figure 4.2) except for the presence of calcite crystals (spectrum B).

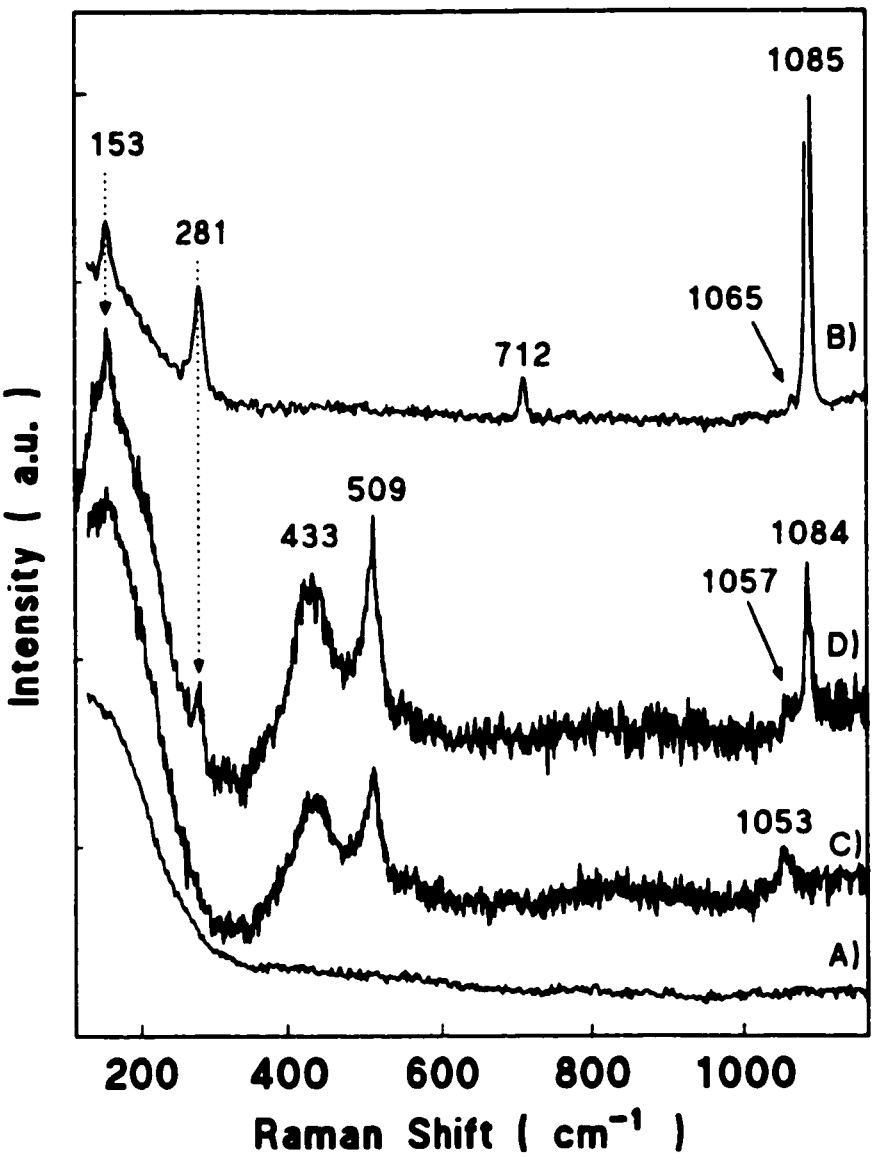


Figure 4. 2 *In situ* Raman spectra of the Fe surface pre-oxidized for 17 h in aqueous solution of calcium carbonate. (A, B) two different locations on the electrode before the injection of CCl_4; (C, D) two different locations on the electrode 1 hour after the injection of CCl_4.

Identification of the rhombohedral crystals was based on the spectral features in the range 100 to 1100 cm^{-1}. The bands at 1085 and 712 cm^{-1} are due to the internal vibrational modes of the carbonate ion (A_{1g} and E_g), while the bands at 281 and 153 cm^{-1} are attributed to lattice vibrational modes of calcite (both of the E_g type) [29]. Other carbonate minerals, such as aragonite, ankerite and siderite, also exhibit four dominant lines in this spectral region, but their locations and intensities

differ [29]. The formation and growth of the calcite crystals was favoured during the immersion period, as indicated by the potential drift and corresponding pH increase. Calcite crystals were however observed on a fresh cathodically-cleaned iron electrode prior to the injection of the contaminant. Initiation of the nucleation process might therefore be due to the cathodic cleaning procedure itself, or more precisely, to the pH increase resulting from the hydrogen evolution reactions. Finally the band at 1065 cm^{-1} (spectrum B, Figure 4.2) is attributed to the symmetric stretch of free CO_3^{2-} ions of saturated carbonate solution [30,31].

Spectrum C (Figure 4.2 and Table 4.1) was recorded one hour after the injection of CCl_4. The bands at ca. 433 and ca. 509 cm^{-1} are assigned respectively to Fe^{2+} - OH and Fe^{3+} - OH stretching modes of green rust. Similar bands were observed by Boucherit and Hugot-Le Goff [21] (420 and 505 cm^{-1}), Simard et al. [22] (434 and 510 cm^{-1}), and Odziemkowski and Gillham [23] (420 and 507 cm^{-1}). The band at ca. 1053 cm^{-1} corresponds to the symmetrical stretching vibration of CO_3^{2-} and indicates that carbonate ions are incorporated into the structure of the green rust. This band is at a lower frequency than would be expected if the CO_3^{2-} species were integrated into the structure of carbonate minerals such as calcite, aragonite, ankerite or siderite (1085-1091 cm^{-1})[29], and at a lower wavenumber than for aqueous CO_3^{2-} (1065 cm^{-1})[30-31]. This shift of symmetric stretching vibrations of CO_3^{2-} ions to lower frequency (1061 cm^{-1}, see Table 4.1) was also observed in experiments [32] where hydroxyl ions in powdered meixnerite were replaced by carbonate ions, resulting in the formation of hydrotalcite. Meixnerite (hydroxide end-member) and hydrotalcite (carbonate end-member) are Mg^{2+}/Al^{3+} minerals that are isomorphous to pyroaurite minerals (Mg^{2+}/Fe^{3+}) and green rust compounds (Fe^{2+}/Fe^{3+}). According to Moroz and Arkhipenko [33], who studied the structure of hydrotalcite and also obtained spectral evidence of interlayer CO_3^{2-} ions, the

shift of stretching vibrations relative to the free ion vibrations gives evidence of a slight electrostatic interaction of the interlayer CO_3^{2-} ions to the octahedral layers of the minerals.

Table 4. 1 Raman bands (in cm^{-1}) and band assignments.

H_2O GR	D_2O GR	Bands Assignment	H_2O* Hydrotalcite	D_2O* Hydrotalcite	H_2O* Meixnerite	D_2O* Meixnerite	Bands Assignment
433	417	Fe^{2+}-OH or OD Stretch	485	484	491	483	Mg^{2+}-OH or OD Stretch
509	494	Fe^{3+}-OH or OD Stretch	554	550	553	543	Al^{3+}-OH or OD Stretch
1053	-	Interlayer CO_3^{2-} Symmetric Stretching	1061	1060			Interlayer CO_3^{2-} Symmetric Stretching

*From Reference 32.

Spectrum D (Figure 4.2) was also recorded one hour after the injection of CCl_4, but at a different location on the electrode surface. Of particular interest is the simultaneous detection of calcite (bands at 153, 281 and 1084 cm^{-1}) and carbonate-containing green rust (bands at 433, 509 and 1057 cm^{-1}). Simultaneous detection of these species at the interface was made possible by using the non-confocal mode of the Raman microscope.

The ratios of the intensity of the Fe^{2+} - OH/ Fe^{3+} - OH peaks shown on spectrum C and D (Figure 4.2) are 1.63 and 1.15, respectively. For stoichiometric GR1(CO_3^{2-}) [15], an Fe^{2+}/ Fe^{3+} ratio of 2 has been found, while for a natural green rust mineral containing OH^- ions only [24], a ratio close to 1 has been reported. This means that the difference between the 2 ratios observed in the present study might be due to a depletion of CO_3^{2-} ions in the interlayers of the green rust formed in the proximity

of a calcite crystal (spectrum D). Since the calcite crystals form the initial sink for the carbonate ions, the subsequent formation of green rust in their proximity will be in a depleted solution. Further away from the calcite crystals, however, the solution is richer in carbonate ions and so is the green rust (spectrum C).

At other locations on the electrode, the situation was even more complex (Figure 4.3). In addition to calcite (band at 281 cm^{-1}) and green rust (bands at 433 and 509 cm^{-1}), iron oxyhydroxide species were detected. The band at ca. 381 cm^{-1} occurs at the same frequency as the strongest bands of α–FeOOH [34].

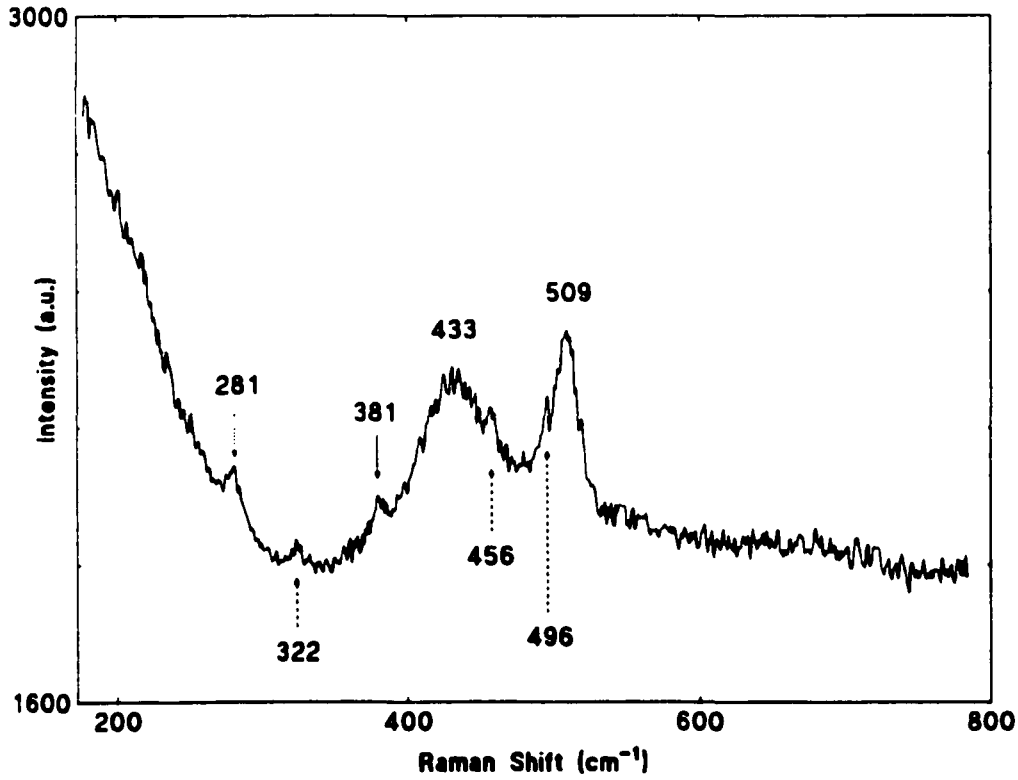


Figure 4. 3 *In situ* Raman spectrum of the Fe surface pre-oxidized for 17 h in aqueous solution of calcium carbonate 1 hour after the injection of CCl_4.

These iron oxyhydroxide species are probably the products of the oxidation of green rust. The band at ca. 456 and the possible band at ca. 496 cm^{-1} do not correlate with any known iron oxide, hydroxide or oxyhydroxide species (see Table 2 in Ref. 35). Such bands were observed on an iron electrode pre-immersed for 24 h in borate buffer after exposure to CCl_4 [3]. In the light of previous findings [35, 36, 21, 22, 3], they are assigned to the E_g and A_{1g} stretching vibrations of the double layer species H_2O - Fe^{3+}- OH_2. These ionic species are probably the products of the hydration of Fe^{3+}_{aq}, which result from the oxidation of Fe^{2+} produced by the corrosion reactions. Finally, the band at 322 cm^{-1} might be attributed to the deformation vibration of H_2O - Fe^{3+}- OH_2. Alternatively, the band at 322 cm^{-1} might be assigned to Fe-Cl vibrations [37] when one or more water molecules in the $[Fe(H_2O)_6]^{3+}$ solution species are replaced by chloride ions produced by the degradation of CCl_4 by iron [1].

To confirm the assignment of Fe^{2+} - OH and Fe^{3+} - OH stretching modes, experiments were repeated in D_2O solution of calcium carbonate (Figure 4.4 and Table 4.1). Raman measurements were performed on the iron electrode kept immersed for 17 h in deaerated solution. Before the injection of CCl_4 (spectrum A), the surface was free of precipitates. Spectrum B was recorded one hour after the injection of CCl_4. Formation of green rust in D_2O solution resulted in a shift of the peaks to lower frequencies, from 433 cm^{-1} for Fe^{2+} - OH to 417 cm^{-1} for Fe^{2+} - OD, and from 509 cm^{-1} for Fe^{3+} - OH to 494 cm^{-1} for Fe^{3+}-OD. These shifts, 16 and 15 cm^{-1} respectively, are consistent with the mass increase when OH groups are replaced by OD groups according to the following equation [38]:

$$\nu_{OD} / \nu_{OH} = \sqrt{(m_{OH}/m_{OD})}$$

Reardon et al. [32] also noticed shifts to lower frequencies when they synthesized hydrotalcite and meixnerite in deuterated water (Table 4.1). In addition, they were able to obtain spectral evidence of the interlayer CO_3^{2-} ions in the hydrotalcite formed in D_2O solution (band at 1060 cm^{-1}; see Table 4.1).

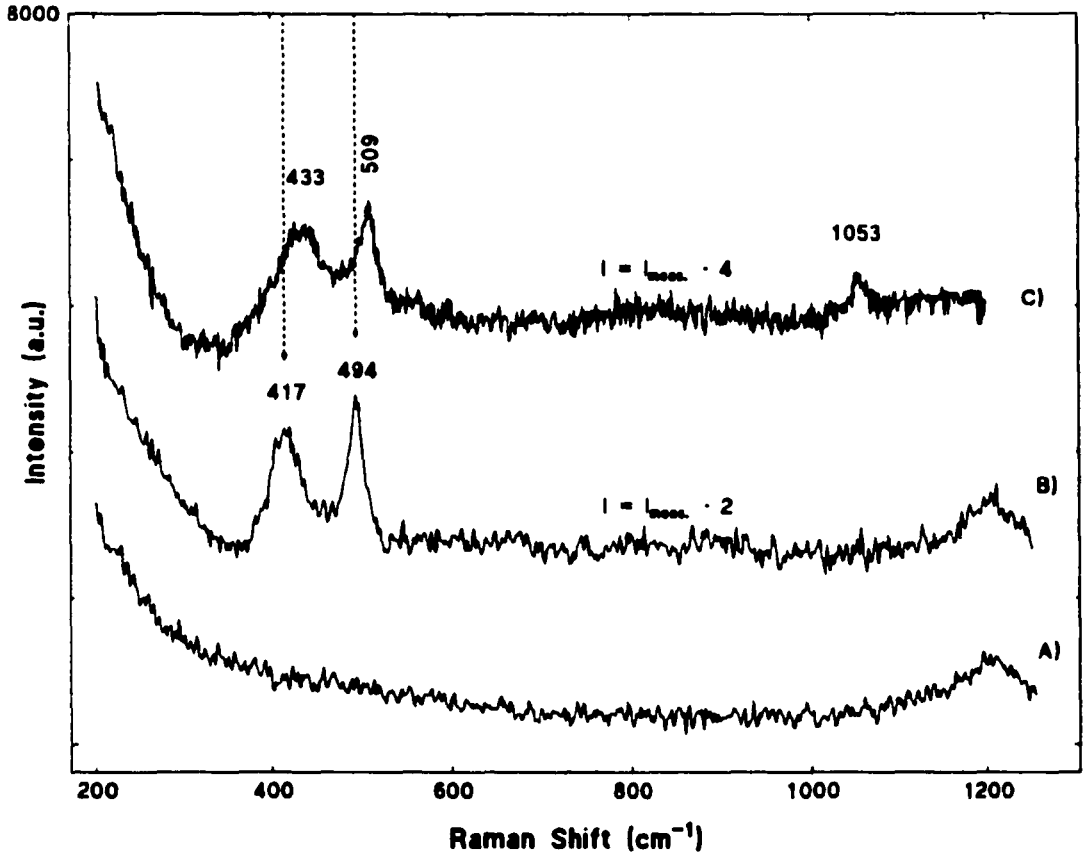


Figure 4. 4 *In situ* Raman spectra of the Fe surface pre-oxidized for 17 h. (A) Before the injection of CCl_4 in D_2O solution of calcium carbonate; (B) 1 hour after the injection of CCl_4 in D_2O solution of calcium carbonate; (C) 1 hour after the injection of CCl_4 in aqueous solution of calcium carbonate.

At other locations on the electrode in D_2O solution, the surface was more heterogeneous (Figure 4.5). In addition to green rust (bands at 417 and 494 cm^{-1}), calcite crystals were detected (bands at 155, 282, 712 and 1085 cm^{-1}; spectrum A). Contrary to what was observed in water, where the formation and growth of calcite crystals was favoured by the cathodic cleaning procedure and

during the immersion period, there were no calcite crystals before the injection of the contaminant. It is not clear why calcite crystals did not form prior to the introduction of the contaminant. Some hypotheses might be that, in D_2O solution, a longer time is required for the precipitation of calcite crystals or that a different process altogether is responsible for the initiation of their nucleation. Finally, bands at 216, 313 and 459 cm^{-1} (spectrum B) are attributed to CCl_4 molecules on the surface of the electrode.

The ratios of the intensity of the Fe^{2+} - OD/ Fe^{3+} - OD peaks shown on Figure 4.4 (spectrum B) and Figure 4.5 (spectrum A) are 1.89 and 1.97 respectively. These ratios, higher than observed in water, indicate a higher proportion of Fe^{2+} and therefore a composition that is closer to non-stoichiometric green rust (with interlayers OD groups), which in fact falls in the category of non-stoichiometric iron hydroxides [39]. The green rust formed in D_2O solution is also probably free of carbonate ions since no spectral evidence of the presence of interlayer CO_3^{2-} ions was obtained. In addition, contrary to what was observed in water, the composition of the green rust formed in D_2O solution does not appear to be affected by its proximity to calcite crystals. Simard et al. [22] reported similar results i.e., spectral evidence of chloride ions in green rust formed in aqueous solutions but no evidence of the presence of Cl^- ions in deuterated solution. Again, it is not clear why a different behavior was observed in deuterated solution. The authors can only speculate that a longer time or a different mechanism might be required in D_2O solution for anions to be incorporated into the green rust structure.

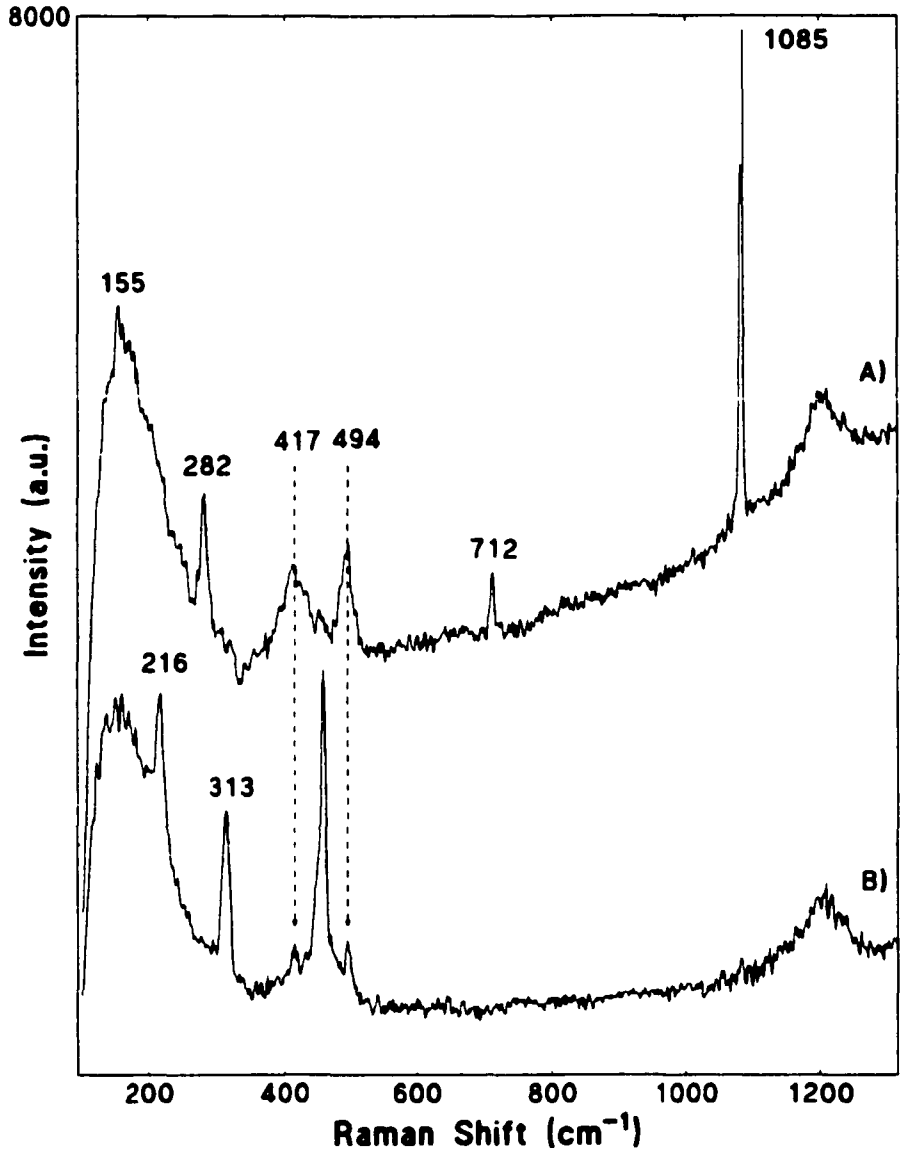


Figure 4. 5 *In situ* Raman spectra of the Fe surface pre-oxidized for 17 h in D_2O solution of calcium carbonate 1 hour after the injection of CCl_4. A) and B) were obtained at two different locations on the electrode.

In the present study, green rusts were observed on pre-oxidized iron electrodes after exposure to CCl_4. It is believed they form due to the oxidizing action of the contaminant on ferrous hydroxides formed during the pre-oxidation period. The Pourbaix diagram of iron in carbonate-containing aqueous solutions (Figure 6, from Ref. 15) predicts the formation of carbonate-containing green rust under the conditions observed in the pre-oxidation experiments after exposure to the contaminant: a

$CaCO_3$ concentration of $1.2x10^{-3}$M, a pH of 6.7, a maximum potential of -0.40 V (■) and a final potential of -0.44 V (❑). In the case of a freshly cathodically-cleaned iron electrode, where the pH was 6.4 and the potential shifted to -0.46 V after exposure to the contaminant (△), the formation of GR1(CO_3^{2-}) is not however thermodynamically favourable and was not observed.

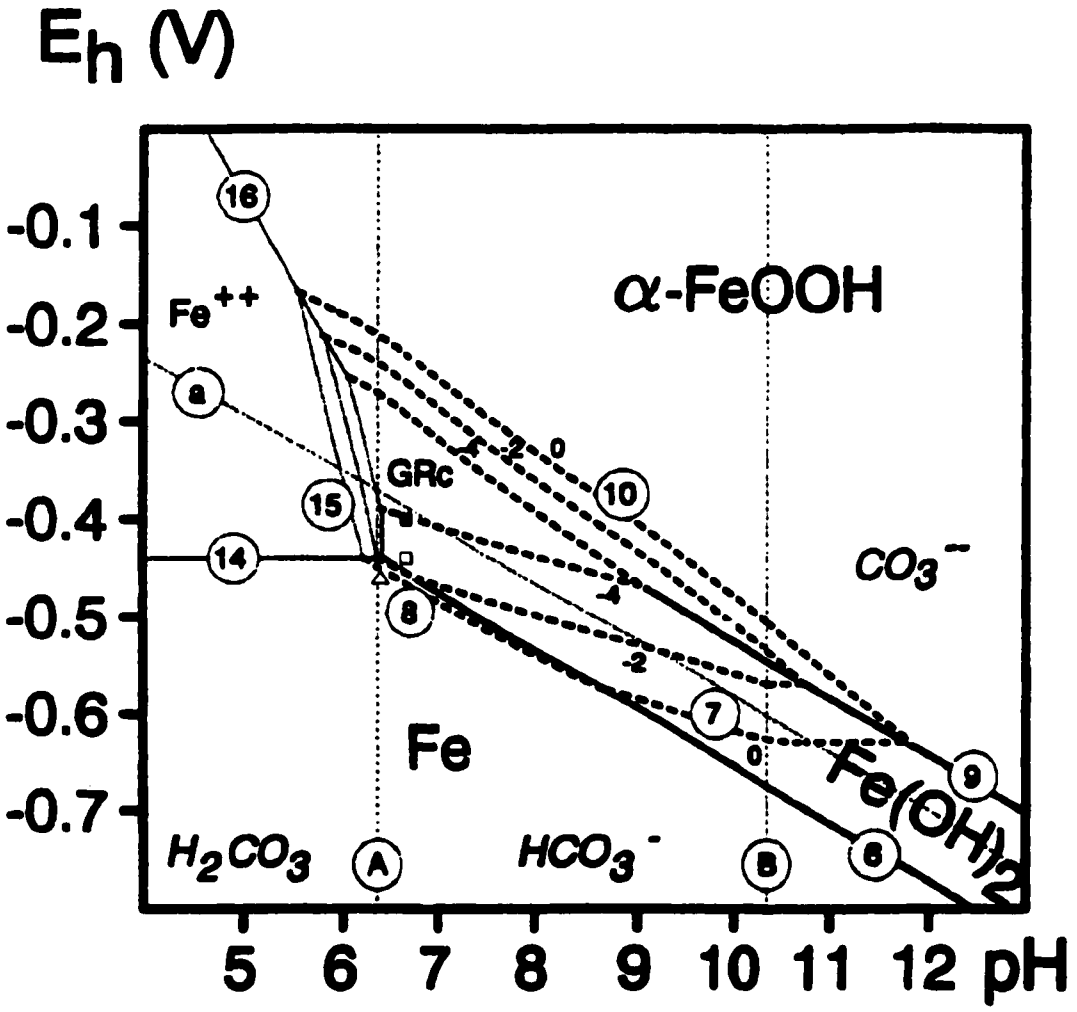


Figure 4. 6 Pourbaix diagram of iron in carbonate-containing aqueous solutions. Pre-oxidized electrode: (■) maximum potential of -0.40 V, (❑) final potential of -0.44 V, pH of 6.7, and $CaCO_3$ concentration of $1.2x10^{-3}$M. Freshly cathodically-cleaned electrode: (△) final potential of -0.46 V, pH of 6.4, and $CaCO_3$ concentration of $1.2x10^{-3}$M. *By permission of the publisher. Copyright ©1995 by Elsevier Science Ltd.*

The same was true in the contaminant-free precipitate study mentioned previously [2]. In that study, the experimental conditions were as follows: a $CaCO_3$ concentration of $1.2x10^{-3}M$, a pH of 9.8, a solution redox potential of -0.3 V, and a maximum corrosion potential of -0.61 V. The only difference between the two studies was that aragonite was observed rather than calcite. This may be due to the higher pH of the solution.

4.5 Conclusion

In the case of a pre-oxidized iron electrode immersed in an aqueous solution of calcium carbonate, the introduction of an oxidizer such as carbon tetrachloride resulted in the formation of a corrosion product referred to as carbonate green rust. *In situ* identification, performed by Raman spectroscopy, was based on bands at ca. 433 and ca. 509 cm^{-1} which were assigned respectively to the Fe^{2+}- OH and Fe^{3+}- OH stretching modes of green rust. A band at 1053 cm^{-1} was attributed to the stretching vibrations of CO_3^{2-}, indicating the presence of carbonate ions in the interlayer regions of the green rust. The composition of the green rust was affected by its proximity to calcite crystals, which were formed before and during the development of the green rust compounds. The presence of $[Fe(H_2O)_6]^{3+}$ ions and of iron oxyhydroxides, as hydrolysis products and products of the oxidation of green rust respectively, was also detected. The assignment of the Fe^{2+} - OH and Fe^{3+} - OH stretching mode bands was confirmed by parallel experiments using D_2O solution. The shifts of the peaks to lower frequency, 16 and 15 cm^{-1} respectively, were consistent with the mass increase due to the replacement of OH groups by OD groups. Furthermore, these experimental data are consistent with the thermodynamic calculations by Drissi et al. [15].

The degradation of chlorinated aliphatic hydrocarbons by iron is a charge transfer process involving oxidation of iron, dissociation of water and reductive dechlorination of the organic compounds [1]. With regards to the granular iron remediation technology, green rust compounds may play a role at several levels. First, as corrosion products due to the oxidizing action of contaminants on iron, as was found in the present study. Secondly, as products of the autoreduction of Fe(III) oxide films, which are present on dry commercial grade granular iron, after exposure to groundwater [23]. In both cases, due to their porosity and lack of protective properties [22], green rust compounds will not prevent charge transfer at the metal/solution interface. Finally as reductants contributing to the total reduction of contaminants in iron systems, as was found by Erbs et al., [40] who reported the reductive dechlorination of carbon tetrachloride using sulfate-containing green rust. In that case, it was found that green rust oxidizes to magnetite during the degradation reactions. Since magnetite is electronically conductive, charge transfer will still proceed but at a slower rate than on bare metal.

Acknowledgements - This study received partial funding through the NSERC, Motorola, ETI Industrial Research Chair held by R.W. Gillham. P.M.L. Bonin was supported by CRESTech through a Co-operative Research Scholarship. Part of this manuscript was presented at the 193rd Meeting of the Electrochemical Society in San Diego, California in May 1998.

4.6 References

1. R.W. Gillham and S.F. O'Hannesin, *Groundwater*, **32**, 958 (1994).
2. M.S. Odziemkowski, T.T. Schuhmacher, R.W. Gillham and E.J. Reardon, *Corros. Sci.*, **40**, 371 (1998).
3. P.M.L. Bonin, M. Odziemkowski and R.W. Gillham, *Corros. Sci.*, **40**, 1391 (1998).

4. V. Rives and M.A. Ulibarri, *Coordination Chemistry Reviews*, **181**, 61 (1999).

5. L. Ukrainczyk, M. Chibwe, T.J. Pinnavaia and S.A. Boyd, *Environ. Sci. Technol.*, **29**, 439 (1995).

6. W. Feitknecht and G. Keller, *Z. Anorg. Chem.*, **262**, 61 (1950).

7. P.P Stampfl, *Corros. Sci.*, **9**, 185 (1969).

8. J.D. Bernal, D.R. Dasgupta and A.L. Mackay, *Clay Min. Bull.*, **4**, 15 (1959).

9. R.M. Taylor, *Clay Miner.*, **15**, 369 (1980).

10. R.M. Taylor, *Clay Miner.*, **17**, 369 (1982).

11. E. Murad and R.M. Taylor, *Clay Miner.*, **19**, 77 (1984).

12. R.M. Taylor, *Clay Miner.*, **20**, 147 (1985).

13. E. Murad and R.M. Taylor, *Hyp. Int.*, 585 (1986).

14. H.C.B. Hansen, *Clay Minerals*, **24**, 663 (1989).

15. S.H. Drissi, Ph. Refait, M. Abdelmoula and J.M.R. Génin, *Corros. Sci.*, **37**, 2025 (1995).

16. M. Abdelmoula, Ph. Refait, S.H. Drissi, J.P. Mihe and J.M.R. Génin, *Corros. Sci.*, **38**, 623 (1996).

17. J.A. Bardwell, G.I. Sproule and M.J. Graham, in *Proceedings of the Symposium on Oxide Films on Metals and Alloys*, Proc. Vol. 92-22, eds. B.R. MacDougall, R.S. Alwitt and T.A. Ramanarayana. The Electrochem. Soc., Pennington, NJ (1992).

18. C.T Chen and B.D. Cahan, *J. Electrochem. Soc.*, **129**, 17 (1982).

19. M. Odziemkowski, M. Krell and D.E. Irish, *J. Electrochem. Soc.*, **139**, 3052 (1992).

20. N. Boucherit and A. Hugot-Le Goff, *Corros. Sci.*, **32**, 497 (1991).

21. N. Boucherit and A. Hugot-Le Goff, *Faraday Discuss.*, **94**, 137 (1992).

22. S. Simard, M. Odziemkowski, D.E. Irish, L. Brossard and H. Ménard, 191st Meeting of The Electrochemical Society, Montreal, Quebec. Meeting Abstracts, **97-1**, p.279 (1997).

23. M. Odziemkowski and R.W. Gillham, 213th ACS National Meeting, San Francisco, CA. Extended Abstracts, Division of Environmental Chemistry, **37**, p.177 (1997).

24. F. Trolard, J.-M.R. Génin, M. Abdelmoula, G. Bourrié, B. Humbert and A. Herbillon, *Geochim. Cosmochim. Acta*, **61**, 1107 (1997).

25. J.-M.R. Génin, G. Bourrié, F. Trolard, M. Abdelmoula, A. Jaffrezic, Ph. Refait, V. Maitre, B. Humbert and A. Herbillon, *Environ. Sci. Technol.*, **32**, 1058 (1998).

26. A.G. Brolo, M. Odziemkowski and D.E. Irish, *J. Raman Spectrosc.*, **29**, 713 (1998).

27. L.D. Burke, *Electrochim. Acta*, **39**, 1841 (1994).

28. M. Fontana and N. Greene, in *Corrosion Engineering*, p.325, McGraw-Hill Inc., New York (1978).

29. R.G. Herman, C.E. Bogdan, A.J. Sommer and D.R. Simpson, *Applied Spectroscopy*, **41**, 437 (1987).

30. J.B. Bates, M.H. Brooker, A.S. Quist and G.E. Boyd, *J. Phys. Chem.*, **76**, 1565 (1972).

31. A.R. Davis and B.G. Oliver, *J. Solution Chem.*, **1**, 329 (1972).

32. E.J. Reardon, R.D. Fagan, M.S. Odziemkowski, H.M. Peemoeller and M. Zhang, Geol. Soc. Amer. Annual Meeting, Toronto, Ontario, October 1998.

33. T.N. Moroz and D.K. Arkhipenko, *Soviet Geology and Geophysics*, No.2, 52 (1991).

34. T. Ohtsuka, K. Kubo and N. Sato, *Corrosion*, **42**, 476 (1986).

35. L.J. Oblonsky and T.M. Devine, *Corros. Sci.*, **37**, 17 (1995).

36. H. Kanno and J. Hiraishi, *J. Raman Spectrosc.*, **12**, 224 (1982).

37. K. Murata, D.E. Irish and G.E. Toogood, *Can. J. Chem.*, **67**, 517 (1989).

38. G. Herzberg, in *Molecular Spectra and Molecular Structure II. Infrared and Raman Spectra of Polyatomic Molecules*, NRC (1964).

39. R. Simpraga and B.E. Conway, in *Proceedings of the Symposium on Oxide Films on Metals and Alloys*, Proc. Vol. 92-22, eds. B.R. MacDougall, R.S. Alwitt and T.A. Ramanarayana. The Electrochem. Soc., Pennington, NJ (1992).

40. M Erbs, H.C.B. Hansen and C.E. Olsen, *Environ. Sci. Technol.*, **33**, 307 (1999).

5.0 ELECTROCHEMICAL AND RAMAN SPECTROSCOPIC STUDIES OF THE INFLUENCE OF CHLORINATED SOLVENTS ON THE CORROSION BEHAVIOUR OF IRON IN BORATE BUFFER AND IN SIMULATED GROUNDWATER

The following manuscript, accepted for publication in November 1999 by the journal Corrosion Science, covers the results of the Tafel plot and corrosion rate measurements performed in borate buffer and in aqueous solutions of potassium bromide and calcium carbonate. The results of the OCP-time and *in situ* Raman spectroscopy measurements in potassium bromide solutions are also included, as well as summary of the results of these experiments in borate buffer and in calcium carbonate solution.

5.1 Cover page

Electrochemical and Raman Spectroscopic Studies of the Influence of Chlorinated Solvents on the Corrosion Behaviour of Iron in Borate Buffer and in Simulated Groundwater

Pascale M.L. Bonin [1*], Wojciech Jędral [2], Marek S. Odziemkowski [1] and Robert W. Gillham [1]

[1] Department of Earth Sciences, University of Waterloo,
Waterloo, Ontario, Canada N2L 3G1

[2] Department of Chemistry, University of Warsaw
Pasteura 1, 02-093 Warsaw, Poland

Abstract - The remediation, by contact with granular iron, of groundwater contaminated with chlorinated halocarbons necessitates a flow of electrons at the iron/solution interface. To refine our understanding of the mechanism and kinetics of the charge transfer process, electrochemical and spectroscopic measurements were performed on iron electrodes in borate buffer and in simulated groundwater solutions of calcium carbonate and potassium bromide before and after exposure to carbon tetrachloride. The results of these measurements highlighted the combined influence of the organic contaminant and inorganic ions on the corrosion behaviour of iron as well as on the nature of the films formed in their presence.

Keywords: iron, borate buffer, calcium carbonate, potassium bromide, carbon tetrachloride, corrosion potential, corrosion rate, Raman spectroscopy, green rust, iron oxides.

5.2 Introduction

A remediation technology for groundwater contaminated with chlorinated aliphatic hydrocarbons is through contact with granular iron [1]. The degradation of halogenated compounds by iron involves oxidation of iron and reduction of the organic molecules. Though considerable research effort has focused on the degradation pathways and rates of reduction for different organic compounds [1-4], many aspects of the charge transfer reactions remain highly speculative. A useful approach to gain insight concerning the mechanism and kinetics of the electron transfer process may be to study the corrosion behaviour of iron under different conditions. This approach was taken in two studies of iron particles in contact with contaminant-free water of different ionic compositions [5,6]. In the first, Raman spectroscopy was used to identify the surface films formed on electrolytic iron particles during contact with simulated groundwater; in the second, corrosion rates were measured by monitoring the hydrogen pressure increase in sealed cells containing commercial iron granules and water.

The corrosion behaviour of iron was also considered in a study [7] where the granular iron/ contaminated groundwater system was simplified to an iron electrode/ borate buffer system in the presence of two model compounds: a degradable compound (carbon tetrachloride-CCl_4) and a non-degradable compound (dichloromethane-CH_2Cl_2). The potentiodynamic polarization of a stationary iron electrode indicated that CCl_4 acts as an oxidizer of iron, while CH_2Cl_2 is non-reactive (a non-oxidizer). The change of the open circuit potential (OCP) of the stationary iron electrode, freshly cathodically cleaned or pre-oxidized by immersion in borate buffer, was also monitored after the addition of CCl_4 or CH_2Cl_2. In both cases, a positive shift of potential was observed after the injection of CCl_4, while the injection of CH_2Cl_2 had no significant effect on

the potential. To gain insight concerning the changes at the interface after the addition of CCl_4, *in situ* Raman spectra of the electrodes were taken. An important advantage of Raman spectroscopy over other methods of surface analysis is its ability to analyze samples *in situ*; the Raman effect is, however, intrinsically weak [8]. In the case of pre-oxidized electrodes, the products of the surface redox reactions, as well as of the ions present in the double layer region, were identified. In the case of freshly cathodically cleaned electodes, however, the surface film, being in an initial stage of formation, was most probably too thin to be detected by Normal Raman spectroscopy (NRS).

In our previous study, CCl_4 was characterized as an oxidizer because its presence caused the corrosion potential, the corrosion current density and the cathodic Tafel slope to increase [1]. For a single reversible reaction (e.g., oxidation/reduction of copper in a highly concentrated acidic solution), the exchange current density can be used to determine the heterogeneous charge transfer rate constant for the reduction reaction. For complex irreversible reactions such as the oxidation/reduction of iron in a basic and/or low conductivity aqueous medium in the presence of CCl_4, this procedure cannot be applied. First, it is not possible to isolate the contribution of the contaminant reduction reaction to the overall cathodic current. Second, in the case of a weak acid (e.g., boric acid), dissociation of the acid will result in higher cathodic currents, while film formation on the electrode surface during anodic polarization will affect the slope of the anodic branch. Other factors will result in additional errors. For instance, when using an electrode of

[1] In our previous study, a decrease of the cathodic Tafel slope was reported. This is because we were not aware of the convention according to which Tafel slopes are to be expressed as absolute values. The decrease of negative values reported should therefore have been expressed as an increase in absolute values. We would like to thank the reviewers of this paper for indicating this convention to us.

large surface area, different parts of the electrode may perform in different ways. This effect will be enhanced by a long polarization time and a low conductivity solution. A solution of low conductivity may also introduce errors in the potential reading due to uncompensated solution resistance (R_u). On the other hand, using an electrode of smaller diameter will result in less precision in the measurements of R_u and current. A good compromise, for approximate measurements such as Tafel slopes in high pH solutions, may be to use a relatively large electrode over short times of polarization, and with IR drop compensation.

In a study of the Fe/borate buffer/CCl_4 system by Scherer et al., [9], it is advanced that near the corrosion potential in the presence of CCl_4, hydrogen evolution is not an important mechanistic intermediate in the reductive dechlorination of the contaminant. On "steady-state j-E curves" obtained in contaminant-free borate buffer and in the presence of CCl_4, the difference in current densities at E_{corr/CCl_4} was attributed to the reduction of CCl_4 and was used to calculate a charge transfer rate constant for the reduction of the chlorinated hydrocarbon. From these measured j-E curves, exchange current density and Tafel slope values for the Fe/Fe^{2+}, $H^+/H_{2(g)}$ and $CCl_4/CHCl_3$ redox couples were also determined. However, it is not clear how these single reaction kinetic parameters were calculated since the Fe/water/CCl_4 system involves three irreversible interdependant redox reactions. In addition, based on thermodynamic calculations and experimental data, it has been found that adsorbed hydrogen will be present at potentials well above the equilibrium potential for hydrogen evolution [10], and thus the assertion that hydrogen evolution is not an important intermediate step would seem to be in question. Finally, the kinetic parameter determinations could be in error since the study was performed without IR drop compensation on a large electrode and with very long polarization times.

The present study was undertaken to determine the kinetic parameters of the charge transfer reactions. The parameters considered included cathodic and anodic Tafel slopes and the corrosion current density, as well as the corrosion rate of iron and the resistance of the metal/solution interface. Our goal was also to refine our understanding of the mechanism of the charge transfer process at the iron/solution interface in borate buffer, in the case of a cathodically cleaned electrode after exposure to carbon tetrachloride, and to extend our investigation to simulated groundwater. More specifically, our objectives were to determine the influence of the organic molecules on the corrosion behaviour of iron, as well as their effect on the structure of the iron/solution interface. In order for the degradation reactions to proceed, there must be a flow of electrons at the iron/solution interface. Determination of the nature and electronic properties of surface films, present before or formed during exposure to contaminants, is therefore important in developing an understanding of the electron transfer process.

To achieve these objectives, Tafel plots and corrosion rates were measured in borate buffer and in aqueous solutions of potassium bromide and calcium carbonate with an iron rotating disk electrode (RDE). Measurements were possible in the low conductivity simulated groundwater by compensating for IR drop. OCP-time and *in situ* Raman measurements were also performed in aqueous solutions of potassium bromide. A summary of the results of OCP-time and *in situ* Raman measurements in borate buffer [7] and in calcium carbonate solution [11] will be provided for reference and comparison purposes.

5.3 Experimental methods

Four aqueous solutions were prepared from distilled water, using chemical grade reagents, and were deaerated with N_2 (except the calcium carbonate solution which was deaerated with a 5% CO_2 / 95% N_2 gas mixture). The four solutions included:

1) (0.15M H_3BO_3 + 0.0357M $Na_2B_4O_7$) borate buffer of pH 8.4;

2) 1.2×10^{-3}M $CaCO_3$ solution of pH 6.4 ± 0.2 after deaeration;

3) 3.4×10^{-4} M KBr solution of pH 7 ± 0.2 after dearation;

4) 3.4×10^{-4} M KBr solution with the pH, after deaeration, adjusted to 10 with KOH.

Solutions 3 and 4 will be referred to as the low and high pH KBr solutions, respectively. The $CaCO_3$ and KBr solutions were prepared to simulate dilute groundwater in carbonate and non-carbonate aquifers, respectively, while solutions of higher pH were intended to replicate conditions in batch and column experiments with granular iron [1-5], where pH values above 9 are commonly observed.

Open circuit potential-time and *in situ* Raman measurements were performed using a 5 mm diameter 99.99% pure iron disk pressed into a Kel-F holder. The working iron electrode was stationary. The auxiliary electrode was platinum. Potentials were measured against a Ag/AgCl electrode and then converted to NHE. Prior to each experiment, the iron electrode was polished with 1200 grade emery paper, washed in copious amounts of distilled water, and ultrasonically cleaned in distilled water. The iron electrode was then immersed in one of the 4 deaerated aqueous solutions and cathodically cleaned by applying a current density of 100 $\mu A/cm^2$ for 15 minutes. In the Tafel plot and corrosion rate measurements, the working electrode consisting of a

¼ inch diameter 99.99% pure iron disk pressed into a Kel-F holder was a rotating disk. The auxiliary and reference electrodes were platinum and Ag/AgCl. Prior to each experiment, the iron RDE was cleaned following a procedure similar to that used for the stationary electrode, the only differences being that it was also polished with a felt polishing cloth using 1 μm alumina powder suspensions and ultrasonically cleaned in methanol.

Open circuit potential-time and *in situ* Raman measurements were performed following a procedure described by Bonin et al. [7]. The OCP of the iron electrode was monitored over time using a high impedance (10^{14} ohm) preamplifier. *In situ* Raman spectra were obtained with a Renishaw 1000 Raman microscope system set-up in non-confocal mode. The chlorinated hydrocarbon (pure phase CCl_4 or CH_2Cl_2) was injected into the deaerated aqueous solutions via a Teflon septum covering the injection port of the electrochemical or Raman cell.

The Tafel plot and corrosion rate measurements were carried out using a Model 273 PAR potentiostat, interfaced to an IBM PC computer via an IEEE-488 interface. Software written in house based on Head Start© architecture was used for data acquisition and potentiostat control. The RDE was installed in an Analytical Rotor (PINE Instruments Company) and set at a rotation speed of 3000 rpm. At such speed, it has been found that mass transport effects are negligible [9]. The experiments were performed with IR drop compensation, using the current interrupt technique described in the instruction manual of the Model 273 PAR potentiostat. The Luggin capillary was shaped and positioned in a way such as to minimize the uncompensated solution resistance (R_u). The chlorinated hydrocarbon (pure phase CCl_4) was introduced into the

deaerated aqueous solutions by flushing the cell with a CCl_4-saturated argon gas, starting 15 minutes prior to the beginning and during the experiments.

The Tafel plot measurements were performed by applying 3 sets of 10 pulses of cathodic current, followed by 3 sets of 10 anodic pulses. Each pulse had a duration of 0.2 s. In the first set, the magnitude of the pulses increased from ≈20 to 200 μA and the electrode was allowed to rest at its OCP for about 4 s between each pulse. In the second set, the magnitude of the pulses increased from ≈200 μA to 2 mA and the rest period lasted 5 s; in the third set, the magnitude of the pulses increased from ≈2 to 20 mA and the rest period was 7 s. In total, it took less than 3 minutes to complete the measurement of one Tafel branch (cathodic or anodic). During each pulse, the electrode potential, corrected for IR drop, was sampled 50 times and the values corresponding to the last 15 sampled points were averaged and used to construct a Tafel plot [12].

The corrosion rate measurements were performed by applying 10 pulses of current, lasting 10 s each, going from cathodic to anodic currents. Between the pulses, the electrode was allowed to rest at its OCP for 35 s. Each measurement took about 7 minutes. During each pulse, the electrode potential was sampled 50 times and the values corresponding to the last 15 sampled points were averaged and used to construct a current-potential plot. The upper and lower current limits in this train of current steps were chosen in such a way that the electrode potential did not deviate more than 10 mV from the corrosion potential (OCP). Under these conditions, the polarization current (pulse amplitude) did not deviate far from the corrosion current.

Consequently, the current-voltage curves were linear and the corrosion current was calculated using the linear approximation of the Butler-Volmer equation [12]:

$$J=J_o\,(-nF/RT)\,\eta \qquad (1)$$

where J is the cell current density

J_o is the corrosion current density

n is the number of electrons (n=2 for iron)

F is the Faraday constant

R is the universal gas constant

T is the temperature

η is the overpotential i.e., $E - E_{corr}$

The corrosion rates, expressed in nm/h, were calculated from J_o using the formula:

$$CR\,(nm/h) = \frac{J_o\,(A/cm^2) \times 55.85\,(g/mol) \times 3600\,(s/h) \times 10^7(nm/cm)}{2 \times 96487\,(C/mol) \times 7.86\,(g/cm^3)} \qquad (2)$$

In the corrosion rate measurements, an average value for the uncompensated solution resistance was first determined and then used to program the potentiostat for the subsequent measurements. R_u was determined by applying a cathodic current pulse (0.05 to 0.1 mA) of a few seconds to the iron electrode followed by a zero current pulse of a few seconds. During each pulse, the current

was interrupted about 1000 times, the value of iR_u was measured and the corresponding R_u was calculated.

5.4 Results and Discussion

5.4.1 Open circuit potential-time measurements on stationary iron electrodes

OCP-time experiments were performed in borate buffer and in simulated groundwater. For the low and high pH KBr solutions, the results are presented in Figures 5.1 and 5.2 and summarized in Table 5.1; for the borate [7] and calcium carbonate [11] solutions, the results are summarized in Table 5.1. In a first set of experiments, the OCP of a cathodically cleaned iron electrode was monitored prior to and after the injection of CCl_4 or CH_2Cl_2. In all the solutions, the injection of CCl_4 resulted in a positive shift of potential; the largest shifts were observed in the KBr solutions (Table 5.1, and curves 1 on Figures 5.1 and 5.2). On the other hand, the injection of the non-degradable compound had no significant effect on the potential (Table 5.1, and curves 2 on Figures 5.1 and 5.2).

In a second set of experiments, the iron electrode was kept immersed in contaminant-free solutions for periods ranging from 17 to 70 h. Immersion of the Fe electrode resulted in its pre-oxidation and probably in the formation of ferrous hydroxide [13,14]. Due to its sensitivity to oxidation and its amorphous structure [15], $Fe(OH)_2$ is difficult to identify by most surface analytical techniques including NRS. The only normal Raman spectral evidence of this compound was obtained on synthesized material in an *ex situ* study by Thanos [15]. Identification of ferrous hydroxide by SERS has, however, been reported by many authors [5,16-18]. Upon introduction of an oxidizer such as CCl_4, the pre-oxidized Fe surface acted as a catalyst in the sense that it promoted faster and further oxidation of the iron electrode and/or the

$Fe(OH)_2$ film covering the electrode surface. Indeed, the potential shifts when the electrodes were pre-oxidized were larger and more rapid (Table 5.1, and curves 3 on Figures 5.1 and 5.2). The magnitude of the shift increased with longer duration of immersion. Subsequent potential declines were observed in all the pre-oxidation experiments. These declines may have been a consequence of a change in impedance of the metal/solution interface.

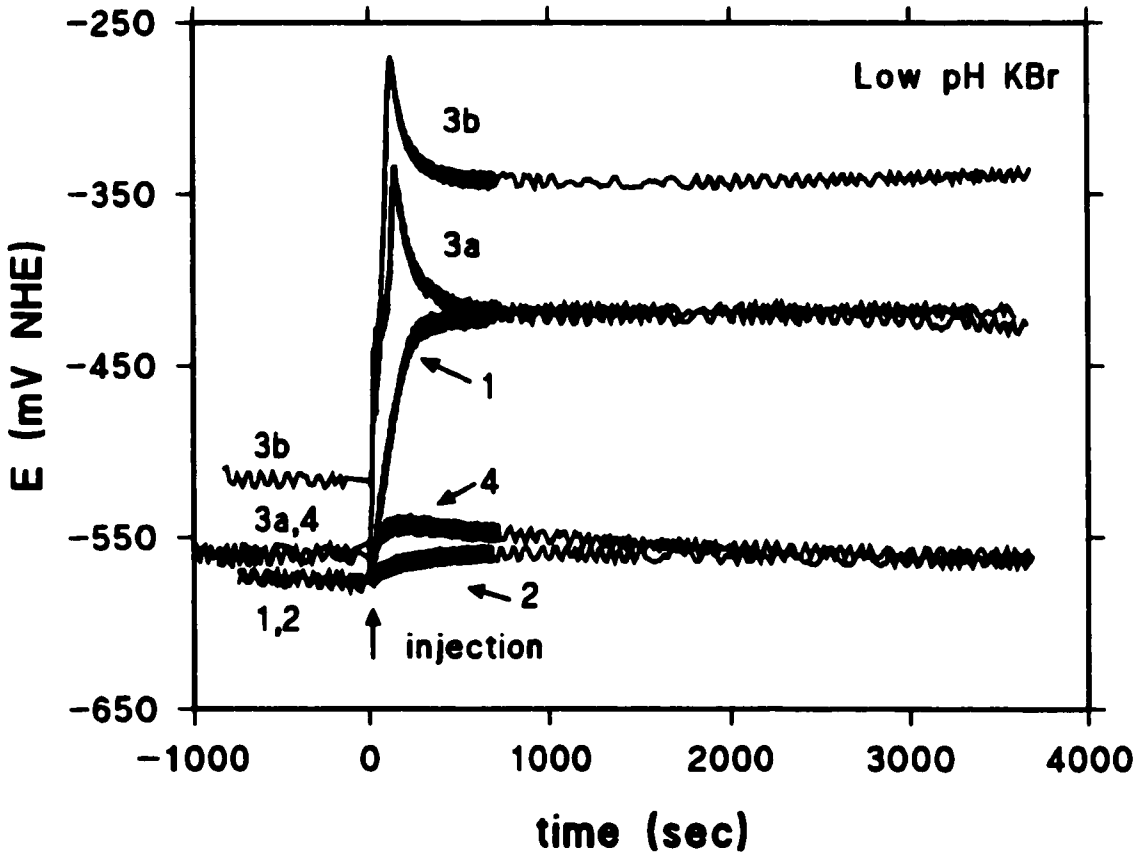


Figure 5. 1 Open circuit potential-time measurements in low pH KBr solution. 1) injection of CCl_4 - electrode freshly cleaned; 2) injection of CH_2Cl_2 - electrode freshly cleaned; 3a) injection of CCl_4 - electrode immersed for 17 h; 3b) injection of CCl_4 - electrode immersed for 70 h; 4) injection of CH_2Cl_2- electrode immersed for 17 h.

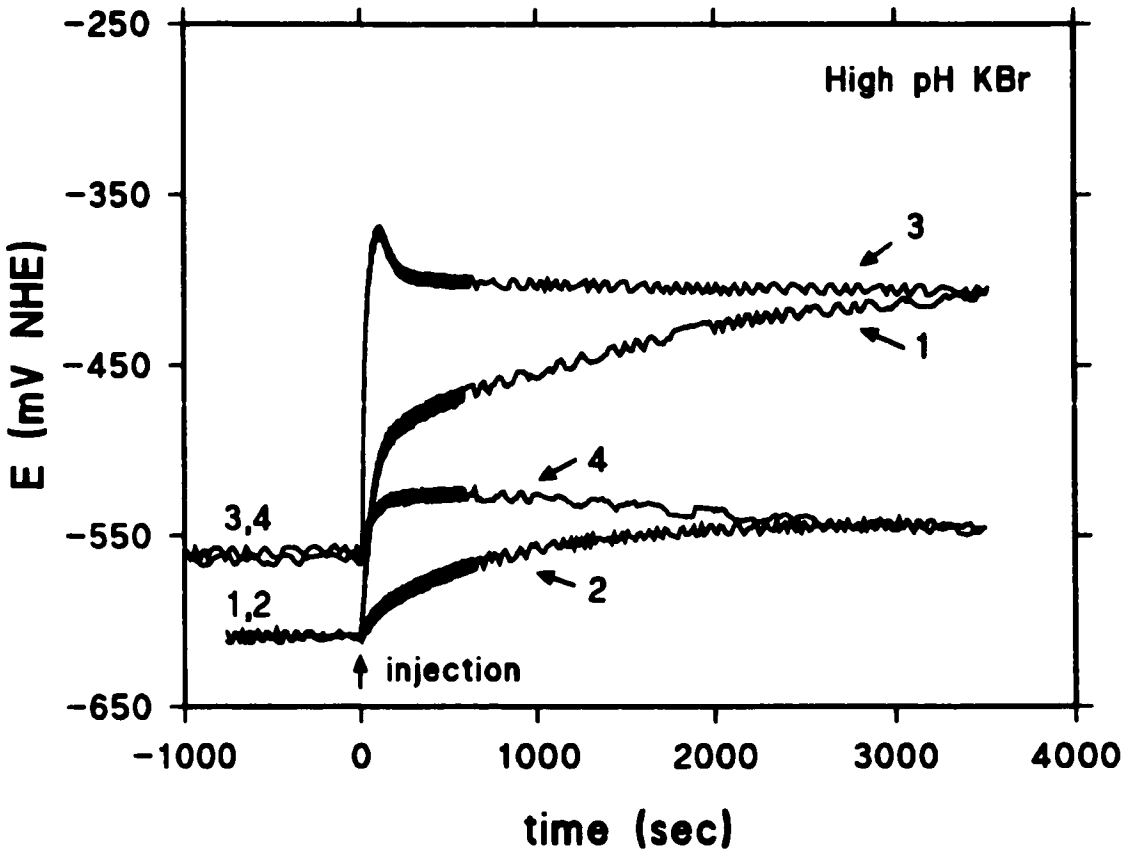


Figure 5. 2 Open circuit potential-time measurements in high pH KBr solution. 1) injection of CCl_4 - electrode freshly cleaned; 2) injection of CH_2Cl_2 - electrode freshly cleaned; 3) injection of CCl_4 - electrode immersed for 17 h; 4) injection of CH_2Cl_2- electrode immersed for 17 h.

In all the solutions, a potential drift was observed during the immersion time in contaminant-free solution (Table 5.1). In borate buffer and in the potassium bromide solutions, the drifts were positive and might be attributed to increases of Fe^{2+} ions in the solutions [7]. These positive drifts may also be due to the oxidizing action of O_2 which, even if precautions were taken to properly seal the cell and if deaeration was pursued during the experiments, may have been present in minute amount in the solutions. The largest drifts were again observed in the KBr solutions. In the calcium carbonate solution, the potential drift was negative, possibly related to a local change of pH in the vicinity of the electrode [11]. Finally, as observed in borate buffer, the

effect of the injection of CH_2Cl_2 after 17 h of immersion in the potassium bromide solutions was similar to the background potential drift (curves 4 on Figures 5.1 and 5.2).

Table 5. 1 OCP-time measurements, on freshly cathodically cleaned and pre-oxidized iron electrodes, in the 4 solutions (all potentials in mV NHE).

OCP of freshly cathodically cleaned iron electrodes in mV NHE

Solution	Contaminant free	After injection of CCl_4		After injection of CH_2Cl_2	
	$E_{at\ t=0}$	$E_{at\ t=1h}$	Potential shift	$E_{at\ t=1h}$	Potential shift
Borate	-540	-460	80	-530	10
$CaCO_3$	-540	-460	80	---	---
Low pH KBr	-570	-420	150	-560	10
High pH KBr	-610	-410	200	-540	70

OCP of pre-oxidized iron electrodes in mV NHE

Solution and time Of immersion	Contaminant free		After injection of CCl_4			
	$E_{after\ imm.}$	Potential Drift	E_{max}	Potential Shift	$E_{at\ t=1h}$	Potential Decline
Borate – 24 h	-530	10	-330	200	-420	-90
Borate – 68 h	-530	10	-280	250	-410	-130
$CaCO_3$ –17 h	-560	-20	-400	160	-440	-40
Low pH KBr – 17 h	-560	10	-330	230	-420	-90
Low pH KBr – 70 h	-520	50	-270	250	-330	-60
High pH KBr –17 h	-560	50	-370	190	-410	-40

5.4.2 *In situ* Raman measurements on stationary iron electrodes

In order to investigate the nature of the changes at the iron/solution interface after exposure to carbon tetrachloride, *in situ* Raman measurements were performed on the iron electrodes pre-oxidized in borate buffer and in simulated groundwater, prior to and 1 hour after the injection of CCl_4. A summary of the Raman bands observed in all the solutions is presented in Table 5.2, while the spectra obtained in the low and high pH KBr solutions are shown in Figures 5.3 and 5.4, respectively.

Prior to the injection of carbon tetrachloride, in the case of an iron electrode pre-oxidized for 70 h in the low pH KBr solution, the majority of the surface was free of Raman features except for the presence of a weak band at 672 cm^{-1}, which is attributed to the A_{1g} mode of magnetite (spectrum a, Figure 5.3).

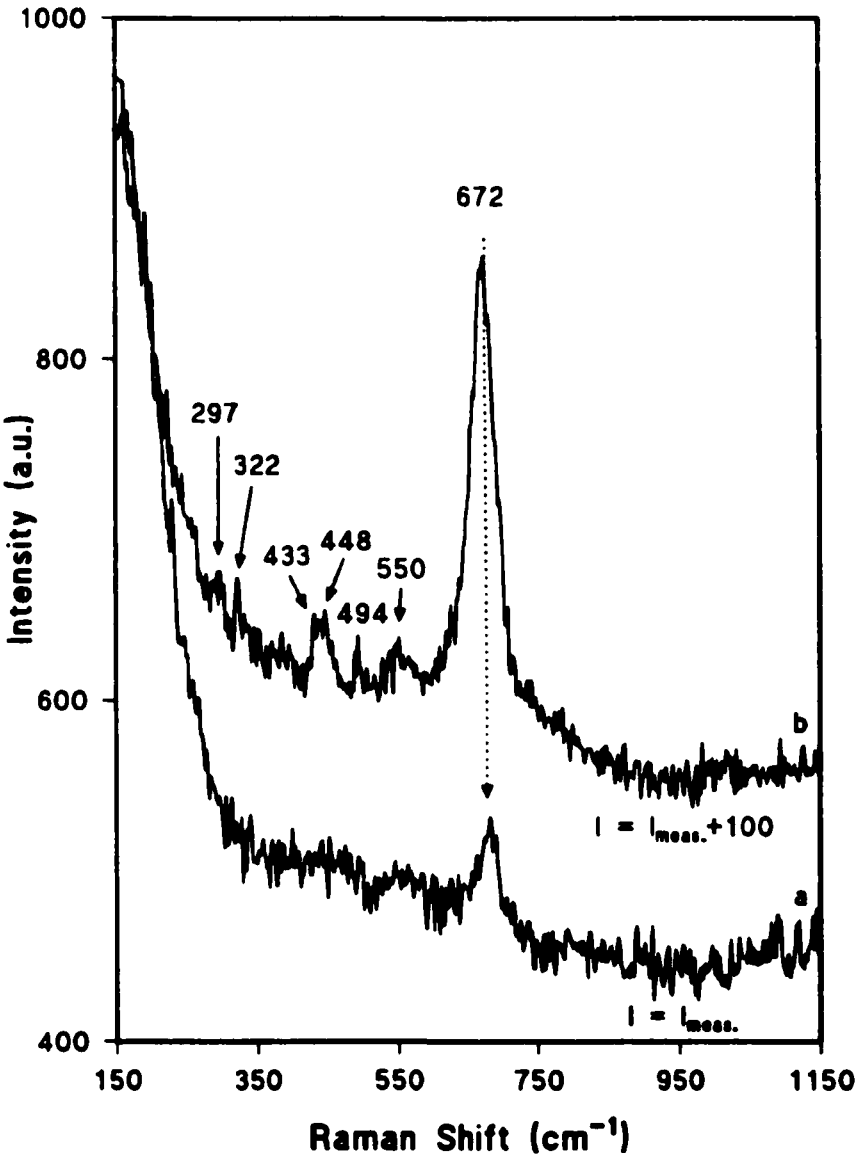


Figure 5. 3 *In situ* Raman spectra of the Fe surface pre-oxidized for 70 h in low pH KBr solution, before (a) and after (b) the injection of CCl_4.

Spectrum b (Figure 5.3) was recorded one hour after the injection of CCl_4 (Table 5.2). The signal of the band at 672 cm^{-1} was then much stronger and two additional bands, at 297and 550 cm^{-1}, assigned to the T_{2g} mode of magnetite, were also observed.

Table 5. 2 Raman bands (in cm^{-1}) observed on pre-oxidized iron electrodes, after the injection of CCl_4, in the 4 solutions.

Borate 24 h	Borate 68 h	$CaCO_3$ 17 h	KBr low pH 70 h	KBr high pH 17 h	Band Assignment	RF
		1084			Internal vibration of carbonate ions in calcite (A_{1g} mode)	19
		1053-1057			Symmetric stretch of carbonate ions in green rust structure	20,21
878	878				Symmetric strech of borate ions	18
669	668		672	675-679	Magnetite (A_{1g} mode) [a]	22,23
547	546		550		Magnetite (T_{2g} mode) [b]	22,23
		509		507-513	Fe^{3+}-OH stretching mode of green rust	24-26
495	495	496	494		Vibration of Fe^{3+}-OH_2 (A_{1g} mode) in $[Fe^{III}(OH)_n(H_2O)_{6-n}]^{3-n}$ ions	27
	479				α - FeOOH	28,29
466					$Fe(OH)_2$	15
454	449	456	448		Vibration of Fe^{3+}-OH_2 (E_g mode) in $[Fe^{III}(OH)_n(H_2O)_{6-n}]^{3-n}$ ions	27
442	425-434		433		Vibration of Fe^{2+}-OH or Fe^{2+}-OH_2 in $[Fe^{II}(OH)_n(H_2O)_{6-n}]^{2-n}$ ions	16
		433		431	Fe^{2+}-OH stretching mode of green rust	24-26
391	390	381		385	Strongest mode of α - FeOOH	28,29
		322	322		Deformation vibration of H_2O-Fe^{3+}-OH_2 in $[Fe^{III}(OH)_n(H_2O)_{6-n}]^{3-n}$ ions [c]	27
				318	Fe-Cl stretches of $[Fe(H_2O)_5Cl]^{2+}$ or $[Fe(H_2O)_4Cl_2]^{+}$ ions	27,30
			297		Magnetite (T_{2g} mode)	22,23
		281			Lattice vibration of calcite (E_g mode)	19
				250	α - FeOOH	28,29
		153			Lattice vibration of calcite (E_g mode)	19

(a) The higher frequency of this band, in the high pH KBr solution, might be due to a contribution from $Fe(OH)_3$ [31].

(b) The higher frequency of this band might be due to a contribution of the strongest mode of $Fe(OH)_2$ [15].

(c) This band might also be attributed to Fe-Cl stretches of $[Fe(H_2O)_5Cl]^{2+}$ or $[Fe(H_2O)_4Cl_2]^{+}$ ions [27,30].

The bands at ca. 448 and ca. 494 cm^{-1} do not correlate with any known iron oxide, hydroxide or oxyhydroxide species [16]. These bands, which were also observed in borate buffer and in calcium carbonate solution after exposure to CCl_4, are attributed to the E_g and A_{1g} stretching vibrations of Fe^{3+}- OH_2 in the double layer species $[Fe(H_2O)_6]^{3+}$. These ions are the products of the hydration of Fe^{3+}, which results from the oxidation of Fe^{2+} produced by the corrosion processes. Assignment of the band at 433 cm^{-1} is less certain. It can be attributed either to the stretching mode of Fe^{2+} - OH_2 [16] or Fe^{2+} - OH in $[Fe(H_2O)_6]^{2+}$ ions, as in borate buffer [7], or to the Fe^{2+}- OH stretching mode of green rust [24-26], as in calcium carbonate solution [11]. In the latter case, however, a band at 509 cm^{-1}, assigned to the Fe^{3+}- OH stretching mode of green rust, was also observed; this band is not present on Figure 5.3. Finally, the band at 322 cm^{-1} might be attributed to the deformation vibration of H_2O - Fe^{3+}- OH_2 in $[Fe(H_2O)_6]^{3+}$ ions. Alternatively, it might be assigned to Fe-Cl vibrations in the instance where one or more water molecules in the cation complexes are replaced by chloride ions, produced by the degradation of CCl_4.

In the high pH KBr solution, after 17 h of immersion and before the injection of CCl_4, either no bands or 3 very weak bands were identified on the electrode (spectrum a, Figure 5.4). The bands at 431 and 513 cm^{-1} are assigned to the Fe^{2+}- OH and Fe^{3+}- OH stretching modes of green rust respectively, while the band at 385 cm^{-1} is attributed to the strongest mode of α-FeOOH. Green rusts are Fe^{2+}-Fe^{3+} layered double hydroxide compounds consisting of positively-charged brucite-like layers separated by interlayers of anions [32]. In the present case, hydroxyl anions are probably occupying the interlayer region; if bromide ions were present, a band at wavenumber lower than 200 cm^{-1} would be expected [33].

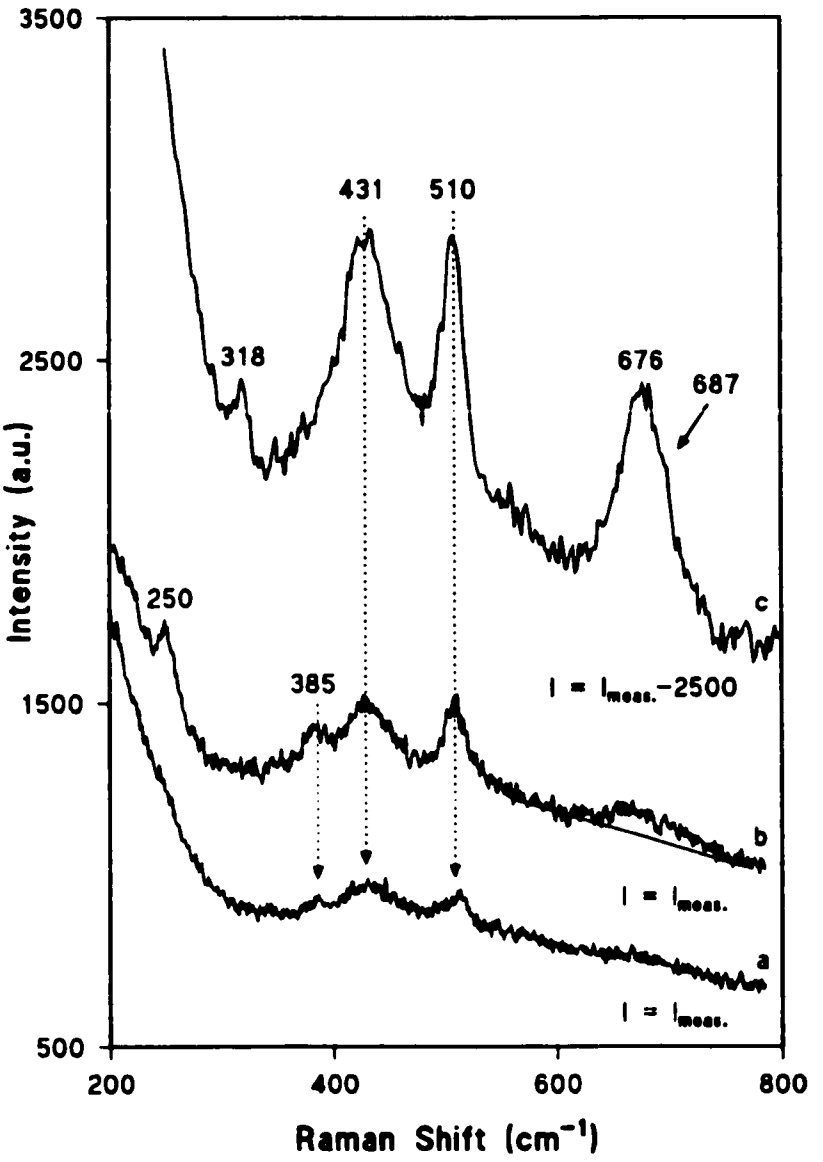


Figure 5. 4 *In situ* Raman spectra of the Fe surface pre-oxidized for 17 h in high pH KBr solution, before (a) and at two different locations after (b,c) the injection of CCl_4.

Spectrum b (Figure 5.4) was recorded one hour after the injection of CCl_4 (Table 5.2). It should be noted that, due to the injection procedure itself, it is difficult to obtain consecutive spectra from precisely the same location. Nevertheless, in this case, stronger signals of the 3 bands present before the injection of the contaminant were detected. In addition, another band indicative of the presence

of α-FeOOH on the surface of the electrode was observed at 250 cm^{-1}. Finally, a very broad, asymmetric band in the 650-750 cm^{-1} spectral range was also detected. Its deconvolution indicated the existence of two bands under the envelope (lower portion of Figure 5.5). The first band, attributed to the A_{1g} mode of magnetite, was fitted by fixing the full width at half maximum (FWHM) at 38 cm^{-1}; for natural magnetite, FWHM values of 34 to 42 cm^{-1} have been reported [22,23]. For the second band, a fit was obtained by fixing the center at 692 cm^{-1}; such a value is characteristic of $Fe(OH)_3$ [31].

Spectrum c (Figure 5.4) was also recorded one hour after the injection of CCl_4, but at a different location on the electrode surface (Table 5.2). The bands at 431 and 510 cm^{-1} are assigned to the Fe^{2+}- OH and Fe^{3+}- OH stretching modes of green rust respectively. Again, the green rust probably contains hydroxyl ions in the interlayers since no Br^- peak was detected. The band at 318 cm^{-1} is attributed to Fe-Cl stretches of $[Fe(H_2O)_5Cl]^{2+}$ or $[Fe(H_2O)_4Cl_2]^+$ ions [27,30]. Alternative assignment of the band at 318 cm^{-1} to the deformation vibration of H_2O - Fe^{3+}- OH_2 in $[Fe(H_2O)_6]^{3+}$ ions is not considered here; concurrent presence of bands at ca. 448 and ca. 494 cm^{-1}, attributed to the E_g and A_{1g} stretching vibrations of Fe^{3+}- OH_2, would then be expected. Finally, the broad, asymmetric band at 676 cm^{-1} is attributed to the A_{1g} mode of magnetite with a contribution from $Fe(OH)_3$, as expressed by the shoulder at 687 cm^{-1}. Deconvolution of this band confirmed the existence of two peaks (upper portion of Figure 5.5). Both were fitted without fixing any parameters. For the magnetite band, the calculated FWHM of 42 cm^{-1} is in very good agreement with literature data [22,23].

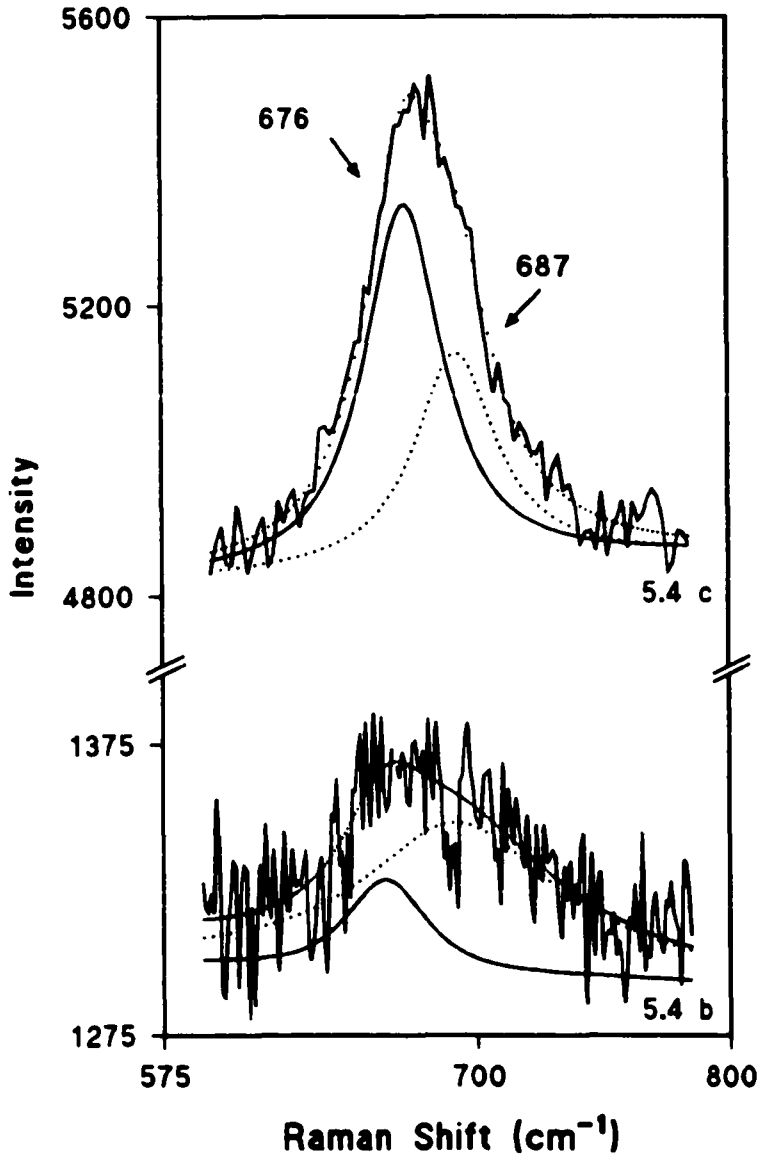


Figure 5. 5 Bandfitting of the *in situ* Raman spectra of the Fe surface pre-oxidized for 17 h in high pH KBr solution after the injection of CCl_4. Lower portion of the figure: spectrum 5.4(b); upper portion: spectrum 5.4(c).

Band fitting of spectra obtained at other locations on the electrode in the high pH KBr solution (not shown here) gave similar results; on each spectrum, a band at 675 to 679 cm^{-1}, having a FWHM ranging from 42 to 51 cm^{-1}, was present. These values, being outside the FWHM ranges reported for natural magnetite, indicate that Fe_3O_4 and $Fe(OH)_3$ were present in each case. On the

other hand, in the low pH KBr solution, the FWHM values observed for the strongest peak of magnetite were always within the range of values for natural magnetite, suggesting that magnetite is the sole product of the surface redox reactions in that solution.

5.4.3 Tafel plot measurements on iron rotating disk electrodes

The results of the Tafel plot measurements performed on the iron RDE in borate buffer (Figure 5.6) confirmed the trends previously reported [7]. In the presence of 2.7×10^{-3} M CCl_4, the corrosion potential increased from –460 to –340 mV, the corrosion current density increased from 0.03 to 0.04 mA/cm^2 and the cathodic Tafel slope increased (from 290 to 340 mV/decade).

Due to their very low conductivity, attempts to measure Tafel slopes in the two KBr solutions were not successful; however, a Tafel plot was measured in the calcium carbonate solution (Figure 5.7). In the presence of 5.3×10^{-3} M CCl_4, there was a positive shift of the corrosion potential (from –500 to –370 mV), an increase in the corrosion current density (from 0.05 to 0.11 mA/cm^2) and an increase in the cathodic Tafel slope (from 320 to 350 mV/decade).

Due to effects related to R_u, the magnitude of the Tafel slopes reported for the borate and calcium carbonate solutions should not be used as a precise source of quantitative information. What is informative, however, is the fact that increases of cathodic Tafel slopes were observed in both solutions, after the introduction of the contaminant, and that these increases were not accompanied by significant changes of uncompensated solution resistance in either solutions.

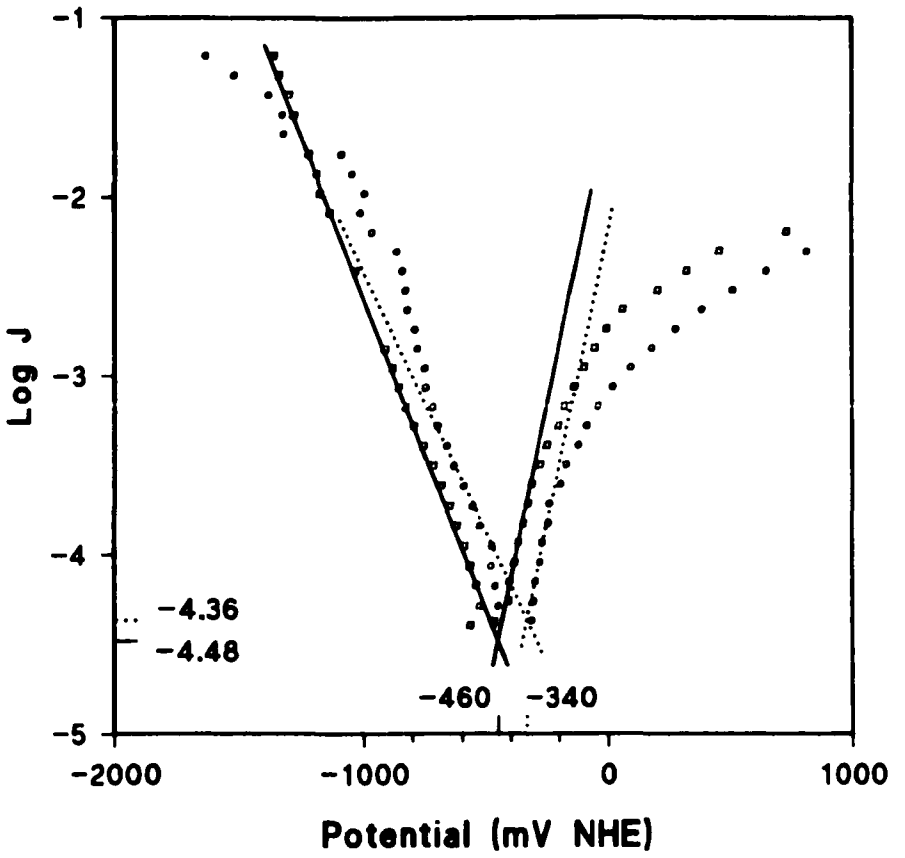


Figure 5. 6 Tafel plot in borate buffer, before (❑, ——) and after (❍, -----) the injection of CCl_4.

The corrosion current density values extrapolated from the Tafel plots were used to calculate iron corrosion rates, with the help of formula 2. Due to the fact that the Log J-Potential curves are possibly not at steady state and that the Tafel behaviour on the anodic side is valid for a very small range in current, one has to keep in mind that these values are very approximate. In contaminant-free solution, the presence of carbonate ions resulted in a higher corrosion rate (68 nm/h) than in borate buffer (44 nm/h), as expected [34]. In the presence of CCl_4, the corrosion rates increased to 149 and 58 nm/h, respectively. The magnitude of these increases was related to the amount of contaminant in solution, $5.3x10^{-3}$ M of CCl_4 in $CaCO_3$ solution, compared to $2.7x10^{-3}$ M in borate buffer.

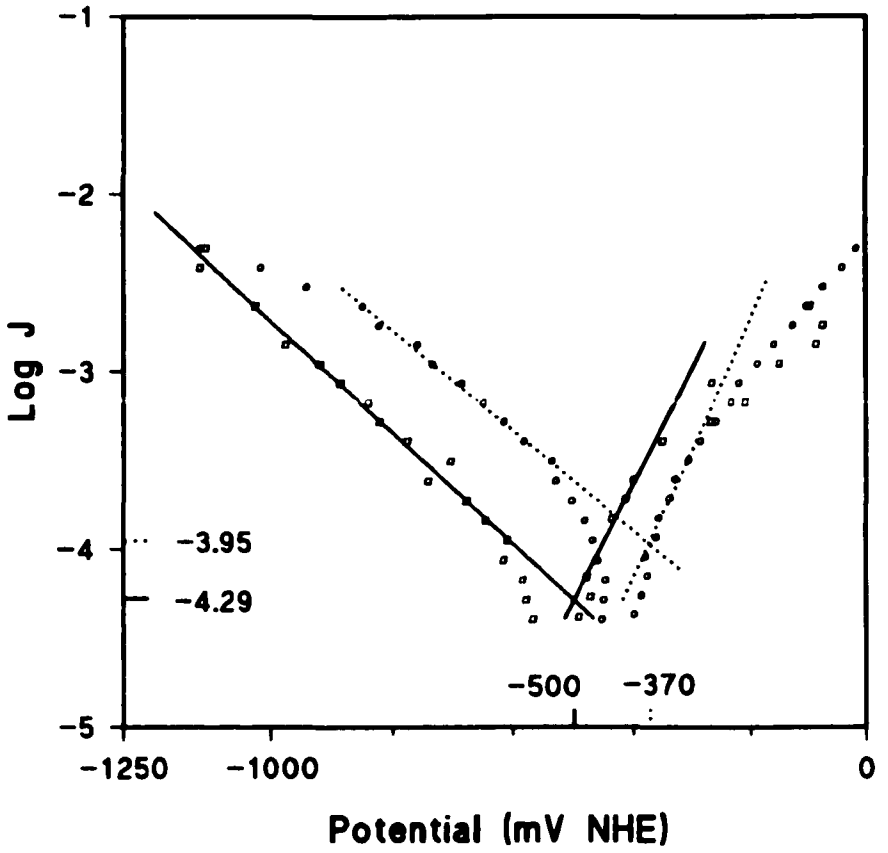


Figure 5. 7 Tafel plot in calcium carbonate solution, before (❑, ——) and after (❍, -----) the injection of CCl_4.

5.4.4 Corrosion rate measurements on iron rotating disk electrodes

Failure to measure Tafel slopes in the two potassium bromide solutions prompted the use of another technique to determine the kinetic parameters in these solutions, and to probe the borate and calcium carbonate systems with more precision. In this technique, current-steps resulting in overpotentials of ±10 mV from the corrosion potential are applied such that the system quasi-equilibrium is maintained, and the overpotential vs current response is linear. The corrosion current density, which is determined from the slope of this line, is used to calculate the iron corrosion rate.

The results of the corrosion rate measurements in borate buffer and in calcium carbonate solution (Table 5.3) are consistent with the results of the Tafel plot measurements. In contaminant-free solution, the presence of carbonate ions resulted in a higher corrosion rate (11.6 nm/h) than in borate buffer (3.0 nm/h). In both solutions, the corrosion potential shifted positively and the corrosion current density increased in the presence of CCl_4. This translated to iron corrosion rates of 26.4 and 5.3 nm/h, respectively. The magnitude of these increases was related to the amount of contaminant in solution, $5.3x10^{-3}$ M of CCl_4 in $CaCO_3$ solution, compared to $3.4x10^{-3}$ M in borate buffer. The uncompensated solution resistance, 3.0 kΩ in $CaCO_3$ solution and 0.2 kΩ in borate buffer, was not affected by the addition of the contaminant.

Table 5. 3 Corrosion rate measurements in the 4 solutions.

Solution		# of data	E_{corr} (mV NHE)		CR (nm/h)		R_u (kohm)	
			Mean	Std Dev.	Mean	Std Dev.	Mean	Std Dev.
Borate	Contaminant free	5	-489	7	3.0	0.2	0.2	0.002
	$3.4x10^{-3}$ M of CCl_4	9	-411	5	5.3	0.9	0.2	0.002
$CaCO_3$	Contaminant free	13	-520	3	11.6	1.1	3.0	0.03
	$5.3x10^{-3}$ M of CCl_4	6	-422	3	26.4	1.3	3.0	0.01
Low pH KBr	Contaminant free	4	-500	1	2.0	0.2	13.7	0.3
	$5.6x10^{-3}$ M of CCl_4	5	-148	25	1.0	0.2	15.8	0.7
High pH KBr	Contaminant free	6	-525	7	0.56	0.03	7.0	0.2
	$4.2x10^{-4}$ M of CCl_4	5	-30	15	0.30	0.03	9.0	1.2

The corrosion rates obtained from these measurements are smaller, by a factor of 10 in borate buffer and 5 in calcium carbonate solution, than those calculated from the Tafel plots. The higher corrosion rates obtained in the Tafel plot measurements are however an artifact due to the

formation of a film on the iron electrode during anodic polarization. The presence of this film affects the slope of the anodic branch, which in turn affects the determination of the intersection between the cathodic and anodic branches and therefore the value of the corrosion potential and corrosion rate. A confirmation of the presence of a film on the electrode after large anodic polarization during the Tafel plot measurements comes from the results of the OCP measurements. In contaminant-free borate buffer, the open circuit potential was more negative for a freshly cathodically cleaned electrode (-540 mV NHE) than for a pre-oxidized electrode (-530 mV NHE). Similarly, in contaminant-free borate buffer, the corrosion potential was more negative in the corrosion rate measurements (-489 mV NHE) than in the Tafel plot measurements (–460 mV NHE). Finally, in the OCP measurements, the addition of CCl_4 to the borate buffer resulted in a smaller shift of potential for a clean electrode (+80 mV NHE) than for an oxidized electrode (+200 mV NHE); the same trend was observed in the corrosion rate and Tafel plot measurements where the shifts were +78 and +120 mV, respectively.

Another factor that might explain the difference between the corrosion rate values obtained from the two methods is that the inaccuracy of the R_u value has a smaller influence on the results from corrosion rate measurements than from Tafel plot measurements. In low conductivity solutions, the values obtained from corrosion rate measurements are therefore more accurate.

In the low and high pH KBr solutions, prior to the introduction of CCl_4, the corrosion rates were 2.0 and 0.56 nm/h, respectively (Table 5.3). These rates are smaller than in borate and carbonate solutions. This is contrary to what one would expect since bromide ions are considered to be aggressive anions [35], while borate and carbonate ions are characterized as passivating anions

[34]. This might be due to the presence of a film on the electrode surface prior to the measurements and despite the cathodic cleaning procedure. Indeed, after immersion and before the injection of CCl_4, the presence of magnetite was detected in the low pH KBr solution, while green rusts and iron oxyhydroxides were detected in the high pH solution. No evidence of such films was obtained, with NRS, in borate and calcium carbonate solution prior to the injection of the contaminant.

In the two KBr solutions, the introduction of the contaminant resulted in the apparent passivation of the electrode. In the low pH KBr solution, following exposure to 5.6×10^{-3} M of CCl_4, the corrosion potential shifted drastically in the positive direction (to −148 mV NHE) and the corrosion rate decreased (from 2.0 to 1.0 nm/h). This is not due to a higher concentration of dissolved CCl_4 in that solution since the corrosion rate also decreased (from 0.56 to 0.3 nm/h) in the presence of a much smaller concentration of contaminant (4.2×10^{-4} M of CCl_4) in the higher pH solution. Rather the apparent passivation was due to the nature and/or thickness of the film on the surface of the electrode after exposure to the oxidizer. For the two KBr solutions, the R_u increased in the presence of CCl_4 (from 13.7 to 15.8 kΩ and from 7.0 to 9.0 kΩ, respectively). The uncompensated solution resistance is the sum of the solution resistance and the resistance of the metal/solution interface (i.e., surface films and double layer region). In all the solutions, it is reasonable to assume that the solution resistance was constant throughout the experiments i.e., that there was no significant iron and/or contaminant dissolution in the time frame of the experiments (7 minutes). Therefore, the increases in R_u corresponded to increases in the resistance of the metal/solution interface, which is probably connected with film formation on the electrode surface, as suggested by the Raman spectral studies.

In summary, it appears that in contaminant-free solution, the anions have the following effect on the corrosion rate: carbonate > borate > bromide at open-circuit potential in these solutions. A similar trend was observed by Reardon [6]. It is worth noting that the corrosion rates of the iron electrode obtained here in contaminant-free solutions (ranging from 0.56 to 11.6 nm/h) are about 5 orders of magnitude greater than the rates for commercial iron granules in different saline solutions reported by Reardon [6]. These very significant differences are due to the fact that commercially-produced iron granules, which are made of various unknown mixtures of low alloyed scrap steel, are covered by a thick heterogeneous oxide layer [24] as a result of the thermal treatment during the production process.

5.5 Conclusion

In borate buffer and in calcium carbonate solution, the corrosion rate increased and the resistance of the metal/solution interface stayed constant in the presence of carbon tetrachloride. This is in agreement with the fact that there was no spectral evidence of the presence of a film, prior to the injection of the contaminant, on the iron electrodes pre-oxidized in these solutions. After exposure to the contaminant, magnetite and hydrated magnetite [$Fe(OH)_2 \bullet 2FeOOH$] were identified as the final products of the surface redox reactions in borate buffer; carbonate-containing green rust complexes were detected in the calcium carbonate solution. Upon aging of the film, hydrated magnetite might convert to magnetite. Since magnetite and green rust are not protective, charge transfer and reductive dechlorination will continue to proceed, but at a slower rate than on the bare metal surface. From a technological point-of-view, green rust complexes might have additional benefits since they can serve as reductants themselves in the degradation reactions [36].

In the KBr solutions, the resistance of the metal/solution interface increased and the corrosion rates decreased after exposure to CCl_4. This could not have been anticipated based solely on the results of the OCP-time experiments, since the potential-time behaviour in these solutions was similar to the behaviour in borate and calcium carbonate solutions. It is, however, in agreement with the results of the *in situ* Raman measurements. After immersion in solutions and prior to contaminant injection, the presence of magnetite was detected in the low pH KBr solution; green rusts and iron oxyhydroxides were detected in the high pH solution. After exposure to the oxidizer, magnetite was the final and only product of the surface redox reactions in the low pH solution; green rust, magnetite, $Fe(OH)_3$ and α-FeOOH were identified in the high pH solution. $Fe(OH)_3$ and α-FeOOH are more protective, and their presence could result in localized passivation of the electrode. For the two KBr solutions, the decrease of the corrosion rates after exposure to CCl_4 was probably due to the nature and/or thickness of the films present before and formed after the injection of the contaminant.

Ackowledgements - The authors wish to thank Professor Jacek Lipkowski, from the Department of Chemistry at the University of Guelph, for technical support through his Electrochemical Research Group. This study received partial funding through the NSREC, Motorola, ETI Industrial Research Chair held by R.W. Gillham. Throughout her studies, P. Bonin was supported by NSERC and by CRESTech Graduate Scholarships.

5.6 References

1. R.W. Gillham, S.F. O'Hannesin, *Groundwater* **32** (1994) 958.
2. L.J. Matheson, P.G. Tratnyek, *Environ. Sci. Technol.* **28** (1994) 2045.

3. R.W. Gillham, *Advances in Groundwater Pollution Control and Remediation*, in: M.M. Aral (Ed.), Kluwer Academic Publishers, Printed in the Netherlands, 1996, p.249-274.
4. T.L. Johnson, M.M. Scherer, P.G. Tratnyek, *Environ. Sci. Technol.* **30** (1996) 2634.
5. M.S. Odziemkowski, T.T. Schuhmacher, R.W. Gillham, E.J. Reardon, *Corros. Sci.* **40** (1998) 371.
6. E.J. Reardon, *Environ. Sci. Technol.* **29** (1995) 2936.
7. P.M.L. Bonin, M. Odziemkowski, R.W. Gillham, *Corros. Sci.* **40** (1998) 1391.
8. R. Greef, R. Peat, L.M. Peter, D. Pletcher, J. Robinson, *Instrumental Methods in Electrochemistry*, John Wiley & Sons, New York, 1985.
9. M.M. Scherer, J.C. Westall, M. Ziomek-Moroz, P.G. Tratnyek, *Environ. Sci. Technol.* **31** (1997) 2385.
10. P. Marcus, E. Protopopoff, *Electrochemical Surface Science of Hydrogen Adsorption and Absorption*, in: G. Jerkiewicz, P. Marcus (Eds.), Proceedings, Vol.97-16, The Electrochemical Society, Pennington, New Jersey, 1997, p.211-224.
11. P.M.L. Bonin, M. Odziemkowski, E.J. Reardon, R.W. Gillham, submitted to *Journal of Solution Chemistry*, May 1999.
12. A.J. Bard, L.R. Faulkner, *Electrochemical Methods: Fundamentals and Applications*, John Wiley & Sons, New York, 1980.
13. D.H. Davies, G.T. Burstein, *Corrosion* **36** (1980) 416.
14. J. O'M Bockris, M.A. Genshaw, V. Brusic, H. Wroblowa, *Electrochim. Acta* **16** (1971) 1859.
15. I.C.G. Thanos, *Electrochim. Acta* **31** (1986) 811.
16. L.J. Oblonsky, T.M. Devine, *Corros. Sci.* **37** (1995) 17.
17. J. Gui, T.M. Devine, *Corros. Sci.* **36** (1994) 441.

18. J.C. Rubim, J. Dunnwald, *J. Electroanal. Chem.* **258** (1989) 327.

19. R.G. Herman, C.E. Bogdan, A.J. Sommer, D.R. Simpson, *Applied Spectroscopy* **41** (1987) 437.

20. E.J. Reardon, R.D. Fagan, M.S. Odziemkowski, H.M. Peemoeller, M. Zhang, Geol. Soc. Amer. Annual Meeting, Toronto, Ontario, October 1998.

21. T.N. Moroz, D.K. Arkhipenko, *Soviet Geology and Geophysics* **2** (1991) 52.

22. M. Odziemkowski, J. Flis, D.E. Irish, *Electrochim. Acta* **39** (1994) 2225.

23. T.R. Hart, H. Temkin, S.B. Adams, *Light Scattering in Solids*, in: M. Balkanski, R. Leite, S. Porto (Eds.), Flammarion Sciences, Paris, 1976, p.254-258.

24. M. Odziemkowski, R.W. Gillham, 213th ACS National Meeting, San Francisco, CA. Extended Abstracts, Division of Environmental Chemistry, **37** (1997) 177.

25. N. Boucherit, A. Hugot-Le Goff, *Faraday Discuss.* **94** (1992) 137.

26. S. Simard, M. Odziemkowski, D.E. Irish, L. Brossard, H. Ménard, 191st Meeting of The Electrochemical Society, Montreal, Quebec. Meeting Abstract, **97-1** (1997) 279.

27. H. Kanno, J. Hiraishi, *J. Raman Spectrosc.* **12** (1982) 224.

28. T. Ohtsuka, K.Kubo, N. Sato, *Corrosion* **42** (1986) 476.

29. D. Thierry, D. Persson, C. Leygraf, N. Boucherit, A. Hugot-Le Goff, *Corros. Sci.* **32** (1991) 273.

30. K. Murata, D.E. Irish, G.E. Toogood, *Can. J. Chem.* **67** (1989) 517.

31. J. Dunnwald, A. Otto, *Corros. Sci.* **29** (1989) 1169.

32. V. Rives, M.A. Ulibarri, *Coordination Chemistry Reviews* **181** (1999) 61.

33. D. E. Irish, T. Ozeki, *Analytical Raman Spectroscopy*, in: J.G. Grasselli, B.J. Bulkin (Eds.), Volume 114 in Chemical Analysis: A Series of Monographs on Analytical Chemistry and Its

Applications; J.D. Winefordner, Series Editor; I.M. Kolthoff, Editor Emeritus, John Wiley & Sons, New York, 1991, p. 67.

34. Z. Szklarska-Smialowska, *Passivity of Metals*, in: R.P. Frankenthal, J. Kruger (Eds.), The Electrochemical Society, Pennington, New Jersey, 1978, p.443-462.

35. K. Ogura, S. Haruyama, K. Nagasaki, *J. Electrochem. Soc. Japan* **37** (1968) 102.

36. M Erbs, H.C.B. Hansen, C.E. Olsen, *Environ. Sci. Technol.* **33** (1999) 307.

6.0 CONCLUSION AND FUTURE WORK

6.1 Conclusion

The results of potentiodynamic polarization experiments, performed on stationary iron electrodes in borate buffer, indicated that only CCl_4 has the ability to oxidize the iron surface while CH_2Cl_2 is non-reactive i.e., a non-oxidizer (Table 6.1). In the presence of CCl_4, there was a positive shift of the corrosion potential, an increase of the corrosion current density and an increase of the cathodic Tafel slope. Thus, with respect to the iron electrode, CCl_4 was clearly acting as an oxidizer. This provides independent evidence that the dechlorination of CCl_4 is a redox process. When the potentiodynamic polarization experiments were performed in the presence of CH_2Cl_2, such changes were not observed. The non-degradability of CH_2Cl_2 may therefore be due to the fact that it does not act as an oxidizer of the iron.

These results are in agreement with the results of polarographic experiments where half-wave reduction potentials of –0.54 and –1.36 V NHE have been measured for CCl_4 and CH_2Cl_2, respectively (Dean, 1987). In the present study, under open circuit conditions, corrosion potentials ranging from –0.54 V NHE (in borate and calcium carbonate solutions) to –0.61 V NHE (in potassium bromide solution) have been measured. At these potentials, the degradation of CCl_4 should be expected but not that of CH_2Cl_2, which requires a potential much more negative than the corrosion potential of the iron in typical groundwater solutions.

Table 6. 1 Summary of the results of the electrochemical and spectroscopic experiments performed on iron stationary and rotating disk electrodes in borate buffer and in simulated groundwater.

Experiments performed on stationary electrodes	State of electrodes	Contaminant	Solution			
			Borate	$CaCO_3$	Low pH KBr	High pH KBr
Potentiodynamic polarization	Clean	CCl_4	Oxidizer	N/A		
		CH_2Cl_2	Non-reactive			
Open circuit potential-time	Clean	CCl_4	Positive potential shift			
		CH_2Cl_2	No potential shift			
	Oxidized	CCl_4	Larger and faster positive potential shift			
		CH_2Cl_2	No potential shift			
In situ Raman spectroscopy	Clean	Contaminant -free	No detectable film			
		CCl_4	No detectable film			
	Oxidized	Contaminant -free	No detectable film		Magnetite	Green rust α-FeOOH
		CCl_4	Magnetite	Green rust	Magnetite	Green rust Magnetite $Fe(OH)_3$ α-FeOOH

Experiments performed on <u>clean</u> rotating Disk electrodes	Parameter measured	Contaminant	Solution			
			Borate	$CaCO_3$	Low pH KBr	High pH KBr
Tafel plot	CR (nm/h)	Contaminant -free	44	68	N/A	
		CCl_4	↗			
Corrosion rate	R_p (kohm)	Contaminant -free	0.2	3.0	13.7	7.0
		CCl_4	≃		↗	
	CR (nm/h)	Contaminant -free	3.0	11.6	2.0	0.56
		CCl_4	↗		↘	

The findings of the potentiodynamic polarization experiments were also supported by the results of open circuit potential-time experiments performed in borate buffer as well as in aqueous solutions of calcium carbonate and potassium bromide (Table 6.1). In all of the solutions, a positive shift of potential was observed after the introduction of an oxidizer such as CCl_4, while no significant change of potential was observed in the presence of CH_2Cl_2. When the OCP-time experiments were repeated on pre-oxidized iron surfaces, the introduction of CCl_4 resulted in larger and faster positive shifts of potential confirming the role of the pre-oxidized iron surface as a catalyst.

The shifts of potential observed in all solutions after the injection of CCl_4, on clean or pre-oxidized iron electrodes, corresponded to surface film formation. To investigate the nature of the changes at the iron/solution interface, *in situ* Raman spectroscopic experiments were performed (Table 6.1). In the case of clean iron electrodes, the film was most probably too thin to be detected by normal Raman spectroscopy. For pre-oxidized electrodes, however, the final products of the surface redox reactions were successfully identified.

On the iron electrodes pre-oxidized in borate buffer and in calcium carbonate solution, there was no spectral evidence of the presence of a film prior to the injection of the contaminant. After exposure to CCl_4, however, magnetite and hydrated magnetite [$Fe(OH)_2 \bullet 2FeOOH$] were identified in borate buffer, while carbonate-containing green rust complexes were detected in the calcium carbonate solution. Identification of the green rust compound was based on bands assigned to the Fe^{2+}- OH and Fe^{3+}- OH stretching modes of green rust but also on a band assigned to the stretching vibrations of carbonate ions located in the interlayer regions of the green rust.

Carbonate-containing green rust, as a corrosion product of iron, was discovered 30 years ago (Stampfl, 1969). However, this study represents the first time that this corrosion product has been identified *in situ* by any technique and also the first time that spectral evidence of interlayer carbonate ions has been obtained.

Contrary to what was observed in borate buffer and in calcium carbonate solution, after pre-oxidation and prior to contaminant injection, the presence of a film was detected in the KBr solutions. In the low pH solution, magnetite was identified; green rusts and iron oxyhydroxides were detected in the high pH solution. After exposure to the oxidizer, magnetite was the final and only product of the surface redox reactions in the low pH solution; green rust, magnetite, $Fe(OH)_3$ and α-FeOOH were identified in the high pH solution

Tafel plot and corrosion rate measurements were performed on iron rotating disk electrodes. The results of these experiments indicated that, in borate buffer and in calcium carbonate solution, the resistance of the metal/solution interface stayed constant and the corrosion rate increased in the presence of carbon tetrachloride (Table 6.1). This was not the case in the KBr solutions where the resistance of the metal/solution interface increased and the corrosion rate decreased after exposure to CCl_4. This could not have been anticipated based solely on the results of the OCP-time experiments, since the potential-time behaviour in these solutions was similar to the behaviour in borate and calcium carbonate solutions. It is, however, in agreement with the results of the *in situ* Raman measurements. After pre-oxidation and prior to contaminant injection, the presence of a film was detected in the KBr solutions; there was no evidence of such a film in the borate and calcium carbonate solutions. For the two KBr solutions, the increase of the resistance

of the metal/solution interface and the decrease of the corrosion rate after exposure to CCl_4 was probably due to the nature and/or thickness of the films present before and formed after the injection of the contaminant. Finally, it appears that, in contaminant-free solution as well as in the presence of CCl_4, the anions have the following effect on the corrosion rate: carbonate>borate>bromide. In term of resistance of the metal/solution interface, a different trend was observed (bromide>carbonate>borate) but this was probably more a reflection of the ionic concentration of each solution than of the type of anions present.

Based on the results obtained in this study, a new conceptual model of the reductive dehalogenation of chlorinated aliphatic hydrocarbons by iron is proposed. According to this model, the introduction of an oxidizer such as CCl_4 will result in surface film formation. The composition and protective properties of these films were shown to be dependent on the potential history of the iron surface prior to and after its exposure to the oxidizer as well as on the ionic composition of the water. With regards to the practical use of iron for the remediation of groundwater contaminated with chlorinated aliphatic hydrocarbons, these surface films may, or may not, affect the reaction rates. For example, magnetite and green rust compounds, being non-protective, will not prevent charge transfer at the metal/solution interface; charge transfer will however proceed at a slower rate than on a bare metal surface. In addition, in the case of green rust compounds, they may also play a role as reductants themselves and thus enhance reaction rates. For $Fe(OH)_3$ and α-FeOOH films, however, the situation is different. Because these compounds are more protective, their presence could result in localized passivation of the iron, as seen in this study, and therefore be detrimental from a technological point-of-view.

Finally, this study demonstrated the usefullness of electrochemical and spectroscopic methods as investigative tools to gain insight on the iron technology. One has to remember however that in field applications of the technology, the chemical conditions are much more complex than presented here.

6.2 Future Work

1) The findings of this study are limited to a single degradable/non-degradable compound couple: carbon tetrachloride and dichloromethane. It would be useful to extend the investigation to other couples, for example chloroform / dichloromethane and trichloroethane / 1-2 dichloroethane, in order to answer questions such as:
   a) Could a compound be degradable in the presence of iron but not act as an oxidizer of iron? For example, chloroform has been found to degrade in the presence of iron (Gillham and O'Hannesin, 1994). As for dichloromethane, however, to be reduced by a redox process, chloroform requires a potential (-1.39 V NHE) which is much more negative than the corrosion potential of the iron in typical groundwater solutions (Dean, 1987). The degradation of chloroform in the presence of iron is therefore probably due to another mechanism, such as catalyzed hydrogenolysis by H_{ads} on the iron or magnetite surface. If chloroform is proven to be a non-oxidizer, experiments performed with the chloroform/ dichloromethane couple could help elucidate the importance of catalyzed hydrogenolysis in the degradation of chlorinated aliphatic hydrocarbons.
   b) Do all the non-degradable compounds have no influence on the corrosion behaviour of iron or are some compounds non-degradable because they actually passivate the iron surface?

c) Can the results of the present study be put to use to develop a screening technique to determine if a particular compound is likely to be degradable?

2) Iron (II) hydroxides, green rust complexes and magnetite have been identified as some of the products of surface redox reactions in simulated groundwater. Being non-protective, the degradation of chlorinated aliphatic hydrocarbons by iron will proceed by charge transfer through these films. In addition, degradation of the halogenated molecules could result from surface reactions with the films themselves, as was found by Erbs *et al.* (1999), who reported the reduction of carbon tetrachloride in the presence of green rust.

To differentiate the relative contribution of these two mechanisms, charge transfer versus surface reactions, to the overall degradation reactions, batch experiments could be performed. These experiments would involve the preparation of vials containing granular particles of iron (II) hydroxide, green rust complexes or magnetite, without an iron core substrate. By comparing the degradation rates there obtained with the rates obtained in the presence of granular iron covered by these films, determination of the contribution of each material to the overall degradation reactions could be established.

3) The surface of as-received granular iron particles used in commercial applications is covered with iron oxides (Odziemkowski, 1997). Some of these oxides are protective and will therefore prevent charge transfer reactions from occurring. In the presence of water (Odziemkowski, 1997) or chlorinated organic molecules (the results of the present study), these oxides have been found to undergo an autoreduction process. This process, by acting as

an activation and/or rejuvenation mechanism, might play a fundamental role in the immediate and long term performance of granular iron remediation systems. Further investigation of these autoreduction proces ses could therefore be beneficial in the production and selection of commercial iron materials.

6.3 References

Dean, J.A. (1987). *Handbook of organic chemistry*. McGraw-Hill Inc., New York, pp. 8.76-8.84.

Erbs, M., H.C.B. Hansen and C.E. Olsen. (1999). *Reductive dechlorination of carbon tetrachloride using iron (II) iron (III) hydroxide sulfate (green rust)*. Environ. Sci. Technol., Vol. 33, pp.307-311.

Gillham, R.W. and S.F. O'Hannesin. (1994). *Enhanced degradation of halogenated aliphatics by zero-valent iron*. Groundwater, Vol. 32, No. 6, pp. 958-967.

Odziemkowski, M.S. and R.W. Gillham. (1997). *Surface redox reactions on commercial grade granular iron (steel) and their influence on the reductive dechlorination of solvent. Micro Raman spectroscopic studies*. 213th ACS National Meeting, San Francisco, CA. Extended Abstracts, Division of Environmental Chemistry, Vol. 37, No. 1, pp. 177-180.

Stampfl, P.P. (1969). *Ein basisches Eisen-II-III-karbonat*. Rost. Corros. Sci., Vol. 9, pp.185-187.